Investigating the effect of Ena/VASP-EVH1 domain-mediated interactions inhibition in immune cells

Inaugural-Dissertation
to obtain the academic degree
Doctor rerum naturalium (Dr. rer. nat.)

submitted to the
Department of Biology, Chemistry, Pharmacy
of Freie Universität Berlin

by
Hafiza Nayab
Berlin

2022

The research for this PhD thesis was conducted from April 2015 until December 2019 at Leibniz Research Institute for Molecular Pharmacology, Berlin under the supervision of Dr. Ronald Kühne.

1. Reviewer: Prof. Dr. Christian Freund
2. Reviewer: Prof. Dr. Hartmut Oschkinat

Date of Oral Examination: 5th July 2022

Affidavit

I declare that my doctoral thesis " **Investigating the effect of Ena/VASP-EVH1 domain-mediated interactions inhibition in immune cells**" has been written independently and with no other sources or aid than those cited.

X _____

Hafiza Nayab

Contents

I.   Introduction

1. Introduction

1.1. Immune system:

The immune system is a precisely developed body's defensive system that has the primary function to protect against foreign invaders (viruses, bacteria, parasites) and antigens by complex biochemical responses [1]. The immune system itself is a complicated system divided into innate and adaptive immune systems based on its responses. Both systems are distinct in occurrence, whereas their functions are overlapping and interconnected [2]. The innate immune system is a non-specific, immediate, and relatively short-lived response that cannot form immune memory. It is the host's first-line defense to invading pathogens. The innate immune system comprises different components from physical barriers like skin and mucosa to effector cells like granulocytes, monocytes, macrophages, natural killer, dendritic cells [3], and chemical mediators [4]. They collectively protect from microbial attack by directly killing them or by initiating proper immunological responses against pathogens. These responses are mediated by receptors (TLR, HLA, MHC, etc.), proteins, enzymes, chemokines, and cytokines [5]. Innate immune response to pathogens relies on pattern recognition receptors (PRRs) which allow immune cells to detect and respond rapidly to a wide range of pathogens that share common structures, known as pathogen-associated molecular patterns (PAMPs). Bacterial cell wall components, lipopolysaccharides (LPS) and double-stranded ribonucleic acid (RNA) produced during viral infection are examples of PAMPs [6].

Innate immune response has characteristics of rapid recruitment of immune cells to infection sites and initiation of the inflammatory response by release of cytokines and chemokines. Key inflammatory cytokines released during the early response to bacterial infections are tumor necrosis factor (TNF), interleukin 1 (IL-1), and interleukin 6 (IL-6). The inflammatory response created is essential for the clearance of pathogens [5]. The complement system of the innate immune system performs pathogen processing and renders them susceptible to phagocytosis by phagocytic cells. The process of phagocytosis is accomplished by neutrophils and monocyte-derived cells (macrophages, dendritic cells). Although both cell types share the same phagocytic function, neutrophils are relatively short-lived cells containing granules and enzyme pathways that assist in eliminating

pathogenic microbes [3]. Whereas macrophages and dendritic cells are long-lived cells that in addition to phagocytosis involved in antigen presentation to T-cells. Therefore, due to their ability to initiate acquired immune responses, macrophages, dendritic cells, and T-cells are considered as the linker between innate and adaptive immune responses [7].

The adaptive immune system is commonly referred to as the acquired system. Unlike the innate immune response, the adaptive immune response is precise and well organized [8]. Maintaining memory is a key feature of the adaptive immune system. The primary adaptive response is to release antigen-specific antibodies upon antigen recognition, which often takes days to mature. Once established, antibody memories are maintained for the rest of life. Memory cells maintain secondary response by reacting rapidly and efficiently to subsequent antigen encounter [9]. This secondary response is often more potent than the primary response. Thus, adaptive immune responses are the basis for adequate immunization against infectious diseases. The cells of the adaptive immune system include T-cells and B-cells [10]. T-cells express a specialized receptor, T-cell receptor (TCR), that controls cell activation by recognizing specific peptides presented by major histocompatibility complexes (MHCs) molecules. The process of antigen presentation initiates T-cell differentiation primarily into either cytotoxic T-cells (CD8+) or T-helper cells (Th) (CD4+) [11]. These cells trigger the humoral immune response by activating antigen-specific B-cells to produce antibodies. For efficient immune response, both innate and adaptive immune systems work in a great synergy against pathogens, tissue damage and toxic chemicals [12]. T-cells and macrophages are important linker between innate ad adaptive immune system. Thus, a functional disruption in any of these cells will results in pathological immune response. This study primarily focuses on T-cells and macrophages due to their significant role in eliciting appropriate immune response.
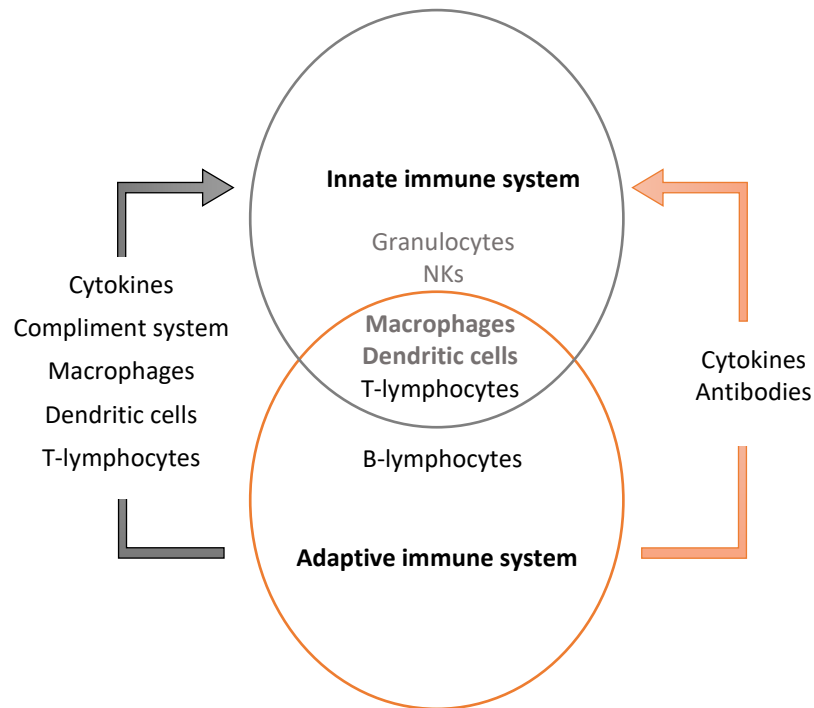
Figure 1.1. Schematic representation of innate and adaptive immune system interplay: The first line responding innate immune system consists of macrophages, natural killer (NK) cells, dendritic cells (DCs) and granulocytes. Antibody producing B-cells, CD8 + and CD4 + T-cells are part of the slow responding adaptive immune system. Macrophages, dendritic cells and T-lymphocytes serve as the linker between innate and adaptive immune system.

1.1.1. T-lymphocytes (T-cells):

T-cells hold a central place in the cell-mediated immune response. They are also known as T-lymphocytes because of their predominant development in the thymus. T-cells are isolated from the bone marrow hematopoietic stem cells. After their development in bone marrow, T-cells migrate to the thymus where they mature and differentiate [8]. During the early stages of development in the thymus, a diverse number of unique antigen-recognizing receptors called T-cell receptors (TCR) express on the T-cell surface by recombination. Consequently, each type of TCR has unique antigen specificity and is capable of recognizing a wide variety of antigens [13]. Unlike antibodies, the TCR cannot bind to antigens directly. Instead, TCR requires special antigen-presenting cells (APCs) for the presentation of antigens. Typical APCs include macrophages, dendritic cells, Langerhans cells, and B-cells [8]. Antigen presentation is accomplished by specialized cell surface receptors called major histocompatibility complexes (MHCs). MHCs are classified as MHC class I (also termed human leukocyte antigen [HLA] A, B, and C) that presents cytosolic endogenous (intracellular) peptides to CD8+ cells. While MHC class II (also termed HLA-DP, DQ, and DR) presents exogenous (extracellular) peptides to CD4+ cells [14]. APCs phagocytose foreign bodies such as viruses or pathogens, process, and display them as antigens-MHC class II molecules. The T-cells recognize antigens upon binding via TCRs and activate T-cells to secrete cytokines which further regulate the relevant immune response. Once activated, T-cells proliferate and differentiate into effector T-cells, regulatory T-cells (T-reg), or become memory T-cells [15,16,17].

CD8+ cells carry out their cytotoxic function by releasing two types of cytotoxic proteins; the granzymes that induce apoptosis in target cells and the pore-forming protein perforin through which the granzymes can enter the cell [18,19]. The CD8+ cells kill not only virally or bacterially infected cells, but also eradicate cancerous cells [19]. The CD4+ cells also known as T-helper cells, play an important role in organizing, activating, and regulating the adaptive immune response. These cells are activated through antigen recognition via MHC class II molecules [7]. Unlike CD8+ cells, T helper cells have a wider range of effector functions and they can differentiate into many subtypes, such as Th1, Th2, Th17, and T-reg cells [15]. The Th1 cells are necessary for host defense against intracellular pathogens. It enhances anti-pathogenic and anti-viral immunity. The Th1 cells release IFN-γ, which triggers the

phagocytic activities of macrophages. Cytokines secreted by Th1 cells participate in the B-cell differentiation to generate opsonizing antibodies [20]. However, exaggerated Th1 responses against self-antigens are evident to be associated with certain autoimmune diseases like Multiple sclerosis (MS), experimental autoimmune encephalomyelitis (EAE) [21]. The Th2 cells are also involved in the development and recruitment of mast cells and eosinophils essential for the initiation of acute inflammatory responses, associated with allergy and asthma. Th2 cells are known to release cytokines (IL-4, 5, and 13) which are responsible for activating B-cells to produce immunoglobulin E (IgE) that are associated with allergic reactions. Therefore, an imbalance in Th2 cytokine production is correlated with the onset of allergic conditions [22]. The Th17 cells produce proinflammatory cytokines such as IL-17 (IL-17A), IL-17F, and IL-22 that are collectively associated with ongoing inflammatory responses, particularly familiar to chronic infections and diseases [20,23]. Memory T-cells are antigen-specific T-cells that exist for a long term after infection. Memory T-cells are well qualified to recognize specific antigens, and quickly converted into effector T-cells upon re-exposure to the specific antigen, thus providing a rapid response to the infection. Memory T-cells are either CD4+ or CD8+ depending on the type of antigen exposure.

T-reg cells are a unique subset of T-cells that have characteristics to regulate other immune cells [24]. T-reg cells release inhibitory cytokines (such as IL-10, IL-35, and TGF-β) and also block the CD8+ activation to suppress the cytolytic response to self and foreign antigens [17]. CD8+ inhibition by T-reg cells can be explained through enhanced IL-2 consumption and high ectonucleotidases CD39 and CD73 expression, which mediate the extracellular conversion of ATP into immunosuppressive adenosine [25]. T-reg cells-mediated immune suppression is crucial for immune tolerance, dysregulation of which results in autoimmunity 39. The increased T-reg cells population in the tumor microenvironment correlates with tumor progression, metastasis, and poor patient outcomes [17].

Lymphocytes are migratory cells, that are constantly circulating in the blood, lymphoid and extra lymphoid tissues in order to search for their cognate antigen. Homing of T-cells into lymph nodes (LNs) occurs constantly with an average of 2.5×10^{10} cells passing each human lymph node per day [26]. T-cell homing occurs in four steps: rolling, firm adhesion, cell spreading, and transmigration (Fig. 1.2) [27]. Upon APC encounter, T-cells recognize antigens presented on the APCs surface.
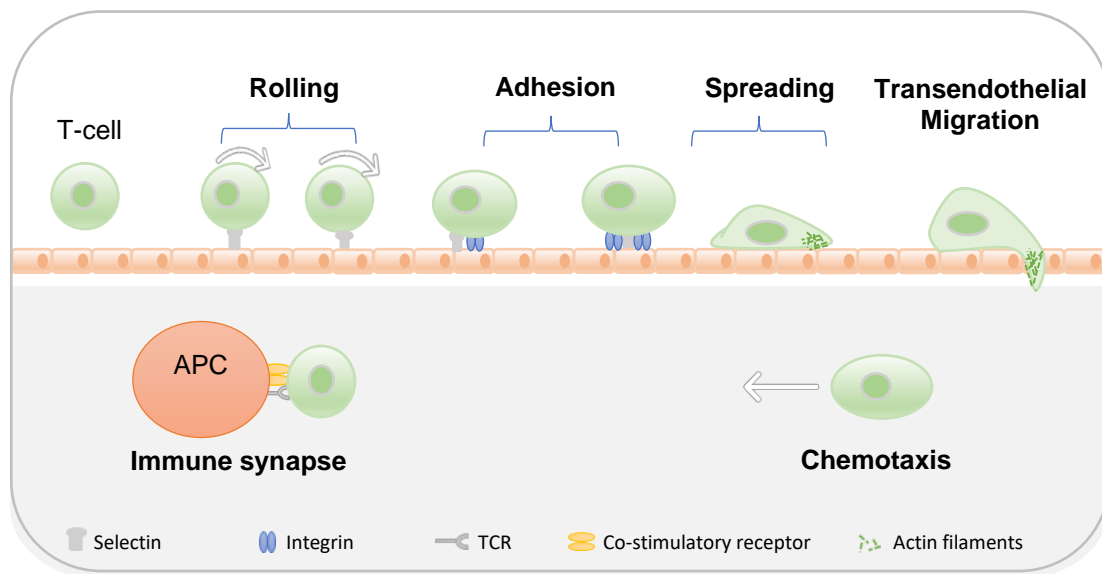
Figure 1.2: T-cell Homing and activation: T-cells homing occur in four steps: Rolling of the T-cells along the endothelium is mediated by selectins expressed on T-cells. Chemokine-activated integrins enable firm adhesion of the T-cells to the endothelium. Subsequently, the T-cells spread over and migrate through the endothelium. In the tissues or LNs, T-cells encounter with an APCs presenting cognate foreign peptide which activate the T-cells to promote their proliferation and differentiation.

T-cells exhibit amoeba-like mobility driven by actin-rich protrusion at the leading edge, working in coordination with contractile forces at the rear of the cell. The structure at the leading edge of the cells, lamellipodium is composed of dense, highly branched actin filaments meshwork. In lamellipodia, thin projections of actin filaments called filopodia, are present that carry out an exploratory function [28]. To cross tissue barriers made of dense extracellular matrix (ECM), immune cells have the capacity to assemble dynamic actin-rich membrane protrusion called invadopodia, which degrade the extracellular matrix through the local deposition of proteases. On the circulating T-cell surface, adhesion molecules such as L-selectin are presented in an active form and bind to its ligand with low affinity. In contrast, integrin binds to its ligand intercellular adhesion molecules 1 (ICAM-1) with high affinity presented in an inactive state [29,30]. This distribution and affinity of adhesion molecules are intended to assist the rolling along the endothelium, while it concomitantly minimizes unspecific adhesion of T-cells. Chemokine receptor stimulation initiates a signaling pathway that leads to the activation of integrins, thus facilitating T-cells to adopt migratory phenotype.

TCR- or chemokine receptors mediated signaling, initiate dynamic cytoskeletal rearrangements, which induce morphological changes crucial for T-cell adhesion, migration, and activation. The binding of chemokine (CXCL12) to their receptor CXCR4 and CCR7 induces signaling pathways via Src family kinases (SFKs) [31,32]. CXCR4 signaling is associated with the TCR and uses its immunoreceptor tyrosine-based activation motifs (ITAMs) for signal transduction. ITAMs act as tyrosine kinase substrates, phosphorylated by Src family tyrosine kinases such as LCK. Upon LCK phosphorylation, Zeta-chain-associated protein kinase 70 (ZAP70) is recruited to the TCR/CD3 complex. Activated ZAP70 then phosphorylates several downstream adaptors, including linker for activation of T-cells (LAT) and SH2 domain-containing leukocyte protein of molecular weight 76 (SLP76) leading to the formation of a signaling complex. SLP76 links with adhesion and degranulation promoting adapter protein (ADAP) in the signaling complex. ADAP binds to Src kinase-associated protein of molecular weight 55 kDa (SKAP55) in the integrin activation pathway [33]. SKAP55 also constitutively interacts with Rap1–GTP-interacting adapter molecule (RIAM) which further binds with VASP and talin to promote cell spreading [34]. SLP76 is associated with a guanine nucleotide exchange factor (GEF) VAV. VAV triggers the GTPase Ras-related C3 botulinum toxin substrate 1 (Rac1) activation, which interacts with Wiskott-Aldrich syndrome protein (WASP) and activates the actin-related protein-2/3 (Arp2/3) complex essential for lamellipodium formation [27,35]

TCR-MHC interactions result in a series of molecular rearrangements, leading to the formation of a distinct structure at the contact site between the T-cells and APCs, termed as immunological synapse (IS) [36,37]. Dynamic actin cytoskeleton polymerization plays a crucial part in facilitating TCR conjugation with MHC and scaffolding protein assemblies and organization [38,39]. Upon TCR activation, signaling proteins arrange in distinct microclusters (also known as 'signalosomes'). The cytoplasmic chain of the TCR is too short to transduce the signal into the cell hence, the co-stimulatory receptor CD3 and ζ polypeptides cooperate in transmitting the TCR signal into the cell via its conserved motifs ITAMs.
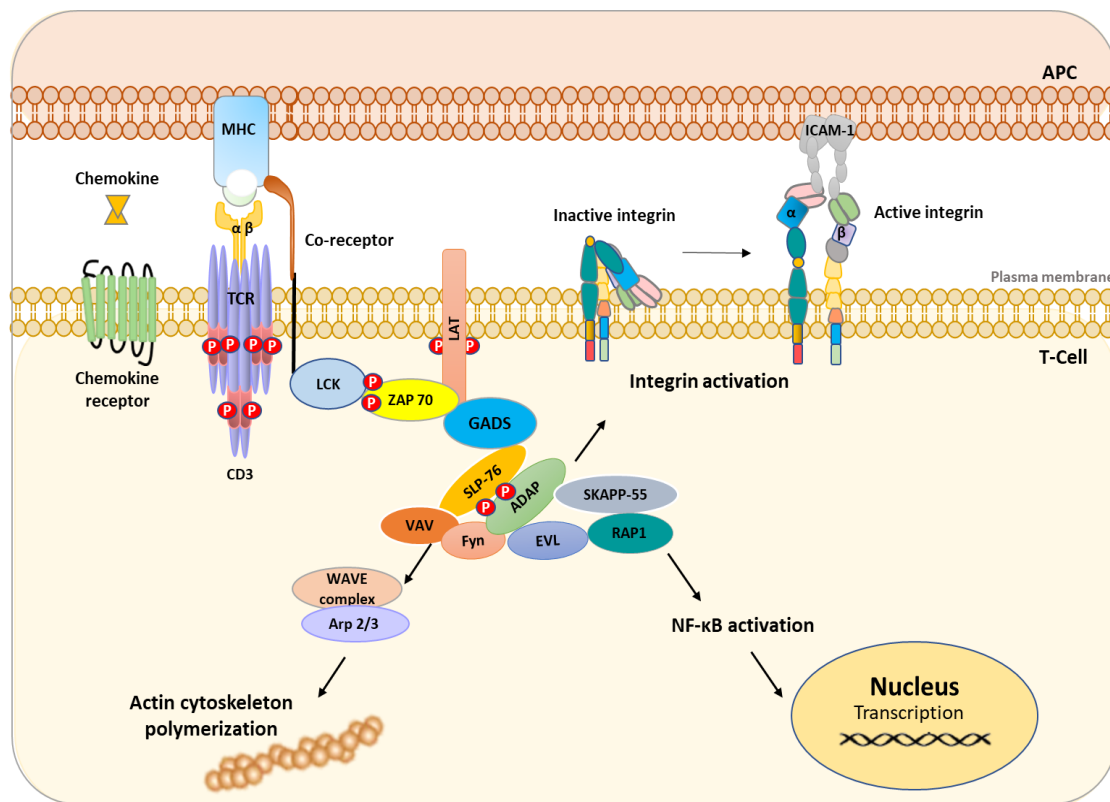
Figure 1.3: Simplified model of T-cell signaling: Chemokine or TCR triggering by their respective ligands activates Src family kinases (SFKs) that phosphorylate the ITAMs of the TCR. Phosphorylation of ZAP70 regulates several signaling molecules involved in gene expression (for T-cell activation, proliferation and differentiation), T-cell adhesion (integrin activation) and migration (actin polymerization).

This signaling complex activates several regulators signaling pathways. Non-catalytic region of tyrosine kinase (Nck) and VAV1 control actin cytoskeletal polymerization by recruiting Wiskott-Aldrich syndrome protein (WASp) and the Wiskott-Aldrich syndrome proteins family member 2 (WASF2 also known as WAVE2) complex to membrane [40,41]. SKAP55 and ADAP are part of the signaling complex that regulates integrin activation [42,43]. Phospholipase Cγ1 (PLCγ1) phosphorylation by ITK leads to the hydrolysis of phosphatidylinositol 4,5-bisphosphate (PIP2) to produce the second messenger diacylglycerol (DAG) and inositol trisphosphate (IP3). DAG activates PKC and the MAPK/Erk pathways, both promoting transcription factor NF-κB (nuclear factor kappa-light-chain-enhancer of activated B-cells) activation [44]. Overall antigen recognition, integrin activation, cytoskeletal reorganization, and gene expression are essential for T-cell activation.

1.1.2. Macrophages:

Macrophages are the professional phagocytes that are highly specialized in the elimination of pathogens. They originate from blood monocytes which have left the circulation and enter the tissues where they differentiate into tissue-specific macrophages [45,46]. Macrophages are the mononuclear white blood cells of the innate immune system that detect, engulf and digest foreign substances like microbes, cellular debris, tumor cells and other non-self-proteins [5,47]. They detect bacterial and other microbial debris using a system of recognition receptors such as Toll-like receptors (TLRs). These receptors bind specifically to different pathogenic components like lipopolysaccharides (LPS), RNA, DNA, or extracellular proteins (for example, flagellin from bacterial flagella). The pathogens during phagocytosis, are trapped in a phagosome that fuses with the lysosome for their ultimate digestion. Post pathogenic digestion, the antigenic peptides are processed within the cell and bind to the MHC class II molecule. Antigen peptide-MHC class II complex then express at the macrophage cell surface where they can be recognized by TCR leading to the activation of effector T-cells [5,13,14].

Besides phagocytosis and T-cell activation, macrophages also regulate the inflammatory immune response. Macrophages exist in a variety of phenotypes which are determined by the stage of inflammation. Peripheral monocytes were differentiated into inactivate tissue-specific macrophages (M0) which then polarized to M1 and M2 phenotypes. M1 macrophages are the dominating phenotype detected in the early stages of inflammation that are activated by LPS and IFN-gamma. M1 phenotypes are known as pro-inflammatory due to their release of pro-inflammatory cytokines like Interleukin-6 and TNF [48]. M1 phenotypes produce cytokines (IL-12, IL-6 and CXCL9) to recruit and stimulate the cytotoxic immune cells to kill tumor cells directly by producing nitric oxide [49].

In contrast, the M2 phenotype generally refers to macrophages that function in wound healing and tissue repair. M2 macrophages turn off damaging immune responses by producing anti-inflammatory cytokines like IL-10 and TGF-β [50,51]. During the wound healing process, macrophages promote re-vascularization and re-epithelialization at the inflammatory site. Thus, overall macrophages acquire dual functions in the promotion and regulation of inflammation. Therefore, dysfunction or impairment in macrophage effector function could lead to some severe disorders.
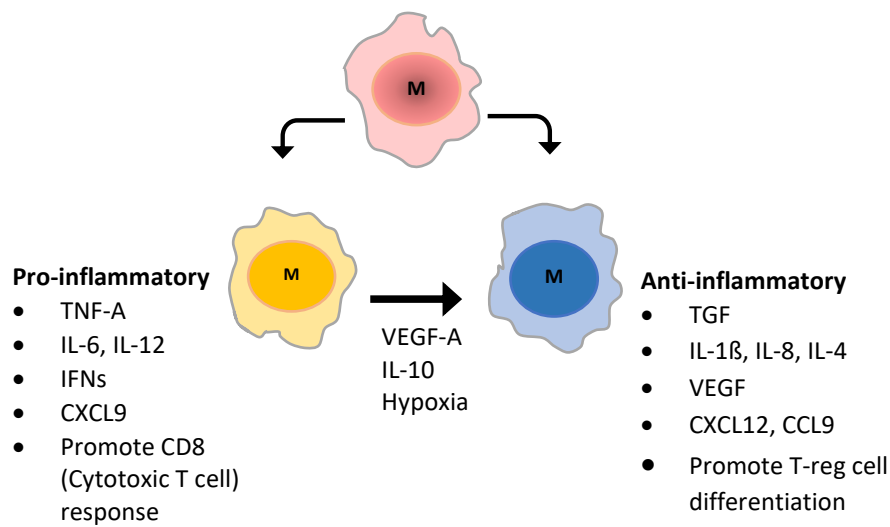
Figure 1.4: Macrophage differentiation: Monocytes in tissue differentiate to tissue specific macrophages M_0. Upon activation by IFNs and Interleukins in initial inflammatory response M_0 differentiate into M1 subset of macrophages. M1 initiate inflammatory response and activate adaptive immune cells. In later phase, under the influence of cytokines and chemokines macrophages differentiate into M2 subset that has Pro-tumor characteristics. It releases cytokines and chemokines to shut down cytotoxic immune cells and help in tissue regeneration.

Inflammation is the characteristic feature of tumor progression and autoimmune diseases. Studies have shown infiltration and differentiation of mononuclear phagocytes (macrophages) contribute to tumor progression and various autoimmune diseases like rheumatoid arthritis, systematic lupus erythematosus, and insulin-dependent diabetes mellitus [3,5,63]. Macrophage recruitment to the tumor microenvironment (TME) is a complicated process that is controlled by the release of several chemokines, cytokines (IL-4, IL-13), growth factor VEGF, and granulocyte-macrophage CSF (GM-CSF) by tumor and stromal cells [57,59]. Macrophages at the tumor site due to rich chemokines and cytokines environment differentiate into distinct subtypes known as tumor-associated macrophages (TAMs). TAMs initiate neoangiogenesis at the tumor site, facilitating tumor growth and metastasis. TAM secrete cytokines to differentiate and recruit regulatory T-cells (T-reg) at the tumor site. Both TAM and T-reg establish an immune-suppressive environment at the tumor site [56]. It is considered a promising strategy to develop agents that inhibit the recruitment and effector functions of macrophages in addressing autoimmune diseases and cancer treatment [53,57].

For efficient immune response, cells of both innate and adaptive immune systems work in a coordinated manner against pathogens, tissue damage and toxic chemicals [12]. Macrophages and T-cells are distinctive immune cells, critical for effective immune system functions. However, characteristic features of these immune cells are often linked to pathological conditions [58]. The pathological immune response is generally characterized as overactive (hypersensitivity reaction), inappropriate (autoimmunity and inflammation), or ineffective immune response (immunodeficiency) [59]. How immunocytes contribute specifically to autoimmune diseases and cancer metastasis is addressed here.

1.2. Autoimmune diseases:

The principal features of the immune system include defence, surveillance and maintaining homeostasis. The components of the immune system are highly efficient in discriminating between the body's own tissues and any foreign bodies. However, in certain individuals, the immune system becomes reactive against the body's own parts, organs, or tissues. The condition that arises from this aberrant immune response is called autoimmune disease [21,3]. There are over a hundred types of autoimmune diseases that exist. Insulin-dependent diabetes mellitus type 1, inflammatory bowel disease, multiple sclerosis is some of the prime examples of autoimmune diseases.

The exact etiologies of autoimmunity remain a conundrum, yet studies have reported the complex interplay of genetic predisposition, infections, internal and external environmental factors [61]. In healthy individuals, autoantibodies and autoreactive immune cells exist that are regulated by a mechanism known as immunological tolerance. In an autoimmune disorder, the loss of immunological tolerance occurs to an individual's own antigens [62]. A common feature of all autoimmune diseases is the presence of autoantibodies and inflammation that is characterized by the infiltration of mononuclear phagocytes, autoreactive T-cells and autoantibody-producing B-cells to the affected site. Autoantibodies attack the body's own tissues, activating the complement cascade-induced lysis or removal of cells by phagocytic immune cells [58]. In tissue-specific autoimmune response, the incursion of phagocytes such as macrophages induces the overproduction of pro-inflammatory cytokines such as IL-1β and TNFα. Steady-state stimulation by proinflammatory cytokines triggers the exaggerated immune response and the release of additional endogenous stimuli like damage-associated molecular patterns (DAMPs), to aggravate autoinflammation [52]. On the other hand, upregulation and accumulation of T helper cells, and downregulation of immune-suppressive regulatory subsets, have a strong influence on the autoantibodies and autoreactive T-cells mediated pathology [21,61,63]. The autoimmune response damages the tissues either by directly targeting cells or indirectly by cytotoxic cytokines, prostaglandins, reactive oxygen, or nitrogen species [64]. Therefore, it has been widely considered that T-cells, B-cells, and macrophages are mainly involved in generating an autoimmune response.

Autoimmune diseases are categorized as systemic or organ-specific based on autoantibodies and immune cells responses. When reactive immune cells or autoantibodies attack the body's specific organs, it is named organ-specific autoimmune diseases [65]. Hashimoto's thyroiditis and Graves' disease, both predominantly affect the thyroid gland and muscles while type I insulin-dependent diabetes mellitus (IDDM), affects the β-cell of pancreatic islets. There are multiple pathways of autoimmunity generation in organ-specific diseases. For instance, in IDDM, macrophages and neutrophils produce cytokines that promote β-cell apoptosis through Fas-Fas ligand and TNF-TNF receptor interactions, besides, there is also increased infiltration of cytotoxic T-cells and the subsequent release of autoantibodies against pancreatic cells [66]. The cytotoxic effector T-cells release granzymes and perforin to destroy β-cells resulting in an IDDM. Autoantibodies also interact with cell surface receptors, resulting in their defective function. Autoantibodies bind to acetylcholine receptors and block transmission at the neuromuscular junction in myasthenia gravis. While in Graves' disease, autoantibodies capture the thyrotropin-stimulating hormone (TSH) receptor and activate thyroid cells to over-produce thyroid hormones and down-regulate TSH production [58,67].

In systemic autoimmune disease, autoimmunity is expressed against many tissues of the body as seen in rheumatoid arthritis (RA), systematic lupus erythematosus (SLE) and multiple sclerosis (MS). RA characterizes by non-organ-specific autoantibody production and chronic inflammation of synovial tissues, leading to cartilage and bone destruction. Autoantibodies bind to normal circulating IgG, forming IgM–IgG complexes that deposit in joints. These immune complexes can activate the complement cascade, which leads to chronic inflammation of the joints. As, macrophages are a potent source of various proinflammatory cytokines in the development of RA [68]. Monocyte/macrophage-derived cytokines, such as TNF-α, IL-1β, IL-12, IL-6, IL-15, IL-18 and IL23 trigger the activation and recruitment of Th1 and Th17 T-cells in the synovial tissues of RA patients [45]. There are ample pieces of evidence that support that the frequency and an absolute number of macrophages markedly increase in the synovial tissues of RA patients [45,66,69].

An optimum phagocytic capacity of macrophages is critical for the clearance of dead cells and debris, which otherwise can lead to a pathological condition. Impaired phagocytosis of cellular debris leads to secondary necrosis, in which the plasma membrane

(PM) disintegrates and releases cellular contents. The cellular contents bind to immunoglobulins and complement proteins to initiate a systemic autoimmune response. Siglec-1 receptor expressed on the macrophage surface has a critical role in the recognition and phagocytosis of foreign antigens [70]. Studies reported the percentage of Siglec-1 expressing macrophages was shown to positively correlate with SLE. Macrophages release cytokines that stimulate B-cells autoantibodies production which leads to pathological conditions such as systemic erythematosus. In systemic lupus erythematosus (SLE), secondary necrosis and late apoptosis extend the autoimmune response by recruiting B and T-cells [48]. The normal function of B and T-cells against apoptotic cells is abolished, instead, B and T-cells are activated by autoantigens. Inflammation is amplified with respect to pro-inflammatory cytokines secreted by activated macrophages and T-cells. Inflammation is further worsened with the generation of autoantibodies by B-cells and the accumulation of autoreactive memory T-cells. The individuals affected by SLE may produce autoantibodies against a vast array of tissues, and interaction of these autoantibodies with their specific antigens produces various symptoms. Autoantibodies specific for erythrocytes and platelets, for example, can lead to complement-mediated lysis resulting in hemolytic anemia and thrombocytopenia, respectively. When the immune complex of autoantibodies with various nuclear antigens is deposited along the walls of small blood vessels, a type III hypersensitivity reaction develops. The complexes activate the complement system to damage the wall of the blood vessel, resulting in vasculitis and glomerulonephritis [71,72].

The autoimmune response generated in multiple sclerosis (MS) is mainly T-cell mediated. The cerebrospinal fluid of a patient with active MS contains activated T-cells. These T-cells infiltrate the brain tissue and cause characteristic inflammatory lesions, which destroy the myelin of nerve fibers and damage various degrees of the axon as well. Since myelin functions to insulate the nerve fibers, the breakdown in myelin sheath leads to numerous neurologic dysfunctions [58]. Research on an animal model of MS encephalomyelitis (EAE) has demonstrated that migration of T-cells and macrophages to the site of lesions in CNS is a vital aspect in the pathogenesis of MS [73].

As the spectrum of autoimmune disease is very broad, the treatment strategies also include a wide range of agents which affect their respective targets. Generally, the treatment of autoimmune disorders revolves around the nature, type and severity of the

disease. Currently, autoimmune disease treatments depend on non-specific immunosuppressant drugs that have high risks and side effects. Therefore, new therapeutic approaches are focused on addressing autoimmune diseases. Therapies targeting monocyte/macrophage have been used against RA. Inhibition of TNF-α produced by synovial inflammatory macrophages promotes IL-10 expression by CD4+ T-cells that enhances Treg cell function, promotes monocyte apoptosis via transmembrane TNF-α, and is associated with an antiosteoclast effect [74]. Another approach is the use of low-dose interleukin 2 (IL-2) for the fact that effector T-cells respond weakly to low doses of IL-2 whereas Foxp3+ Treg cells, which express the high-affinity IL-2 receptor (CD25), following low-dose IL-2 treatment proliferate in vivo. However, the non-specific expansion of the Foxp3+ Treg population may influence susceptibility to infections and cancer in some individuals. Immune cell trafficking towards the site of inflammation can also serve as ideal targets for therapeutic intervention for autoimmune diseases [75]. Autoimmune disorder studies have shown enhanced embracement of migratory attributes by immune cells in some cases. Chemokines and chemokine receptors upregulation in blood and cerebrospinal fluid of MS patients is familiar [76,77]. Further, overexpression of adhesion molecules also contributes to enhanced macrophage migration and activation in active SLE patients which is associated with tissue recruitment and inflammatory cytokine production [52]. T-cells displayed an enhanced ability to traffic to the peripheral lymph nodes due to increased levels of the adhesion molecules ICAM-1 and P-selectin. Over-expression of VCAM-1 has been associated with several autoimmune disorders such as rheumatoid arthritis and asthma [78]. Activated T-cell trafficking to lymph nodes and spleen depends upon actin cytoskeletal regulatory proteins EVL and VASP. In experimental autoimmune encephalomyelitis mice models, activated T-cells deficient of EVL/VASP expressed defective migration to the inflamed central nervous system [73].

One of the targeted drugs preventing T-cell migration into the CNS is natalizumab. Natalizumab targets the VLA-4 over the lymphocyte surface to pass the blood-brain barrier and de-escalate annual recurrence rates and disability progression. However, post-treatment there is still a 1/300 chance of developing progressive multifocal leukoencephalopathy (PML) [79]. Fingolimod acts as a Sphingosine 1 phosphate (S1P) receptor agonist, helping in S1P receptor downregulation, thereby preventing lymphocyte migration

from lymph nodes. This drug has shown a temporary adverse effect on the heart rate but otherwise shows remarkably few side effects. Conclusively, preventing immune cell migration to inflamed tissues in autoimmune diseases is one of the promising approaches. Thus, new therapy targeting different aspects of cell migration will be served as a target for the control of autoimmune diseases. Further, it is assumed, co-administration of such anti-migratory drugs with conventional immunotherapies would benefit the effectiveness of therapy and inhibit the chances of relapse as seen in many cases.

1.3. Metastasis:

The most lethal attribute of cancer is the ability to metastasize. It is the primary cause of cancer-associated morbidity and mortality [80]. Metastasis is referred to as a condition in which tumor cells evade their primary site and via the bloodstream or lymphatic system reach the distant sites where they start growing. Despite the advanced techniques in controlling cancer, approximately 90% of cancer-associated deaths are still caused by metastasis [81]. Based on invasion tendency, cancer is clinically categorized into three broad types. **Localized** cancer is confined to the area of its origin and has not spread to other parts of the body. **Regional** cancer diffused into surrounding tissues or organs and spread to nearby lymph nodes, while **Distant** cancer means that cancer is in a part of the body farther from its primary site [82]. US National Cancer Institute (SEER) published a report comparing 5-year survival data of the most common cancer types. According to the report, the 5-year survival rate for most localized cancer was improved over the last 5-year. However, metastatic patients with regional and distant tumors expressed a lower 5-year survival rate with almost less than 20% in most types of cancers [83]. A similar pattern has been observed in female breast cancer cases. Statistics revealed a 5-year relative survival rate is 99% to 86% in the case of localized breast cancer, which falls to 27% in the case of breast cancer metastasis [84].

The process of metastatic dissemination is very complicated that encompasses the interplay between intrinsic properties of tumor cells (genetic and epigenetic) and extrinsic factors (host tumor microenvironment) [80]. Cancer metastasis involves several sequential steps, each of which is crucial and correlated. Initially, tumor cells detach from their primary site after acquiring the capacity to invade into adjacent tissue or lymphatic/circulatory system. Within the circulation, tumor cells survive immune cells attack and interact with the endothelium to extravasate into the secondary tissues [85]. Upon arrival to the secondary site tumor cell quickly develop a pre-metastatic niche to enable their colonization and outgrowth within the new microenvironment. Each of these steps requires tumor cells to exhibit remarkable plasticity, allowing them to invade, adapt to continuous changes and encounter new challenges within their surroundings [86,87]. The development of invasive characteristics by tumor cells and the modulation of tumor microenvironments are considered as the principal hallmarks of metastasis [86]. Invasion to surrounding tissues

initiated by epithelial-mesenchymal transition (EMT) of tumor cells. The epithelial-mesenchymal transition (EMT) is generally described as a rapid and reversible modulation of epithelial cell phenotype. The EMT initiates alterations in the phenotype of epithelial cell that enables them to lose cell-cell adhesion, change in the expression of cell surface proteins, reorganizational variations in actin cytoskeletal proteins, activation of transcription pathways, and production of ECM degrading enzymes [88,89].
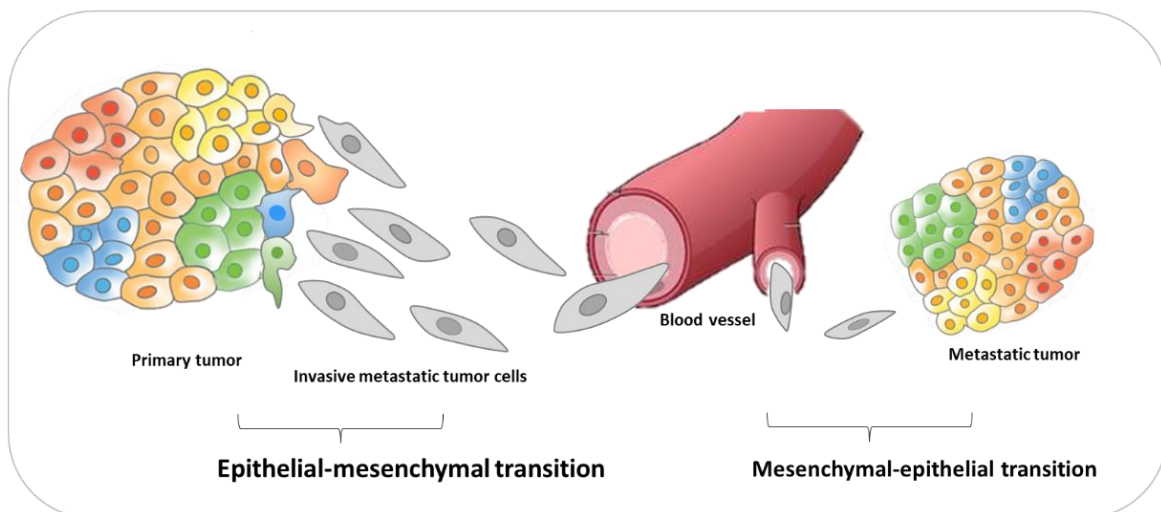
Figure 1.5: Epithelial mesenchymal transition as contributing factor in cancer progression: Cancer progression begins with reversible epithelial to mesenchymal transition of tumor cells phenotype. Transition to invasive stage enables tumor cells to intravasate the circulation and exit at remote site, where they undergo MET to generate secondary metastatic tumor.

Various actin filament nucleating proteins are not transcriptionally regulated during the transition but are differently localized and regulated [88]. The actin cytoskeleton organization is tightly linked to cell-cell junctions in the epithelial cells and due to the downregulation of E-cadherin during EMT, cells dramatically lose their adherence at tight junctions. Consequently, the actin-related proteins like Scar/WAVE complex, N-WASP, Arp2/3 complex, and cortactin are released from cell-cell junctions and redirected to cells leading edges for cellular migration and invasion [90]. There are shreds of evidence available claiming in breast cancer, cells undergoing EMT modulate the expression of actin-binding protein Mena to its invasive isoform (Mena^INV) [91,92].

The tumor microenvironment (TME) is a dynamic and complex network that includes stromal cells like fibroblasts, neuroendocrine cells, lymph-vascular endothelial cells, infiltrating immune cells, and ECM along with tumor cells [93]. A thick stromal layer surrounding the cancerous mass creates a physical barrier for cytotoxic immune cells. These stromal cells generate a unique microenvironment that modifies the neoplastic properties of the tumor cells. In the tumor microenvironment, immune cells function as both positive and negative regulators for cancer development. Normally, immune cells kill tumor cells or prevent tumor growth. However, tumor cells ditch immune cells in various ways including genetically manipulating their surface proteins to become undetectable by immune cells. Tumor cells modulate the tumor microenvironment by recruiting and differentiating immune cells that further promote cancer progression. Thus, immune cells ultimately facilitate tumor cell evasion and survival [94].

Macrophages facilitate tumor cell invasion, stromal remodeling through matrix metalloproteases. Macrophages are known to initiate vascularization and EMT that leads to metastatic tumor cell dissemination [53,57,95,96]. Macrophages at the tumor site differentiate into immunosuppressive phenotypes known as tumor-associated macrophages (TAMs). TAMs are the most abundant immune cells in the tumor microenvironment [53]. Characteristic features of TAMs are neo-angiogenesis and establishing an immune-suppressive environment at the tumor site. TAMs promote angiogenesis by producing IL-10, VEGF, and CCL22. TAMs inhibit NK cells, cytotoxic T-cells, and DCs by arginine deprivation through arginase expression for the generation of immune-suppressive environment [97]. It is evident that the chemokines released by TAM activate the transcription pathways for the expression of Mena^{INV} [92]. Mena^{INV} is the splice variant of the member of the Ena/VASP protein family (Mena) which is expressed in invasive tumor cells. Mena^{INV} expression is upregulated in breast cancers that promote invasion and motility of tumor cells [91]. However, there is also an indication exist that Mena^{INV} presents chemoresistance by altering microtubule dynamics and their ratio in breast tumor cells [98].

TAMs population in TME regulates the differentiation of cytotoxic CD8+ T-cell to immunosuppressive regulatory T-cells [49]. The increased T-reg cells population in the tumor microenvironment correlates with tumor progression, and poor patient outcome [17]. T-reg cells suppress cytolytic immunological reactions to self and foreign antigens by releasing

inhibitory cytokines (such as IL-10, IL-35, and TGF-β), blocking CD8+ T-cell activation by depletion of IL-2, direct suppression of enzyme and perforin dependent cytolysis of tumor cells [12,24]. T-reg cells alter other immune cells differentiation and maturation to maintain immunosuppressive cell populations at the tumor site [94]. Inhibition of CD8+ T-cells by T-reg cells can be explained through enhanced IL-2 consumption and by expression of high levels of the ectonucleotidases CD39 and CD73, which mediate the conversion of extracellular ATP into immunosuppressive adenosine [25]. Cytotoxic immune response serves as a strong checkpoint against cancer progression and metastasis formation [99]. Therefore, immunotherapy has gained a prominent place in recent years against various types of cancer. However, due to lack of specificity, only a small subset of patients respond favorably to immunotherapy [100]. Tumor cells possess high plasticity that manipulates not only immune cells but also is responsible for the ineffectiveness of immunotherapy due to the development of mutations and resistance [101]. Tumor cells evade immune attack by various mechanisms, like by upregulation of checkpoint receptor ligands, T-reg cells upregulation, or by the production of immune suppressive cytokines such as IL-10 and TGF [100,102].

Similar to immunotherapy, other conventional cancer therapies targeting metastasis proved ineffective due to the plasticity and unstable morphological transformation of tumor cells [85,103]. Although, traditional cancer treatments, including surgery, chemotherapy, and radiation therapy, have shown encouraging improvement in the disease. Yet 90% of cancer mortality is associated with metastasis [82]. The development of anti-metastatic therapy is a challenge due to the heterogeneous, unstable nature of tumor cells and the lack of ideal biomarkers for early detection and diagnosis. Therefore, innovative and site-specific targeted cancer therapies are urgently needed to address cancer. So far, drugs employed to prevent metastasis act upstream of the signaling pathways, as depicted in (Fig. 1.6) [104]. Whereas many of the initial steps in metastasis are complex and a high degree of cellular efficiency enabled them to bypass these signaling pathways [104]. Therefore, it is proposed to target the ultimate downstream of the cell migration signaling pathway, which would be difficult to bypass. The process of actin polymerization is highly unlikely to be substituted or alternated by tumor cells to invade or migrate. Therefore, we focus on an important regulator protein of actin cytoskeleton machinery, Ena/VASP, as a novel target for metastasis drug therapy.
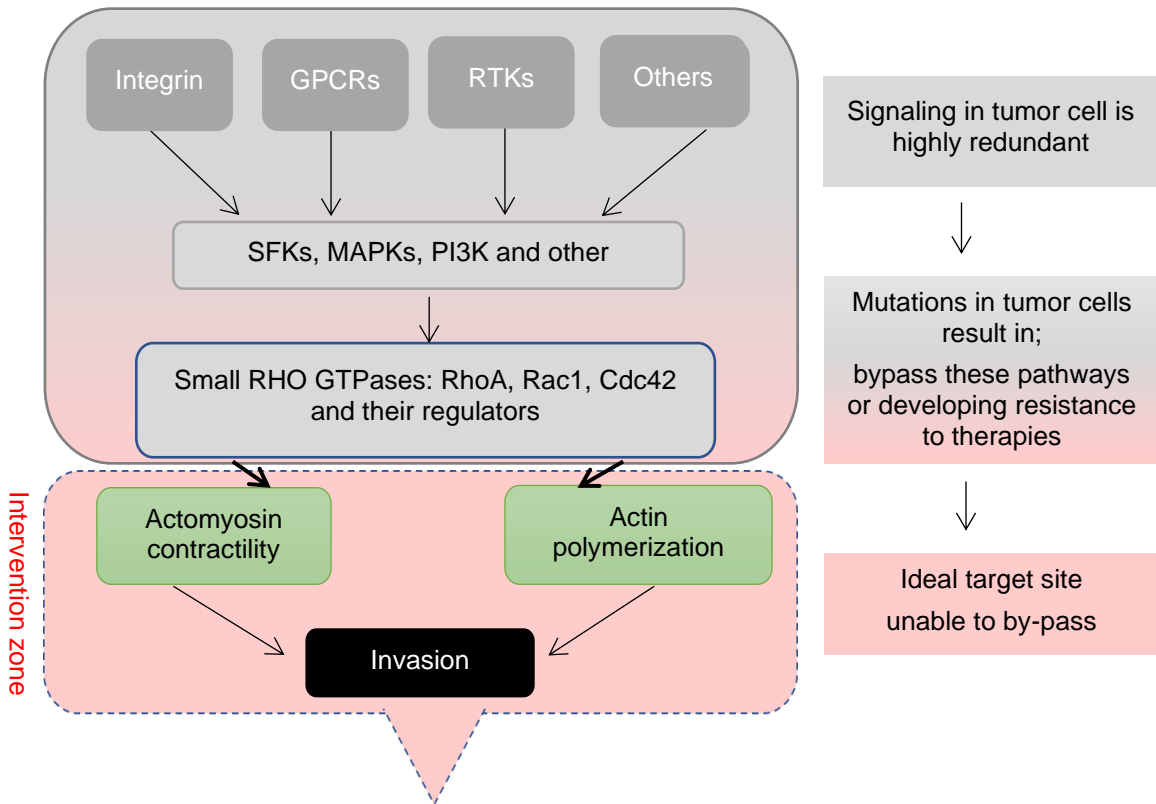
Figure 1.6: Anti-metastatic drug target: Schematic presentation of different signaling pathways involved in tumor metastasis. Tumor metastasis signaling pathways initiated by various extracellular stimuli. Tumor cells follow cascade of events to reach successfully at secondary site. Drug therapy utilized so far as anti-metastatic therapy act at the very upstream of these pathways. However, tumor cells can bypass or develop mutations in these pathways. This will result in non-responsiveness or resistance to therapy. Therefore, it is suggested to target the downstream of the pathways like actomyosin contractility and actin polymerization process, that cannot be by-passed. This approach can target directly two essential mechanisms driving cell migration.

1.4. Ena/VASP homology proteins:

Ena/VASP proteins are the important regulators of actin cytoskeleton [105]. They are involved in developing the nervous system in an embryonic phase and regulate actin cytoskeletal-related cellular responses [106–108]. Ena/VASP proteins directly modulate actin filament elongation by antagonizing F-actin capping proteins at barbed ends and binding profilin at actin polymerization sites [109]. Ena/VASP protein family in vertebrates consists of three paralogues, EnaH (Enabled homology), VASP (Vasodilator-stimulated-phosphoprotein), and EVL (Ena/VASP like). All family members have overlapping properties and expression pattern [110]. Ena/VASP family members exhibit a tripartite structural organization consisting of homologous N-terminal Ena/VASP homology 1 domain (EVH1), a central proline-rich region, and common C-terminal Ena/VASP homology 2 domain (EVH2) [111]. The Ena/VASP proteins function in tetrameric form. Overall, they act as actin elongation factors by employing the actin stress fibers at the tips of filopodia, lamellipodia, or focal adhesion sites [112,113].
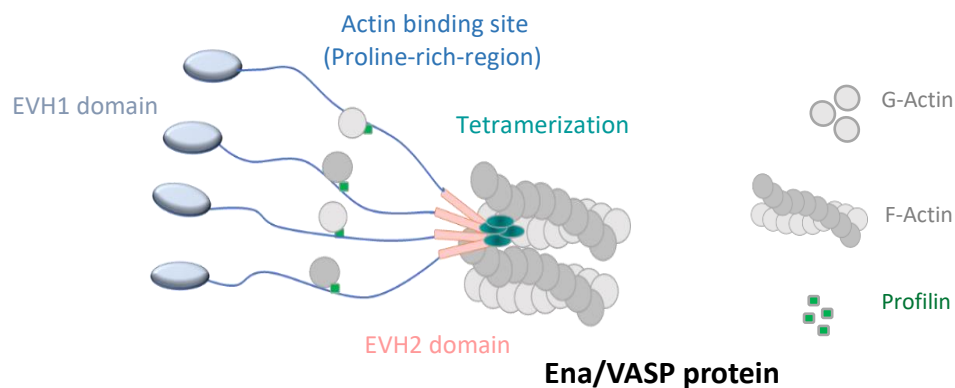
Figure 1.7.: Structure and domains of Ena/VASP homology proteins: Ena/VASP homology proteins contain a N-terminal EVH1 domain, which can bind to effector proteins though a poly-proline sequence (FPPPP) and are responsible for cellular localization of actin machinery. The central proline-rich region is a profilin binding site, whereas the C-terminal EVH2 domain is involved in tetramerization of Ena/VASP which is crucial in actin bundling and filament formation.

Structural insight into Ena/VASP protein domains:

1.4.1. EVH1 domain

The Ena/VASP homology domain 1 (EVH1) is an about 115 amino acid residue structure, that mediates multiprotein complex assembly associated with actin cytoskeletal remodeling [107,114]. The EVH1 domain is involved in the formation of multiprotein assemblies and helps in the recruitment of actin machinery at the tips of filopodia, lamellipodia, or focal adhesion site [112,113]. The EVH1 domain embraces a pleckstrin homology (PH) domain-like structure. However, conversely to the PH domain, the EVH1 domain does not bind to phospholipids [114,115]. Instead, the EVH1 domain mediates specific protein-protein interactions with proline-rich short peptide motifs like Src homology 3 (SH3), WW, and GYF domains. EVH1 domain of Ena/VASP proteins recognizes (D/E)-(F/W/Y/L)-P-P-P-P-X-(D/E) motifs, where X can be any amino acid residue [114]. The intracellular pathogen *Listeria monocytogenes* takes control over host actin machinery to propel itself to neighboring cells [116,117]. The pathogen spreads from cell to cell by using proline-rich motif (FPPPP) of its surface protein ActA to recruit Ena/VASP to the PM. Ena/VASP proteins generate actin filaments protrusion at the PM to push pathogen into the neighboring cell [118]. The proline-rich motifs are commonly found in cytoskeletal proteins, such as Vinculin, Zyxin, and lamellipodin [112].

The structural analysis revealed that the EVH1 domain comprises two antiparallel beta-sheets followed by an alpha-helix at the C-terminal. Further, the X-ray structure demonstrated the formation of a deep groove (binding pocket) by beta-strands within the EVH1 domain [115,119]. The proline-rich peptide adopts a left-handed poly-L-proline II helix that binds primarily to aromatic amino acids within the deep groove of the EVH1 domain [116] as shown in the figure below.
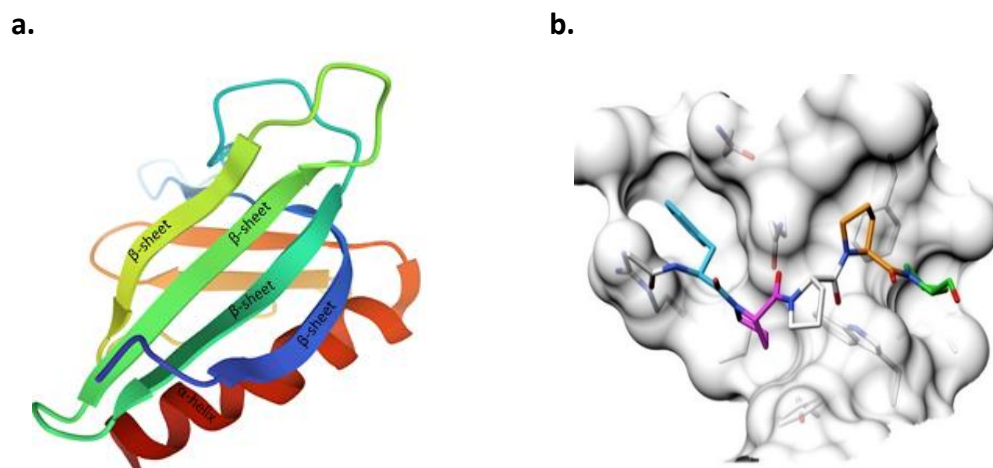
Figure 1.8: Structure of the EVH1 domain of VASP/EnaH: a. The solution structure of EVH1 domain of human VASP (PDB code: 1EGX) reveal the presence of alpha helix and antiparallel beta sheets in its structure. **b**. Structure of EnaH-EVH1 domain resolved through the X-ray crystallography by Dr. Matthias Barone, showing poly proline-rich ligand (in multicolor) adopting a conformation to fit in the binding pocket of EVH1 domain.

The EVH1 domain binds to the effector proteins via extended sequence to the main polyproline FPPPP consensus motif [114]. Studies have shown that the charged residue at the N- and C-terminal of EVH1-binding peptide boasted the specificity and affinity to the EVH1 domain. Thus, the binding affinity of EVH1 ligands with flanking residues (D/E)-(F/W/Y/L)-P-P-P-P-X-(D/E) is increased as compared to the peptide with only FPPPP motif [120]. The impact of flanking residue in the binding affinity to the EVH1 domain was described by Dr. Linda J Ball [121].

Table 1.1: Binding affinities of ActA peptides with VASP/EnaH-EVH1 domain determined by fluorescence spectroscopy

Peptide	Binding constant in µM	
	VASP-EVH1	EnaH-EVH1
Ac-FPPPPT-CONH$_2$	N.B*	417 ± 82
Ac-SFEFPPPPT-CONH$_2$	214 ± 32	201 ± 82
-FEFPPPPTEDEL- CONH$_2$	19 ± 3	17 ± 1

*N.B; Not binding

Data revealed by implicating negatively charged residues at the N-terminal of the core motif (FPPPP) boast binding affinity from 400 µM to 200 µM. However, full-length ActA peptides with intact N and C-terminal flanking residues showed a 21-time higher binding constant. Consequently, flanking residue along with the core motif for EVH1 binding ligand collectively contribute to their binding affinity.

1.4.2. Proline-rich site:

The central proline-rich domain is the least conserved region within the Ena/VASP proteins [122]. This region is the most divergent within the family and therefore has different binding partners and regulation mechanisms. The central proline-rich region harbors binding sites for SH3, WW domain-containing proteins and the actin monomer-binding protein profilin. The proline-rich site of Mena is distinct from VASP and EVL as it bears a highly charged site of unidentified function. Three isoforms of Mena are found expressing additional exons within this central region [123].

1.4.3. EVH2 domain:

The EVH2 domain contains three highly conserved sites, a G-actin-binding site (GAB), an F-actin-binding region (FAB), and a coiled-coil site [111,124]. GAB is an actin monomer binding site and is required in the role of Ena/VASP actin nucleation [125]. FAB region of the EVH2 domain mainly allows elongation of the actin filament, promoting filament bundling [111]. The ability of FAB to bind F-actin is necessary for the anti-capping activity of Ena/VASP. Ena/VASP protein functions in tetrameric form and the EVH2 domain mediate this oligomerization. EVH2 mediated tetramerization enables the cross-linking of the EVH1 domain binding partners (zyxin, vinculin) to central proline-rich region [112]. Hence, the EVH2 domain of the Ena/VASP protein is sequentially conserved and functionally critical.

In general, Ena/VASP proteins are involved in the regulation of cytoskeletal dynamics crucial for coordinating cell migration, adhesion, and cell shape change. The EVH1 domain is critical for the recruitment of actin machinery to the site of action. The actin cytoskeleton holds a fundamental place in the cellular processes of cancer cells. Thereby, the proteins that are functionally linked to the actin cytoskeleton are expected to be

involved in the cancer progression [126]. The expression level of different actin-related proteins (Ena/VASP proteins, Arp2/3 subunits, WAVE, and WASP) altered in cancer [127]. Studies have shown enhanced VASP and Mena expression in lung adenocarcinoma cells [128] and most breast cancers, respectively [105,129]. Another study revealed significant upregulation of VASP, gelsolin, and profilin during tumor angiogenesis. Similarly, EVL overexpression is associated with pancreatic cancer, lymphoma, and breast cancer [130]. Considering the potential of Ena/VASP proteins in the regulation of altered cell motility and invasiveness of the cancer cells, it seems a promising subject for cancer treatment and new drug development.

1.5. Adhesion and degranulation-promoting adaptor protein (ADAP):

Adhesion and degranulation-promoting adaptor protein (ADAP) is also referred to as SLP76 associated phosphoprotein of 130 kDa (SLAP130) or Fyn binding protein (FYB). ADAP is a cytosolic adaptor protein expressed in various hematopoietic cells like T-cells, platelets, mast cells, dendritic cells, natural killers, granulocytes, monocytes, and macrophages [40,131]. Alternative splicing generates two isoforms of ADAP, ADAP120 and ADAP130. The ADAP130 isoform contains 46 additional amino acids close to the C-terminus and is predominantly found in mature cells. The shorter ADAP120 isoform is abundant in immature thymocytes [132–134].

ADAP is a multifunctional scaffold protein involved in various signaling pathways in T-cells, including integrin-mediated inside-out and outside-in signaling, the activation of NF-kB pathway for subsequent production of proinflammatory cytokines (e.g., IFN-g and IL-2), T-cell trafficking and in the formation of the immunological synapse [40]. Adaptor proteins bear multiple specific modular domains that mediate protein-protein interactions and these proteins colocalize effector molecules for assembling the macromolecular signaling complex [30]. ADAP possesses an unstructured N-terminal region of unknown function, a proline-rich domain, two helical Src homology 3 (hSH3) domains, an Ena/VASP homology 1 (EVH1)-binding site, and several tyrosine-based signaling motives [135,138,139].
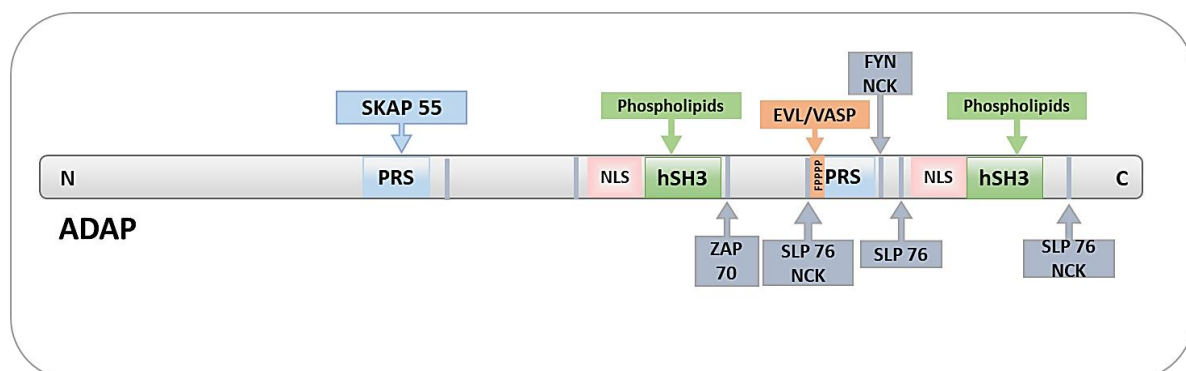
Figure 1.9: Schematic view of molecular domains of ADAP: Known domains of ADAP with their interaction partners, protein-rich sequence (PRS), nuclear localization signal (NLS), helically extended SH3 domain (hSH3), phosphorylation mediated interactions are displayed in grey color, Ena/VASP proteins bind to the N-terminal proline-rich region of ADAP.

hSH3 domains are an unusual variant of the Src homology 3 (SH3) domain where an N-terminal α-helix packs against the β-sheet of the canonical SH3 domain structure. This increases the stability of the hSH3 domain [137]. These hSH3 domains do not bind proline-rich domains instead, the N-terminal α-helix displays several positively charged amino acid side chains that likely favor membrane lipid binding. Compared to the N-hSH3 domain of ADAP, the C-terminal hSH3 domain shows *in-vitro* higher affinity for lipids and possibly be involved in PM recruitment of ADAP [138]. Deletion of the N-terminal α-helices of both hSH3 domains leads to reduced T-cells adhesion and migration. Whereas complete loss of the C-hSH3 domain has no effect in cellular functions [138]. ADAP contains a number of proline-rich motifs that mediate the interaction with the SH3 domain of SKAP55 [42]. The interaction of ADAP with SKAP55 is essential for integrin-mediated function regulation. This constitutive interaction with ADAP stabilizes the expression of both SKAP proteins by protecting them from degradation [140]. Between the two SH3 domains of ADAP, a proline-rich-sequence (PRS) (FPPPP) exist, which binds with Ena/VASP-family proteins via their EVH1 domain [140,40]. Although there is evidence available for ADAP-Ena/VASP-EVH1 interaction yet the precise role of this interaction in T-cell migration, adhesion, and antigen recognition has to be addressed. The detailed functional analysis of the ADAP-Ena/VASP module is focused on as part of this study.

1.5.1. ADAP signaling in Immune cell adhesion and trafficking:

Maintenance of effective immune response requires precise regulation of lymphocyte differentiation, trafficking, and immunological synapse formation. Integrin-mediated signaling is crucial for the regulation of these processes. Integrins are adhesion receptors regulating the interaction with the extracellular matrix as well as with neighboring cells to provide mechanical support. Moreover, they are involved in signaling pathways that modulate T-cell motility, proliferation and differentiation [141]. Integrins are the transmembrane signaling receptors, comprised of two distinct, noncovalently associated subunits (α and β). Each subunit consists of a large extracellular domain contributing to ligand binding and a smaller unstructured cytoplasmic tail [142]. The cytoplasmic tail is the binding site for signaling proteins and cytoskeleton-associated proteins, which altogether

play an essential role in integrin bidirectional signaling (inside-out signaling and outside-in signaling) [141,143].

The integrins in T-cells are β2-integrin LFA-1 (αLβ2 or CD11a/CD18) and β1-integrin VLA-4 (α4β1 or CD49d/CD29) [141,144]. LFA-1 binds to its ligand intracellular adhesion molecule-1 (ICAM-1) [30,145,146]. While VLA-4 binds to vascular cell adhesion molecule-1 (VCAM-1) and the extracellular matrix protein fibronectin. Inside-out signaling positively regulates integrin activation in T-cells [147]. Previous studies observed two modules for "inside-out" signaling. Rap1-RapL-RIAM and adaptor proteins SLP76, ADAP, and SKAP55 mediated [42,142]. Upon T-cell receptor (TCR) activation, Src kinases such as lymphocyte-specific protein tyrosine kinase (LCK) are phosphorylated and activated. A tyrosine kinase ZAP70 is then recruited to the TCR complex and is phosphorylated by LCK. Activated ZAP70 phosphorylates many downstream adaptor molecules, including the linker for activation of T-cells (LAT) and SH2 domain-containing adaptor protein SLP76 [131]. SLP76 is the central scaffolding protein that is associated with a guanine-nucleotide exchange factor (GEF) Vav1, while VAV1 activates the GTPase Rac1, which interacts with Wiskott-Aldrich syndrome protein (WASP) and activates the actin-related protein-2/3 [148]. Arp2/3 complex initiates actin branching that helps in cell spreading and migration [149].

On the other hand, phosphorylated SLP76 via the SH2 domain interacts with ADAP. Whereas ADAP further binds directly to SKAP55. Several studies revealed ADAP/SKAP55 signaling module is so crucial that any disruption that hampers the binding of ADAP and SKAP55, strongly reduces integrin activation [33,150]. Additionally, disruption in the ADAP/SKAP55 interaction leads to the displacement of small GTPase Rap1 from the plasma membrane without influencing its GTPase activity [132]. SKAP55 constitutively interacts with Rap1–GTP-interacting adapter molecule (RIAM). Previous studies revealed that the ADAP/SKAP55 module relocalized RIAM and Rap1 to the PM following TCR activation to facilitate integrin activation [42,151]. This proposed the potential function of ADAP and SKAP55 as a scaffold, indirectly involved in active Rap1 PM recruitment. Continue to that, SKAP55/RIAM interaction disruption diminished T-cell adhesion to fibronectin and ICAM-1 as well as the ability of T-cell to form an immunological synapse with APCs [152]. Integrin-mediated adhesion is a prerequisite essential not only for transmigration but also during the immunologic synapse formation during the contact between naive T-cells and APCs.

Talin is the integrin cytoplasmic tail linked protein that further involved in RIAM based actin cytoskeleton polymerization via its binding to VASP. Thus, it is concluded that the ADAP/SKAP55/RIAM trimolecular complex is responsible for activated Rap1 localization to the PM in inside-out signal activation of integrin [33,136].
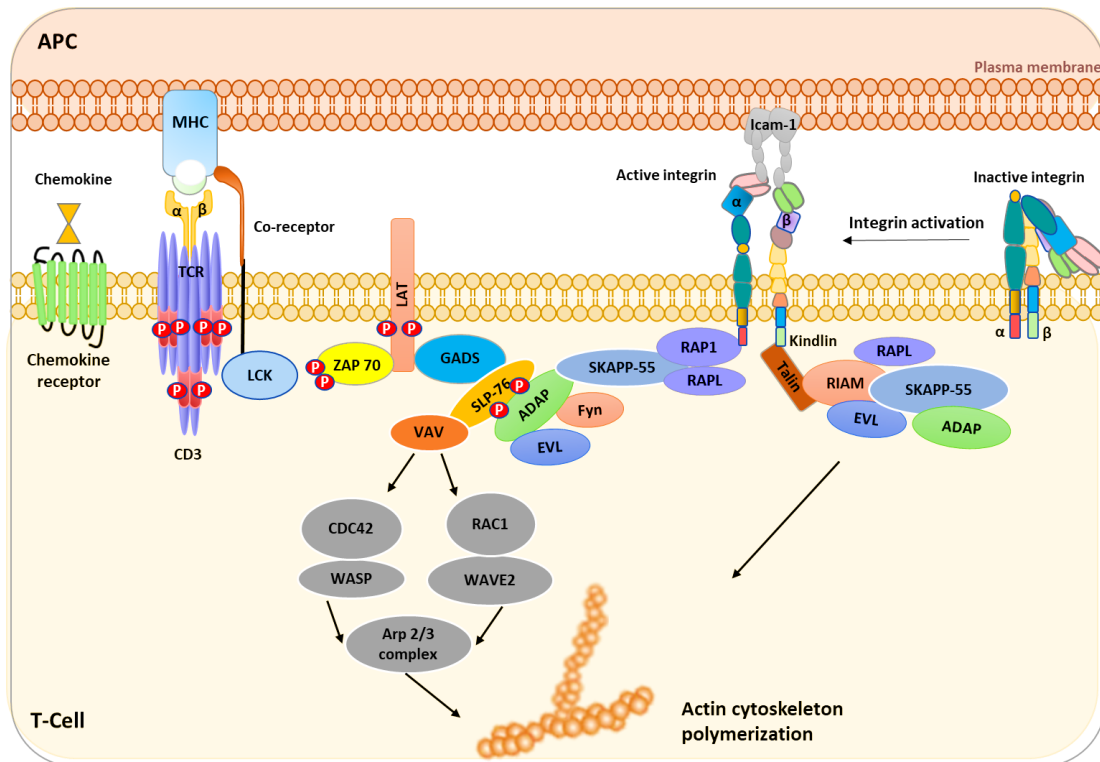
Figure 1.10: Model of T-cell signaling pathway for actin cytoskeletal polymerization: Chemokine/TCR triggering activates the Src kinase LCK. In turn, LCK activates ZAP70, which then phosphorylates the adapter proteins LAT and SLP76. A signaling scaffold associated around LAT and SLP76 triggers guanine-nucleotide exchange factor (GEF) VAV1, while VAV1 activates the GTPase Rac1, which interacts with Wiskott-Aldrich syndrome protein (WASP) and activates the actin-related protein-2/3. Arp2/3complex initiates actin polymerization. SLP76 scaffold also interacts with ADAP and SKAP55. SKAP55 further binds to RIAM. Thus ADAP-SKAP55 controls the recruitment of RIAM to the membrane where it initiates actin polymerization.

1.6. WASp family Verprolin homologous protein-2 (WAVE2):

WASp family Verprolin homologous protein-2 (WAVE2) is a member of the Wiskott-Aldrich syndrome protein (WASp) family and is known as an actin regulatory protein [153]. WAVE2 protein serves as a linker at the upstream signals to the Arp2/3 complex activation, thereby mediating the propagation of signaling cascades that lead to actin nucleation and polymerization [154]. Among the WAVE family, WAVE2 is ubiquitously expressed in hematopoietic cells, where it plays an important part in controlling vital cellular properties, such as cell proliferation, shape, motility, extravasation, and adhesion.

WAVE2 is associated with multiple signaling pathways. WAVE2 possesses verprolin-homology cofilin- homology acidic (VCA) domain at their C-terminal, which is responsible to interact and activate the Arp2/3 complex [155]. Adjacent to the VCA domain, a proline-rich domain (PRD) represents a binding site for proteins containing Src homology 3 (SH3) domains while the N-terminal WAVE homology domain (WHD), immediately followed by a section of basic residues [153,156]. WAVE2 protein is linked with four other proteins via its WHD to form the WAVE regulatory complex (WRC). The pentameric heterocomplex of 400 kDa comprised of Abi (Abelson-interacting protein), Sra-1, Nap1/Hem-2, and HSPC300. GTP activates Rac1 which in turn binds to the N-terminus of Sra-1 and Nap1. Nap1 interacts with Abi1/2, which is associated with HSPC300 and WAVE2 via its WHD domain [157]. Thereby Rac1 recruits the WRC to the cellular membrane where the WAVE2 protein promotes actin filament reorganization, lamellipodia formation, dorsal ruffling, and cellular migration by interacting with the Arp2/3 complex via its VCA domain [158].

a.

b.
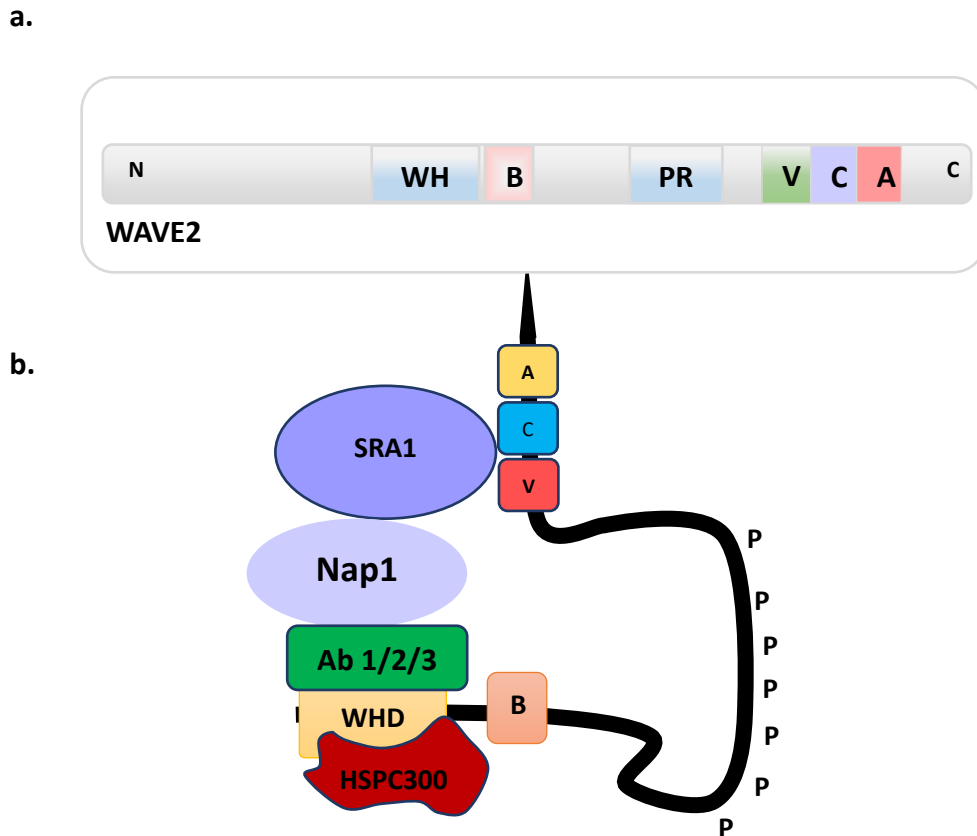
Figure 1.11: Schematic view of the molecular domain structure of WAVE2: a. WAVE2 domains, WAVE2 homology domain (WHD), Proline rich domain (PRD), Basic region (B), Verprolin-homology domain (V), Cofilin homology domain (C), Acidic region (A). b. WAVE2 regulatory complex (WRC), is a heteropentameric protein complex consisting of HSPC300, Abi 1/2/3, Nap1, SRA1, Arp 2/3 and WAVE2.

Chemokine-mediated directional migration involves the formation of protrusion at the leading edge of the cells. These protrusions are the actin filament-rich structures; filopodia and lamellipodia. WAVE2 switches from the inactive form in the cytosol to functionally active upon activation signals by forming the WAVE2 regulatory complex (WRC). Upon activation, WRC localizes to the PM, where it mediates lamellipodial formation[135]. Moreover, as discussed earlier, WAVE2 is also involved in integrin-mediated adhesion and cell spreading [136]. Rho GTPase binding proteins function as activators of the actin cytoskeleton remodeling and are key players in the transendothelial migration of tumor cells [158]. The Rho GTPase activation of WAVE2 protein is considered to be an important regulator in tumor cell motility. A study has shown that invasion and metastasis are effectively suppressed when WAVE2 activity is restricted or inhibited in highly

metastatic B16F10 and MDA-MB 231 cells [156]. Thus, interference in the WAVE2 activity might prove encouraging in preventing tumor cell metastasis [159].

WAVE2 protein is well known to be part of the WAVE complex that is involved in lamellipodial protrusion formation[158]. WAVE2 directly interacts with Ena/VASP protein through its EVH1 domain hence the significance of this interaction in T-cells will be elucidated here. EVH1-binding motif in WAVE2 has already been identified by Dr. Matthias Müller (Fig. 1.13.). The data obtained from spot array assay suggested that WAVE2 protein bears only one binding motif **XEDNLPPPPAEX** to EVH1-domain. The binding dissociation constant, 240 µM was measured by isothermal calorimetry (ITC) between VASP-EVH1 and detected WAVE2 peptide.
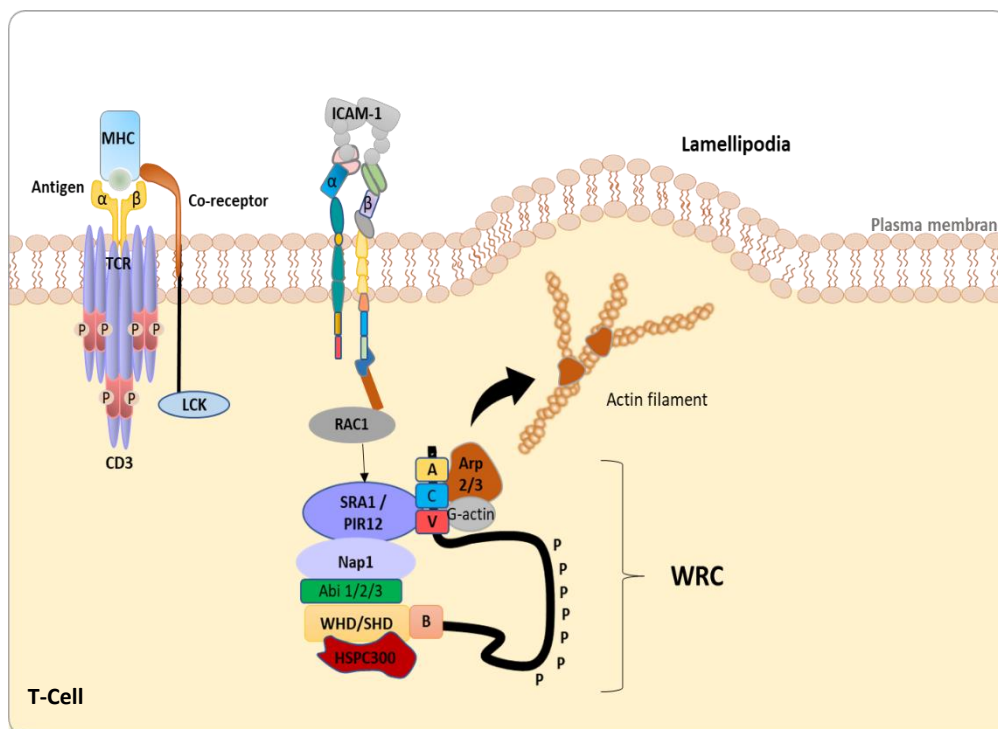
Figure 1.12: Simplified model of WAVE2 mediated lamellipodial protrusion formation in T-cell: Upon activation of TCR or integrin, signaling pathway initiate the actin cytoskeletal polymerization. WAVE2 protein in the WRC translocate to the plasma membrane (PM) downstream to activated Rac1 through its direct interaction with Sra1. WAVE2 protein via its VCA domain interact with Arp2/3 complex to promote actin filament reorganization during lamellipodia formation and cellular migration.

a.
b.

GST
VASP-
GST EVH1   **WAVE2 Peptide**

SPSPSFSEDNLPPPP
SPSFSEDNLPPPPAE
SFSEDNLPPPPAEFS
SEDNLPPPPAEFSYP
DNLPPPPAEFSYPVD
LPPPPAEFSYPVDNQ
PPPAEFSYPVDNQRG

WAVE2 peptide	Protein	K_D
Ac-SEDNLPPPPAEF-NH$_2$	VASP-EVH1	240 µM
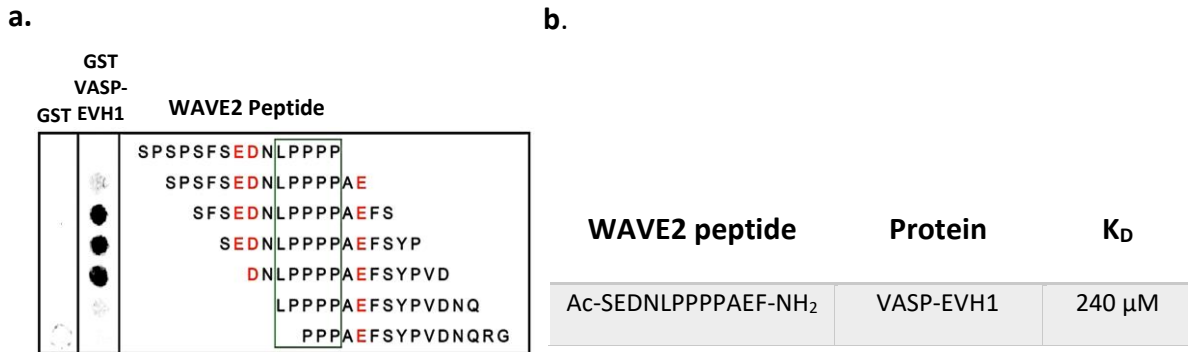
Figure 1.13. WAVE2 epitope mapping and binding affinity with EVH1-domain*: **a.** Spot-peptide membrane array epitope-mapping for WAVE2 against EVHI-domain of VASP by immunostaining. GST antibody treated blot was served as negative control. Dark spots represented binding of peptide sequence to the GST VASP-EVH1 domain. Red colored amino acids refer to negative charged amino acids essential for binding. **b.** Binding dissociation constant (k_D) was measured by ITC between WAVE2 peptide and VASP-EVH1 domain.

WAVE2 deficiency results in defective T-cell activation impairs IL-2 production and decreases actin cytoskeletal mediated functions [130]. Mice model deficient in WAVE2 did not exist because of gestational death due to embryonic lethality [138]. However, there are some shreds of evidence available that fibroblasts of RNAi-depleted WAVE2 or WAVE2 mutant mouse models show defects not only in Rac1-mediated migration but also in both lamellipodia formation and dorsal ruffling [139]. Another study supports that WAVE2 depleted murine macrophages showed a significant decrease in 2D migration [138]. WAVE2 is a multidomain protein and its complete deletion will result in severe impairments in cellular functions. Here, we are specifically interested in WAVE2 and Ena/VASP-EVH1 domain interaction. Therefore, as part of the current study, we aimed to characterize the WAVE2-EVH1 interaction mediated responses in immune cells.

1.7. EVH1 inhibitor:

The Ena/VASP-EVH1 domain has a significant role in the subcellular localization of the actin machinery [121]. The EVH1 domain is the highly conserved domain that binds with specific poly-proline rich motif (D/E)**FPPPP**X(D/E)(D/E) that possesses left-handed polyproline helix II conformation [109,160]. Several proteins like zyxin, vinculin, and lamellipodin utilize their proline-rich motif to capture the EVH1 domain and recruit Ena/VASP at the effector site [118,121]. Any substitution in the core motif (FPPPP) of the EVH1 ligand will lead to the loss of interaction with the EVH1 domain [121]. Thus, loss of EVH1 mediated interaction will strongly influence cellular localization of actin machinery at the effector site. Based on this finding, the EVH1 domain is predicted as a potential drug target for addressing tumor cell invasion/migration (metastasis).

Highly specific structural conformation and conserved amino acid sequences are critical parameters for developing EVH1 inhibitors. Although not much work is available, however, few attempts have been made previously in developing EVH1 domain inhibitors. ActA derived peptide Ac–SFEFPPPPTEDEL–NH$_2$ occupying the EVH1 domain of Ena/VASP protein, showed an 89% decrease in speed of L. *monocytogenes*. However, this small peptide has robust metabolic instability [161]. Hence, it was a challenge to design a molecular entity that shares structural analogy with a core-binding motif of the EVH1 ligand along with improved binding affinity and can overcome the pharmacokinetic limitations.

To chase this concept, Dr. Ronald Kühne at Leibniz Institute for Molecular Pharmacology Berlin has designed a peptidomimetic small molecular weight compound by utilizing the *in-silico* approach. The basis of developing a novel conformational proline mimetic (ProM) scaffold was to replace strictly conserved di-prolines in the core motif of EVH1-ligand [160]. Different ProM scaffolds were generated intending to replace prolines of the core-motif completely. The combination of 2 ProM scaffolds demonstrated a conformational analogy to the natural EVH1 ligand (Fig. 1.14) and also improved binding affinity (Tab 1.7).
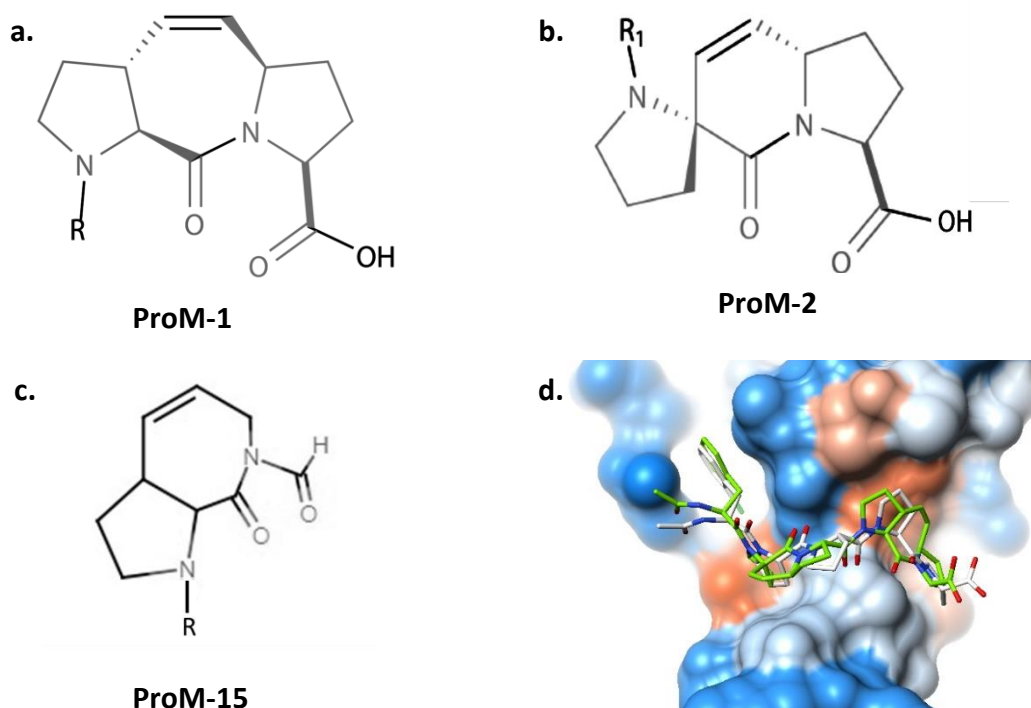
Figure 1.14: Structural representation of ProM scaffolds: a.b.c. ProM scaffolds able to mimic two prolines in the core motif of EVH1 ligand. **d.** Superposition of the Xray structure of EnaH-EVH1 domain (PDB code: 4MY6) with ActA peptide, Ac-FPPPP-OH in white and Ac-[2-Cl-F]- [ProM-2]-[ProM-1]-OH in green (Dr. Matthias Barone).

While structural and affinity modification, the *in-silico* approach suggested the introduction of a hydrophobic substituent (chlorine) at the ortho position of the phenylalanine ring within the core motif will result in a gain in affinity (Tab 1.5). Moreover, to achieve ideal left-handed PPII helix conformation of the ActA peptide, X-ray structure suggested, proline mimetic scaffold-1 (ProM-1) can replace the second pair of prolines in the core motif (FPPPP). In contrast, ProM-2 can replace the first pair of prolines in the FPPPP motif. Thus, overall, it generates Ac-[2-Cl-F]-[ProM-2]-[ProM-1]-OH inhibitor. However, the inhibitor presented poor cell permeability due to the hydroxyl group's presence that was resolved by the substitution of ester linkage at the C-terminal of the inhibitor, which enhances cellular uptake in colorectal cancer HCT-116 cells [120].

Table 1.2: Binding affinity of ActA peptide in comparison to di-proline mimetic scaffolds with EnaH-EVH1 measured by fluorescence titration:

	ProM inhibitor	K_D µM (SE)
-	Ac-FPPPP-OEt	153 (8)
-	Ac-SFE-FPPPP-TEDEL-NH2	13 (0.6)
-	Ac-SFE-[2Cl-F]-PPPP-TEDEL-NH2	1.5 (0.3)
Inhibitor a	Ac-[2Cl-F]- [ProM-2]-[ProM-1]-OMe	4.4 (0.7)
Inhibitor b	Ac-[2Cl-F]- [ProM-2]-[ProM-15]-OMe	0.47 (0.03)

The binding affinity of the ProM inhibitors to EnaH-EVH1 was measured by a colleague, Dr. Matthias Barone, by fluorescence titration. In this study, two EVH1 inhibitors, Ac-[2Cl-F]-[ProM-2]-[ProM-1]-OMe and Ac-[2Cl-F]-[ProM-2]-[ProM-15]-OMe are investigated in T-cells. From now, Ac-[2Cl-F]-[ProM-2]-[ProM-1]-OMe will be addressed as **inhibitor a** and Ac-[2Cl-F]-[ProM-2]-[ProM-15]-OMe as **inhibitor b**.

Biophysical binding data revealed that inhibitors a and b substantially inhibit EVH1 mediated interactions by mimicking the proline-rich sequence of the EVH1 ligand. This attribute proposed that it can ultimately serve as a potential antimetastatic agent. The efficacy of **Inhibitor-a** as the anti-metastasis agent was investigated by Dr. Matthias Müller in MDA-MB 231, an invasive breast tumor cell line. *In-vitro* data suggested **inhibitor a** can displace all-important interaction partners of the EVH1 domain when observed through pull-down assay. Interestingly, MDA-MB-231 assay data demonstrated **inhibitor a** had significantly reduced the MDA-MB 231 cell line invasion across matrigel in transwell assay setup. Consequently, EVH1 inhibitors were considered a promising class of antimetastatic drug candidates

1.8. Aim of the study:

Immune cell trafficking and antigen recognition are the necessary processes for the efficient function of the immune system. T-cells rely on actin network remodeling in order to migrate through diverse tissue environments [162]. During the process of antigen recognition and activation T-cells also exhibits extensive cytoskeletal remodeling. Therefore, it is believed that by targeting actin cytoskeletal remodeling in T-cells, infiltration of immune cells in the tumor microenvironment or autoimmune diseases (MS and EAE) can be controlled. This study focused on the key regulators of actin cytoskeletal polymerization protein, the Ena/VASP-EVH1 domain. EVH1 domain mediated interaction of Ena/VASP proteins with effector proteins (zyxin, lamellipodin, ADAP, and WAVE2) is responsible for the activation and localization of actin machinery at the site of action (focal adhesion site, lamellipodia, immune synapse).

In this study, I have addressed two main questions.

First, what is the impact of Ena/VASP-EVH1 domain-mediated interaction inhibition on immune cell functioning?

A small novel peptidomimetic (ProM) molecule has been designed and developed by Dr. Ronald Kühne. These molecules were used to inhibit the Ena/VASP-EVH1 domain-mediated interactions. Initial data obtained from EVH1 inhibitor in the MDA-MB-231 cell line has revealed that by targeting the EVH1 domain-mediated interactions, actin-based migration and invasion can be prevented. Thus, the effects of the EVH1 inhibitors were investigated in Jurkat cells (T-cells) and U-937 (macrophages) cell lines to understand the ultimate impact on immune cell function.

Second, what is the functional relevance of ADAP and WAVE2-EVH1 domain interaction in T-cell homing and antigen recognition?

A mutation was introduced at the EVH1 domain binding site in both proteins (to block the interaction to Ena/VASP proteins). ADAP and WAVE2 were downregulated by small hairpin RNA (shRNA) in Jurkat cells. ADAP and WAVE2 mutants (ADAP$_{MUT}$/WAVE2$_{MUT}$) and wild types (ADAP$_{WT}$/WAVE2$_{WT}$) were then overly expressed. The effect of ADAP$_{MUT}$ and WAVE2$_{MUT}$ was observed, and its significance was assessed in immune cell phenotypes.

I.   Materials and Methods

2. Material and Methods

2.1. Materials:

2.1.1. Equipment:

Equipment	Source
Agarose gel running system	BIO-RAD
ÄKTA purifier 10 G	GE
Autoclave	H+P
Beckman centrifuge, rotor JLA-10.50	(Avanti J-25)
Automated cell counter	BIORAD
Cell chamber	oko touch
Centrifuge 5224	Eppendorf
Centrifuge 5415R	Eppendorf
Centrifuge 5418	Eppendorf
Centrifuge 5810R	Eppendorf
Confocal microscope	LSM710-ConfoCor3
Culture hood	BIOHIT-ANTARES
Electrophoresis system Mini-PROTEAN®	BIO-RAD
Gene-Pulser X	BIO-RAD
Epi-TIRF-phase contrast	Nikon
FACS-Fortesa	BD Bioscience
Fluorescence plate reader	TECAN Saphire
Glutathione Sepharose 4B	GE
Glutathione Sepharose FastFlow	GE
HiLOad 16/60 Superdex 75	GE
Incubator (with rotator, bacteria)	Infors HT multitron
Incubator for bacterial plates	Binder

ITC 200	microCal
Lyophilizer	Christ-Alpha
Microscope	Nikon
Milli-Q® Integral Water Purification System	MERCK MILLIPORE
Ni-NTA column	BioRad
Nanodrop 1000	ThermoScientific
Odyssey 2.0	LI-COR Biosciences
PCR machine	BIOER Gene Touch
pH meter	Schott CG 840
pH meter (Ligand)	Mettler Toledo
Profinia protein purification system	BioRad
High precision Scale (ligand)	KERN PLE
Shaker for gels	NeoLab DRS-12
Thermo-shaker	BioEr
Speed vac	BIO-RAD
Trans Blot Turbo-transfer	BIO-RAD
Ultrasonifier	Cole-Parmer
UV nanodrop	Vortex 2 genie
UV/Vis Spektrophotometer UV mini 1240	Shimadzu
Vortex	GFL
Water bath	Memmert

2.1.2. Consumables:

	Source
15 ml and 50 ml falcon tubes	SARSTEDT
6/12/24-well cell culture plates	TPP
8 well glass bottom chamber	Ibidi
96-well cell culture plates	BD Bioscience
96-well cell culture plates (U bottom)	Costar
Blotting/Whatman paper sheets	GE
Chemotaxis µ slide	Ibidi
Cryo Pure Tube 1.6 ml	Sarstedt
Eppendorf tubes (0.5 ml,1.5 ml, 2 ml)	Eppendorf
FACS tubes	BD Bioscience
Glass coverslips	Carl Roth
Glutathione sepharose agarose beads	Biosciences
Mini Protean TGX 4-20% 10 well	BIORAD
Mini Protean TGX 4-20% 15 well	BIORAD
Mini Protean TGX 7.5% 15 well	BIORAD
Miniproteax 4-20% SDS gel	BIORAD
Nitrocellulose membrane	BIORAD
Parafilm	Parafilm
PCR soft tubes	Biozym
Pierce Protein A-magnetic beads	Thermo scientific
Pierce Protein G-magnetic beads	Thermo scientific
Pipette tips	Surphob Biozym
Pipette tips (special for Ibidi chamber)	Ibidi
Plastic cuvettes	Sarstedt

Syringe filters (0.22, 0.45, 0.8 μm)	Sartorius stedium
Syringes (2ml, 20ml,50ml)	BD Bioscience
Tissue culture flask	BD Bioscience
Transfection cuvettes	VWR
Transwell insert (5.0μm pore, 3 μm pore)	Milicell
VIVA-SPIN	Sartorius Biotech

2.1.3. Chemicals and Reagents:

10Kbp DNA ladder
2-mercaptoethanol
2-propanol
30% Acrylamide
4-(2-hydroxyethyl)-1-piperazineethanesulfonic acid (HEPES)
Agar-Agar
Agarose
Alamar blue
Ammonium persulfate (APS)
Ampicillin
Arp2/3 inhibitor (CK666)
BD FACS Flow™ Sheath Fluid
BD FACS™ Clean Solution
BD FACS™ Rinse Solution
Blocking buffer (Odyssey)
Bovine serum albumin (BSA) fraction V
Bromophenol blue
CFSE

CMTPX

Complete protease inhibitor tablet (Roche)

CXCL12 human

Deoxyribonucleoside triphosphate (dNTP) set

Dimethyl sulfoxide (DMSO)

Ethanol (99% v/v)

Ethidium bromide (10 mg/ml)

Ethylenediaminetetraacetic acid (EDTA)

Calcium chloride (CaCl2)

Fetal Calf Serum (FCS)

Fibronectin

Fuse-It-P (Ibidi)

GelRed (Biotium)

Glycerol

Hank's balanced salt solution (HBSS)

Hydrochloric acid (HCl; 37% v/v)

Hygromycin

ICAM-1 Fc chimera

Isopropyl-β-D-thiogalactopyranoside (IPTG)

Kanamycin

Lipopolysaccharide (O_{55-135}), ($O_{127-138}$)

Manganese chloride (MnCl2)

Methanol (99.9%)

Nonidet P40 (NP-40, Ipegal CA-630)

OVA peptide $_{257-264}$

OVA peptide $_{323-339}$

Pageruler prestained protein ladder

Paraformaldehyde (PFA)

PBS Dulbecco (phosphate-buffered saline, without Ca2+, Mg2+)

Penicillin/Streptomycin (10000U/10000µg/ml)

Phalloidin-Alexa Fluor R633

Phenylmethylsulfonyl fluoride (PMSF)

Phorbol-12-myristate-13-acetate (PMA)

Ponceau S

Potassium chloride (KCl)

Puromycin (Santa Cruz)

Sodium azide (NaN3)

Sodium chloride (NaCl)

Sodium dodecyl sulfate (SDS)

Sodium fluoride (NaF)

Sodium hydroxide (NaOH)

Sodium orthovanadate (Na4VO3)

Tris(hydroxymethyl)-aminomethane (Tris)

Triton X-100

Trypan Blue Solution (0.4%)

Trypsine/EDTA (0.05% v/v, 0.02% v/v)

Tween 20

VCAM

2.1.4. Kits:

Type	Source
GeneJET Plasmid Miniprep kit	Thermofisher Scientific
PureLink HiPure Plasmid Midiprep kit	Invitrogen by Thermofisher Scientific
QIAquick PCR Purification kit	QIAGEN
Bio-spin ™ 30	BIORAD
Neon transfection system (NMPK/10025)	Invitrogen
Hi-yield PCR cleanup/Gel extraction kit	SLG

2.1.5. Antibodies:

Antibody	Organism	Concentration use		Ref no./ Company
ADAP	Rabbit polyclonal	WB	1:1000	PAS 20401
		IP	4 µg	Thermo Fischer Scientific
ADAP	Rabbit polyclonal	WB	1:1000	07-546 Merck
EVL	Mouse monoclonal	WB	1:1000	Sc373793
		IP	4 µg	Santa Cruz
VASP	Mouse monoclonal	WB	1:1000	Sc46668 Santa Cruz
EnaH	Rabbit polyclonal	WB	1:1000	SAB4502350 Sigma Aldrich
WAVE2	Rabbit monoclonal	WB 1:1000		D2C8 Cell Signaling

GFP	Rabbit polyclonal	WB 1:1000 IP 4 µg		A6455 Thermofisher Scientific
mCherry	Rabbit polyclonal	WB 1:1000 IP 4 µg		PA5-34974 Invitrogen
GAPDH	Mouse monoclonal	WB 1:1000		Sc47724 Santa Cruz
Alpha-Tubulin	Mouse monoclonal	WB 1:1000		DM1A Cell Signaling
p-Erk	Mouse monoclonal	WB 1:1000		sc-7383 Santa Cruz
PE Antihuman CD29	Mouse	FACS 1:100		556049 BD Bioscience
IR800	Donkey anti-mouse	WB 1:50000		926-32212 Odyssey
IR800	Donkey anti-rabbit	WB 1:50000		926-32213 Odyssey
GST	Rabbit polyclonal	WB 1:1000		Sc459 Santa Cruz
CD3 OKT3	Mouse monoclonal	T-cell activation 1 µg/ml		SAB4700040 Sigma Aldrich
p-Tyrosine PY-20	Mouse monoclonal	WB 1:1000		P-4110 Sigma Aldrich
CD28	Mouse monoclonal	T-cell activation 5 µg/ml		MAI-10166 Thermofischer

			Scientific
IgG mouse	IP	4 µg	Gift from Dr. Michael Krauß
IgG rabbit	IP	4 µg	Gift from Dr. Michael Krauß

2.1.6. Buffers:

PBS	(NaCl 137 mM, KCl 2.7 mM, Na_2HPO_4 10 mM, KH_2PO_4 1.8 mM, pH 7.4)
Buffer A	(EDTA 10 mM, 2-Merceptoethanol 0.5 mM, in PBS pH 7.4)
Buffer B	(Reduced GSH 20 mM in Buffer A, pH 7.4)
EVH1 buffer	(NaH_2PO_4 10 µM, Na_2HPO_4 30 µM, NaCl 100 µM, TCEP 2 µM, pH 7.3)
Pyrophosphate buffer	NaPi 40 mM, NaCl 100 mM, pH 7.3
RIPA buffer	Tris HCl 50 mM, NaCl 150 mM, $MgCl_2$ 20 mM, NaF, 10 mM, NP-40 1.0% (v/v), Sodium Deoxycholate 0.5% (w/v), EDTA 0.5 mM, SDS 0.1% (w/v), Benzonase 3 U/ml, Na_3VO_4 1 mM, complete protease inhibitor tablet 1/10 ml, pH 8
FACS buffer	2-5% (v/v) FBS (or BSA), EDTA 2 mM, NaN_3 1 mM, in PBS, pH7.5
SDS running buffer	Tris base 250 mM, Glycine 2 M, SDS 35 mM, pH 8
Destainer buffer	Methanol 30%, Acetic acid 10%
TAE buffer	TRIS 50 mM, Acetate 50 mM, EDTA 1 mM, pH 8
Western blot transfer buffer	Tris 25 mM, glycine 192 mM, 20% methanol, pH 8.3
20 mM HEPES buffer	HEPES 20 mM, pH 7.4 adjusted with NaOH
250 mM imidazole	250 mM Imidazole, 50 mM sodium phosphate pH 8.0, 300 mM NaCl

2.1.7. Enzymes and their buffers

T4 DNA-Ligase	**NEB**
T4 DNA-Ligase buffer 10X	NEB
Alkaline Phosphatase	NEB
KOD *Hot Start* DNA-Polymerase	Merck
Thrombin	Merck
GC buffer 5X	Thermo scientific
BamHI	NEB
BstBI	NEB
XbaI	NEB
XhoI	NEB
BsrGI	NEB
CIP	NEB
Dpn1 enzyme	NEB

2.1.8. Cells:

Bacterial strains:

BL21	Electrocompetent
XL1-blue	Electrocompetent
HB101	Electrocompetent/Chemocompetent

Eukaryotic cell lines

Cell Line/no.		Organism	Company
Jurkat Clone E6-1	TIB-152	Human	ATCC

MDA-MB-231	HTB-26	Human	ATCC
U-93	CRL-1593	Human	ATCC
HUVEC	PCS-100-010	Primary Human cells	ATCC
HEK 293T		Human	A gift from Matthias Müller
BJAB	ACC-757	Human	DSMZ (gift)

2.1.9. Media:

2xYT	**Roth**
LB media	Roth
RPMI 1640	Merck
RPMI 1640 (without Phenol Red)	Gibco
Endothelial cell media	Promo cell
FBS	Gibco
Penicillin/streptomycin	
Trypsin / EDTA	Biochrom

2.1.10. Peptides:

ADAP peptide (for binding affinity measurements)

Ac-SGSGGIFPPPPDDDIY-NH2

Ac-EDADDGFPAPPKQLDM-NH2

Ac-SLPPPPPSHPAS-NH2

Ac-SKPTFPWPPGNKPSL-NH2

Ac-ARFPKAPSKLTV-NH2

EVH1/ProM Inhibitors

	AC- 2Cl-F- [ProM2]-[ProM1]-NH2
Inhibitor a	AC- 2Cl-F- [ProM2]-[ProM1]-OMe
Inhibitor b	AC- 2Cl-F- [ProM2]-[ProM15]-OMe

2.1.11. Oligonucleotides:

Cloning primers	Sequence
ADAP-mut-Fw	TTCGGTTCACCACCAGATGATGACATTTATGAC ATT TATG
ADAP-mut-Rev	CAGTCAGAGTGGAAGTGGAGGGATATTCGGTT CACCA
BstBI-pET28a-Fw	ACCTTCGAAACCACCACTGAGATCCGGCT GCTAACAAAG
BstBI-pET28a-Rev	GGTTTCGAAGGTGCTCGAGTGCGGCCGCAAGC TTG
BsrGI-pET28a-Fw	GACTGTACAAGCAAATGGGTCGCGGATCCGAA TTC

BsrGI-pET28a-Rev	GCTTGTACAGTCCACCAGTCATGCTAGCCATAT GGC
BstBI-Fw-ADAP	AAT TTCGAA ATGTTCAGAGTCACAGGGCC
XbaI-Rev-ADAP	ATA TCTAGA CTAGTCATTGTCATAGATGCA GCCATCAGC
Fw-XbaI_mut_ADAP_A1296T	CTGATGGTGCTGGAAATCTtGATGAGGAACAA GACAGTGA
Rev-XbaI_mut_ADAP_A1296T	TCACTGTCTTGTTCCTCATCaAGATTTCCAGCAC CATCAG
Fw-XbaI_mut_ADAP_A2286T	GGTAAAACCTGGTGAATCTCTtGAAGTTATACA AACCACA
Rev-XbaI_mut_ADAP_A2286T	TGTGGTTTGTATAACTTCaAGAGATTCACCAGG TTTTACC
BstBI-WAVE2 primer-Fw	AATTTCGAAATGCCGTTAGTAACGAGGAACATC
XbaI-WAVE2 primer-Rev	ATATCTAGAATCGGACCAGTCGTCCTC

Sequencing Primers	Sequence (5' to3')
EnaH-Fw	TTTTTGGATCCATGAGTGAACAGAGTATCTGTCAG
EnaH-Rev	TTTTTTTTTCGGCCGCTCATAACATTCTAAGGCATGCA TCATGG
EVL-Fw	GAAAGGGATCCATGGCCACAAGTGAACAGAGTATC
EVL-Rev	TTTTTGCGGCCGCTTACATGATGTTCAGGCAAACAGC
LentipGK-vector-Fw seq	GATGCTGCAGGAACACCAAGGATATCATGAAAGAGA

LentipGK-vector-Rev seq	GAGGGGCAGCAAAATCAGGGTGAGGTGGGAAAGAT
pGK-ADAP-BstBI-Fw seq	GAGGAAAGAATGAACTGAGCTTCAAGCAAGGAGAG
pGK-ADAP-XbaI-Rev seq	CTAGAGATTCACCAGGTTTTACCTGTAGATCTCTG
pGK-WAVE2-BstBI-Fw-seq	GGTTCGTCGACTAGTCCAGTGTGGT
pGK-WAVE2-XbaI-Rev-seq	GCGTATCCACATAGCGTAAAAGG
CMV-Fw	CGCAAATGGGCGGTAGGCGTG

2.1.12. Constructs:

Construct	Vector backbone	Source	Restriction sites
GST-VASP-EVH1 (1-113)	pGEX-4T-1	A gift from Dr. Linda Ball (FMP)	-
GST-EnaH-EVH1 (1-112)	pGEX-4T-1	A gift from Dr. Anne Diehl (FMP)	-
GST-EVL-EVH1 (1-115)	pGEX-4T-1		-
HIS-ADAP-fl	pET28a-mod	A gift from Prof.Dr. Christian Freund	BamHI, XhoI
Lentiviral envelope Plasmid	pMD2.G	Addgene 12259	-
Lentiviral packaging plasmid	psPAX2	Addgene 12260	-
Knockdown - ADAP	TRC1-pLKO-puro-shRNA	Sigma Aldrich TRCN0000159548 TRCN0000161163	-
Knockdown - WAVE2	TRC2-pLKO-puro-shRNA	Sigma Aldrich TRCN0000382403 TRCN0000123069	-
Control Plasmid shRNA	TRC2 pLKO.5-puro non-Mammalian shRNA	Sigma Aldrich MFCD07785395	-
Lentiviral plasmid for ADAP	pLJM1-EGFP	Addgene 19319	BsrGI,BstBI
Lentiviral plasmid for WAVE2	pLV-mCherry	Addgene 36084	XbaI, BsrGI
Lentiviral plasmid (ADAP/WAVE2)	pLentiPGK Hygro DEST H2B-mRuby2	Addgene 90236	XbaI, BstBI
Lifeact	pmEGFP-N1-Lifeact	Addgene 6085-1	

2.1.13. Software and Statistics:

Chemotaxis and Migration Tool	Ibidi
ImageJ	NIH
rITC	R script
Uniprot	http://www.uniprot.org/
ZEN 2010	Carl Zeiss Jena
GraphPad Prism	Prism
FlowJO	V10-CL

GraphPad software (Prism 6) was used for statistical analysis of results and for plotting graphs. Data were expressed as mean ± sem with respect to the number of independent experiments unless mentioned otherwise. ANOVA followed by Dunnett's multiple comparison test was performed to analyze significant differences between more than two groups. To analyze the difference between the two groups, a paired Student's t-test was applied. A confidence interval greater than 95% was set to consider as a significant difference. Statistical significance is indicated as $*$ $p < 0.05$, $**$ $p < 0.01$, $***$ $p < 0.001$.

2.2. Methods:

2.2.1. Cell handling:

2.2.1.1. Cell culture:

Cells (Jurkat cells (E 6.1), B-cells (BJAB) and HEK 293T cells) were cultured in RPMI 1640 medium added with 10% FBS and 5% penicillin/streptomycin. Cells were maintained at 37°C and 5% CO_2 concentration. Human umbilical vein cells (HUVECs) were cultured in endothelial cell growth medium from Promo cells with provided growth factors included. Cells were passaged every 48-72 h to keep them at a density of 1-2 x 10^5 cells/ml. Cells were counted using the BioRad automated cell counter (mix of an equal volume of cell suspension and trypan blue). Trypan Blue was used to differentiate between dead and viable cells.

2.2.1.2. Liposome formation and lipofection:

EVH1 inhibitor delivery into the Jurkat cells was accomplished using commercially available liposomal preparation. A fusogenic liposome for protein transfection, **Fuse-It-P**, was purchased from Ibidi. EVH1 inhibitor was reconstituted in PBS at pH 7. The stock solution of EVH1 inhibitor was diluted in 20 mM HEPES buffer to a final concentration of 400 µM. The fuse-It-P lipids film was formed and loaded with EVH1 inhibitor according to the supplier's instructions. Jurkat cells were incubated for 3-5 min at 37°C with liposomal mixture for EVH1 inhibitor efficient delivery. The process of liposomal fusion was stopped by replacing liposomal media with the fresh medium and returned the cells to incubator until ready for the assay.

2.2.1 3. Jurkat cell lysis:

Jurkat cells were lysed with RIPA buffer (containing protease inhibitor). Jurkat cells (4 X 10^6) were harvested, cell pellet was washed with PBS and resuspended in ice-cold RIPA lysis buffer (50 µl). Cells were incubated on ice for 30 min with an intermittent vortex. The lysate was centrifuged at 4^0C, 12000 g for 15 min to separate cellular debris. The supernatant was carefully separated from the pellet. The concentration of proteins was determined by NanoDrop^{TM} ND-1000 spectrophotometer (ThermoScientific) at 280 nm and expressed as µg/µl. The formula of the Beer-Lambert law was used to calculate the concentration of the protein sample.

$$\textbf{A280 = \varepsilon280} \times \textbf{c} \times \textbf{d}$$

A280   Absorption at 280 nm

$\varepsilon280$ Extinction coefficient of the protein in cm^{-1} M^{-1}

c   Protein concentration in M

d   Light path length in c

2.2.1.4. Jurkat cell transduction:

Stable clones of Jurkat cells were generated by lentiviral transduction. Infection of Jurkat cells with lentiviral particles was attained via the spinoculation technique [31]. In the first step, the lentiviral producer cell line HEK293T is transiently co-transfected using calcium phosphate transfection method. The vector encoding the transgene of interest (25 µg), a second-generation envelope plasmid (pMD2.G; Addgene Plasmid #12259) and a second-generation packaging plasmid (psPAX2; Addgene Plasmid #12260) were added to HEK 293T cells to generate lentiviral particles. Later, lentiviral particles were collected from the HEK293T supernatant and used to infect Jurkat cells (2×10^6 cells/ml). In spinoculation technique for Jurkat cell transduction, Jurkat cells were incubated with lentiviral particles and centrifuged at 12000 g for 1 hour at 30^0C. After that, Jurkat cells were incubated for 2 hours at 37^0C and 5% CO_2. Following that the medium was carefully removed and replaced with a fresh medium including 10% FBS and antibiotic (as selection marker). The media was replaced every second day. Once stably transduced clones were obtained, cells expanded on a large scale [163].

2.2.2. Recombinant protein expression:

2.2.3.1. Plasmid transformation in E. Coli:

The plasmids were transformed into bacterial strains via electroporation. The electroporation was performed using the Gene-PulserX cell (Bio-rad) that applies high-voltage (1800V) electric pulses to create tiny pores in the cell membrane through which the DNA penetrates. 0.3 µl of the purified plasmid was mixed with 50 µl electrocompetent cells in an electroporation cuvette (1 mm gap, Bio-rad) while maintaining the temperature of the system at around 4^0C. Following electroporation, the bacterial cells were resuspended in 1 ml of 2xYT media and incubated for 1 h at 37 °C under constant shaking. The bacterial cells

were then plated strategically on antibiotic-containing agar plates and incubated for 16-24 h at 37^0C. Single colonies formed on agar plate were picked and proceeded for the next steps.

2.2.2.1. Recombinant expression of EnaH/VASP/EVL-EVH1:

GST-EnaH/VASP/EVL-EVH1 constructs were expressed in electrocompetent E. *coli* (BL21) grown in 2xYT medium. Plasmids (pGEX-4T-1) were transformed into bacterial strains as the method explained above. Single colonies were picked and incubated in 1 L 2xYT medium at 37^0C, 180 RPM until OD_{600} 0.4-0.5 was achieved. The culture was cooled down till 18^0C, 1.5 mg/ml ampicillin, and 100 µM IPTG was added to it. The culture was then induced overnight at 18^0C and 180 RPM. E. *coli* were harvested by centrifugation for 15 min at 6000 g. The cell pellet was then stored at -20^0C.

2.2.2.2. Recombinant expression of His-ADAP and variants:

His tag ADAP full-length (fl) in PET28a-mod vector was a gift from Prof. Dr. Christian Freund (Freie University Berlin). His-ADAP$_{WT}$ and His-ADAP$_{MUT}$ (full length) were expressed in the electrocompetent Rosetta (DE3) strain of E. *coli*. Following the same method described above, except for the culture media, 2xYT containing kanamycin 1 mg/ml and 100 µM IPTG. Culture was induced at 18^0C overnight for protein expression.

2.2.2.3. Protein purification:

E. *coli* cell pellet (as described in section 2.2.2.1) was resuspended in PBS containing EDTA and protease inhibitor cocktail tablet (Roche). Cells were then subjected to lysis by ultrasonication for 30 min at 10-15^{0}C temperature. The lysate was spun down at 6000g for 30 min to remove cell debris. The supernatant was filtered with 0.8 and 0.45 µm filters before proceeding to purification. Two different chromatography techniques (Affinity- and Size-exclusion) were used to purify recombinant proteins of interest. The filtered supernatant was subjected to a fast flow glutathione matrix at 1-2 ml/min to purify protein by affinity chromatography. GST-tagged protein was eluted by GSH buffer (GSH 20 mM, EDTA 10 mM, 2-β mercaptoethanol 0.5 mM, in PBS pH 7.4). To cleave off the GST tag, 1 U/ml of thrombin and 2-β mercaptoethanol 5 mM was added to eluate from the glutathione matrix. The Protein-thrombin mixture was incubated in the water bath at 27^0C

overnight. To check the efficiency of cleavage, the eluate was analyzed on SDS-PAGE. Generally, GST was cleaved entirely off from the EVH1 domains by this method.

His-ADAP$_{WT}$ and His-ADAP$_{MUT}$ were purified by an automated affinity tag purification system, "Profinia" (BIO-RAD), using the Ni-NTA column. Recombinant protein is His tagged, allowing affinity binding to Ni2$^+$, which was part of the Ni-NTA matrix in the column. When recombinant protein was loaded to the column, 2 of the 6 histidine bind with one Ni2$^+$ ion, trapping the tagged protein in the column while unbound protein was washed out. After the washing step, 250 mM imidazole buffer was run through the column. Imidazole buffer competes with the histidine for the Ni2$^+$ binding. This process effectively released the recombinant protein from nickel resin and eluted purified recombinant protein. After affinity tagged purification, the protein was further purified by size exclusion chromatography. For this purpose, the sample was loaded on a preparative Superdex75 16/600 column of the ÄKTA purification (FPLC) system. Protein absorbance at 280 nm was analyzed over time. Fractions corresponding to the purified protein peak (280 nm) were tested on SDS-PAGE for purity. Fractions that showed high protein purity were pooled down and concentrated using vivaspin tubes (MWCO 10,000) by centrifugation. The protein concentration was measured by nanodrop, shock frozen in liquid nitrogen and stored at -80^{0}C in small aliquots.

2.2.3. Molecular Biology Methods:

2.2.3.1. Polymerase chain reaction (PCR):

The Polymerase Chain Reaction (PCR) is applied to amplify or modify a specific region of DNA. Regular PCR components are primers, a DNA template, a thermostable DNA polymerase and nucleotides (dNTPs). Primers are short oligonucleotides that bind to the DNA template. They can introduce flanked restriction sites to the DNA template compatible with the vector. The three main steps of a PCR reaction include; i. Denaturation of the DNA template, ii. Annealing of the primers and iii. Extension (DNA-polymerase copies the DNA template). These steps were repeated several times, amplifying the DNA template (up to 25 cycles or more). KOD Hot Start DNA polymerase (Merck) was used to generate protein constructs. The PCR was performed according to the manufacturer's instructions.

2.2.3.2. Agarose gel electrophoresis:

DNAs were analyzed/separated by agarose gel after PCR or DNA ligation to verify insert and restriction sites. 0.7% (w/v) agarose gel made in TAE buffer was used for large DNA vectors, while 1.5% (w/v) was used for small DNA like the PCR products. GelRed (Biotium) was added (1/10,000) to agarose gel to detect DNA. Samples were supplemented with 2 µl of 5X loading buffer. 5-10 µl 1 Kbp (NEB) DNA ladder was applied in parallel to the samples for size reference. The electrophoresis was done in a BIO-RAD Mini DNA system in TAE buffer at a constant voltage of 100-140V for 45-60 min (depending on the size of the DNA/DNA fragment of interest). The DNA was visualized and recorded under blue light transilluminator.

2..2.3.3. DNA extraction:

According to the manufacturer's instructions, PCR products were extracted from the agarose gel with the QIAquick Gel Extraction Kit (Qiagen).

2.2.3.4. Ligation:

For ligation, first purified PCR fragments and vectors were undergone restriction enzyme digestion. PCR fragments were then incubated in a 4:1 ratio with the vector in the presence of T4 DNA ligase overnight at 16^0C. Ligated products were high in salt content due to the ligation buffers, which can compromise transformation efficiency. Therefore, the ligated vector was purified by a Micro Bio-spin ^{TM} 30 column to remove excess salt before transformation in E. *Coli*.

2.2.3.5. Vector transformation in E. Coli:

A purified ligated vector was then transformed into a suitable electrocompetent strain of E. *coli* (HB101) following the earlier described method (section 2.2.3.1). E. *coli* were incubated in LB medium at 37^0C for an hour with continuous shaking. After an hour, E. *coli* were plated on agar plates with suitable antibiotics and let the colonies grow overnight at 37^0C. Single colonies were picked and left to grow in 15 ml LB medium overnight at 37^0C with 180 RPM shaking.

2.2.3.6. DNA isolation, purification and sequencing:

E. *coli* were harvested from overnight culture by centrifugation at 2000 g for 20 min. DNA was purified by GeneJET Plasmid Miniprep Kit (ThermoScientific) or PureLink HiPure Plasmid Midiprep Kit (Invitrogen) according to the manufacturer's instructions. The purified DNA sequence was validated by Eurofins MWG Operon. The NanoDropTM ND-1000 spectrophotometer was used to measure the DNA concentration in ng/µl.

2.2.4. Biophysical and analytical method:

2.2.4.1. Binding affinity measurement:

The binding affinity of ADAP peptides to the EVH1 domain was determined by isothermal calorimetric titration (ITC200). ADAP peptides representing putative binding sites were synthesized by Dr. Rudolf Volkmer. The stock solutions of peptides and EVH1 domains were made in the same buffer (NaH$_2$PO$_4$ 10 µM, Na$_2$HPO$_4$ 30 µM, NaCl 100 µM, TCEP 2 µM) and closely adjusted the pH 7.3 of both systems to avoid background noise during measurements. Peptide and protein solutions were degassed prior to the experiment. Protein concentration was taken 500 µM, while 7.5 mM peptide solution was injected into the protein chamber at the rate of 2.5 µl per injection at a continuous stirring speed (750 RPM). The system temperature was maintained at 25^{0}C. The spacing time between two injections was set to 240 sec, while filter time was kept at 5 sec. The observation was made until 16 times peptides was injected into the protein solution. This change in thermodynamics during the binding enables accurate determination of binding constants (KD). At least three replicas of each measurement were made. To remove background noise in the measurements, peptides were titrated against system buffer and the values were subtracted from actual measurements. Results were quantified and analyzed by a script designed by Dr. Robert Opitz in R-program.

2 2.4.2. Tryptic in-gel digestion:

For mass spectrometric analysis, SDS-gel from pull-down assay was coomassie stained then cut precisely (so each lane cut at the same level). SDS-PAGE was destained by washing them with 50% acetonitrile in 50 mM ammonium bicarbonate. The slices were then

dehydrated with 100% acetonitrile, dried in a vacuum centrifuge and re-swollen in 25 µl of trypsin in 50 mM ammonium bicarbonate. The trypsin digestion (0,05 µg trypsin) was performed overnight at 37°C. Then 10 µl of 0.5% (v/v) trifluoroacetic acid in acetonitrile was added to stop digestion. After sonification for 5 min, the supernatant of each slice was filled in a glass vial and completely dried in a vacuum centrifuge. The samples were dissolved in 6.5 µl of 0.1% (v/v) TFA, 5% (v/v) acetonitrile in water. The samples were stored at -20°C till ready for mass spectrometry analysis.

2.2.4.3. Mass spectrometry (MS):

The mass spectrometric analysis was conducted to identify interaction partners of the EVH1 domain that were displaced by the EVH1 inhibitor. A label-free quantification method was used for mass spectrometric analysis. For this purpose, pull-down eluates with and without inhibitor were run on SDS-PAGE followed by 'tryptic in-gel digestion' protocol as described earlier. Data obtained was sorted based on the intensity and number of peptides (proteins) deficient in the sample with an inhibitor.

2.2.5. Biochemical Methods:

2.2.5.1. Pull-down assay:

Pull-down experiment was performed to identify EVH1 domain interaction partners in Jurkat cells. GST-tagged EVH1 domains were bound to the glutathione sepharose matrix (GST beads). The interaction partners of the EVH1 domain were pulled down from Jurkat cell lysate (which was made as described in section 2.2.1.3. EVH1 inhibitor was used at different concentrations to investigate the concentration-dependent displacement of interaction partners. In detail, glutathione sepharose beads (15 µl of 50% slurry) (GE) were washed three times with washing buffer (PBS, 1% NP-40) and incubated with purified GST-EVH1 domains (50 µg) of EnaH, VASP, or EVL at 4^0C while continuously shaking for 30 min. EVH1 domain-loaded beads were allowed to settle down, the supernatant was removed. EVH1 domain loaded beads were washed three times with washing buffer. 2 µg/µl cell lysate was added to the beads along with the EVH1 inhibitor at different concentrations (0, 1, 10, 100, 200 µM) and incubated overnight at 4^0C while continuous shaking. Remove the lysate supernatant from the beads, giving them a twice gentle wash with washing buffer. During

the final wash, beads were transferred into microcentrifuge tubes. Protein complexes were eluted from the beads by adding 20 µl of 2X SDS sample buffer and incubated at 95^{0}C for 10 min, followed by centrifugation at 12000g for 1 min. Pull-down samples obtained in the presence or absence of EVH1 inhibitor were then applied to SDS-PAGE and run in BioRad gel electrophoresis system at constant current (25 mA) for about 50 min. A prestained protein marker (Pageruler) was used to identify proteins based on their size.

2.2.5.2. Western Blot:

Western Blot is an analytical method for protein detection. Proteins were separated by 4-20% gradient SDS-PAGE (BIO-RAD) and then electrophoretically transferred to nitrocellulose membrane for 10 min at 250V in a fast turbo-blot system (Bio-Rad). After protein transfer, the membrane was treated with the blocking buffer (Odyssey) for 45 min. The membrane was incubated with primary antibodies (1:1000) in blocking buffer overnight at 4^{0}C while continuously shaking. The next day membrane was washed thrice with PBS (0.05% tween20) and incubated with IR (800) conjugated secondary antibody (1:50000) for 45 min at room temperature. Finally, the membrane was washed three times with PBS before scanning on Odyssey (LI-COR) IR scanner to reveal proteins.

2.2.5.3. Co-Immunoprecipitation:

Pierce Protein A/G magnetic beads were loaded with respective antibodies (2-4 µg/µl) after washing 3x with PBS containing 1% NP-40. Beads were then incubated in cell lysate (2 µg/µl) overnight at 4^{0}C while continuously mixing [164]. The next day, the magnetic beads were separated from the lysate with a magnetic rack's help. The beads were washed once with PBS and the protein complex was eluted with 2x SDS sample buffer. Beads were incubated at 95^{0}C for 5 min and the eluate was separated from beads magnetic rack. The protein sample was run on SDS-PAGE, followed by transferring on the nitrocellulose membrane. The membrane was fixed with Odyssey blocking buffer and then exposed to antibodies against proteins of interest overnight at 4^{0}C. Finally, the membrane was incubated by IR conjugated secondary antibodies to reveal interaction partners by the Odyssey IR scanner (LI-COR).

2.2.6. Cell biological methods:

2.2.6.1. Integrin activation assay:

The β1 integrin subunits (CD29) were activated by treating Jurkat cells with 100 ng/ml PMA for 10 min. Cells were then washed twice with PBS and resuspended in a fresh medium. 1×10^6 activated and non-activated (as control) Jurkat cells were labeled with (1:100) CD29 antibody conjugated with PE (BD Bioscience) in the presence of 200 μM $MnCl_2$ for 30 min at room temperature [165]. Cells were washed with PBS and resuspended in FACS buffer at 4^0C [166] [167]. Living cells were gated based on sideward and forward scattering. CD29 activation was measured for 20,000 cells/condition based on the PE intensity of the population at 570 nm. FACS data were analyzed in FlowJO software and expressed as histograms of PE intensity.

2.2.6.2. Cell spreading assay:

1×10^6 Jurkat cells were transiently transfected with pmEGFP- lifeact-N1 plasmid (10 μg) by using the neon transfection system (Invitrogen) (pulse voltage (v) 1400, pulse number 3). 24-hour post-transfection cells were analyzed by fluorescent microscopy. 8 well chamber glass-bottom slide (Ibidi) was coated with 3 μg/ml ICAM-1 and VCAM-1 overnight at 4^0C. ICAM-1 and VCAM-1 were removed and let the slide dry at room temperature. Before the assay, the plate surface was washed once with PBS and lifeact (GFP) transfected Jurkat cells were added 1×10^3 per well. The glass-bottom slide was incubated at 37^0C, 5% CO_2 for 30 min. Suspended cells were removed and observed spreading of the adhered cells on the surface of the slide with Epi-TIRF (488 nm) by providing 10 ng/ml CXCL12 gradient to one corner of the chamber. Images obtained were analyzed by ImageJ software to quantify cell spreading. Aspect ratio (height divided by the length of the major-axis in the *x-y* plane) correlates with the degree of cell spreading.

2.2.6.3. Transendothelial migration assay:

HUVECs were seeded on the basal side of 24 well PET transwell inserts (5 μm pore size membrane) coated with human fibronectin and culture HUVECs until confluent [168]. Transwell inserts were then inverted and placed in a growth medium. Jurkat cells were incubated in a starvation medium (without FBS) for 24 hours. Jurkat cells were stained with

5 μM CFSE dye (absorbance 488 nm, emission 520 nm) for 15 min, washed with PBS and resuspend in starvation medium. 100 μl of stained Jurkat cells (3 X 10^6/ml) were added to the apical chamber of the insert. The chemokine CXCL12 final concentration 100 ng/ml was added to the lower chamber of the well, and cells were incubated at 37^0C, 5% CO_2 for 2.5 hours. Afterward, the insert was removed, and the fluorescent intensity of migrated cells in the lower chamber was measured by the fluorescent reader (TECAN) at 488 nm with multiple reads per well. Data obtained after three replicates were normalized with respect to control (without chemokine gradient). Statistical significance was determined by One-way-ANOVA followed by Dunnett's test in Prism software (6).

2.2.6.4. Chemotaxis assay:

2D cell migration was performed in chemotaxis μ-Slide (Ibidi) coated with 10 μg/ml fibronectin. Jurkat cells or macrophages were starved for 24 hours before the assay. The cells were washed with PBS and resuspended 2 X 10^5 cells/ml in a starvation medium. 6 μl of cell suspension was added to the observation chamber and let the cell adhere to the surface at 37^0C, 5% CO_2, for an hour. 60 μl of the starvation medium was loaded in both reservoirs. 5 μl of the starvation medium was replaced with 6 ng of CXCL12 in one of the reservoirs to establish a gradient (-/+). For a control experiment (-/-), both reservoirs were filled with 60 μl of the starvation medium. Cells were observed under bright field microscopy with 4X objective. Cells were tracked for 120 min, with 1 min intervals between recordings.

For 3D migration Jurkat cells 5 X 10^5 cells/ml were embedded in collagen gel (bovine collagen I 1.3 mg/ml, $NaHCO_3$ 7.5%, 10x MEM, in RPMI 1640 media) in a μ-dish (35 mm, Ibidi). The μ-dish was sealed with a glass coverslip in such a way that the coverslip covered 80% of the bottom of μ-dish. 70% of the space between a coverslip and the μ-dish were filled with collagen I + Jurkat cell matrix. The μ-dish was incubated at 37^0C, 5% CO_2, for 1 hour to solidify. The remaining space was filled with chemokine (CXCL12 100 ng/ml) containing medium. Cell migration was observed by a 10x objective under bright field microscopy for 4 hours, setting 2 min intervals between each recording. Cell tracking data were analyzed by ImageJ and quantified by an automated tracking plugin.

2.2.6.5. Immunological synapse formation:

Immunological synapse formation between T-cells and antigen-presenting cells is critical for the execution of T-cell immune response. Here we analyzed conjugation between Jurkat cells and B-cells by flow cytometry [36]. Jurkat cells were exposed to OVA antigen 10 µg/ml for 48 h at 37^0C. Jurkat cells (6 X 10^5) were stained with 5 µM cell track green dye (CFSE) for 15 min and B-cells (2 X 10^5) were stained with 5 µM cell tracker red dye (CMTPX) for 20 min at room temperature. Cells were centrifuged at 1500g for 5 min, remove supernatant and washed cells 3 times with RPMI media. Add 10 µg/ml OVA antigen to B-cells, mix Jurkat cells and B-cells in 3:1 ratio and incubated at 37^0C for 30 min. Jurkat cell-B-cells conjugates were analyzed using dual-color flow cytometry. Unstained control was analyzed to set voltage and gates (FSC, SSC, fluorescence signals). Fluorescence of 50,000 cells was observed for each condition. Control of conjugation assay were the samples untreated with OVA peptide. Results were quantified using FlowJO software and expressed in terms of the mean percent population in a specific quadrant.

III. Results

3. Results

3.1. Recombinant expression of proteins:

### 3.1.1. Recombinant expression of EVH1 domain of Ena/VASP proteins:

For the proteomic study, the purified form of recombinant EVH1 domain of Ena/VASP protein was expressed in E. *coli* (BL21). The N-terminal GST tag pGEX-4T-1 vector was used to express the EVH1 domain of all Ena/VASP family proteins. Similarly, for biophysical study, untagged EVH1 domains of the Ena/VASP family were expressed. Äkta purified recombinantly expressed protein. Purified fractions were obtained after size exclusion chromatography. The purity of protein fractions was determined by SDS-PAGE, stained by coomassie blue (Fig. 3.1-c).

3.1.2. Recombinant expression of His-ADAP (fl) and His-ADAP$_{MUT}$:

Recombinantly expressed wild type His-ADAP$_{WT}$ full length (fl) and mutated His-ADAP$_{MUT}$ (fl) in E. *coli* (Rosetta). The expression protocol was almost similar to the above-explained protocol, except E. *coli* was grown overnight at 18^0C in media containing kanamycin antibiotic. Once bacterial pellet was harvested and lysed, cell lysate was loaded on the Ni-NTA column in the Profinia automated system. His tag purified protein bound to the matrix of a column and later eluted with 250 mM imidazole. After affinity purification, His-ADAP(fl) and its variant were purified by size exclusion chromatography. Fractions were loaded on SDS-PAGE and stained by coomassie blue before pooled down (Fig. 3.1-d). Fractions that exhibited a high ADAP concentration were combined, fast-frozen in liquid nitrogen, and stored at -80^0C. For ADAP-EVH1 binding site investigation, a mutation was introduced at its EVH1 domain binding site (DBS) by replacing two crucial amino acids of the core motif from F<u>PP</u>PP (617-618) to F<u>GS</u>PP. By designing a suitable oligonucleotide primer, the site-specific mutation was introduced by PCR. The mutation was confirmed by DNA sequencing.
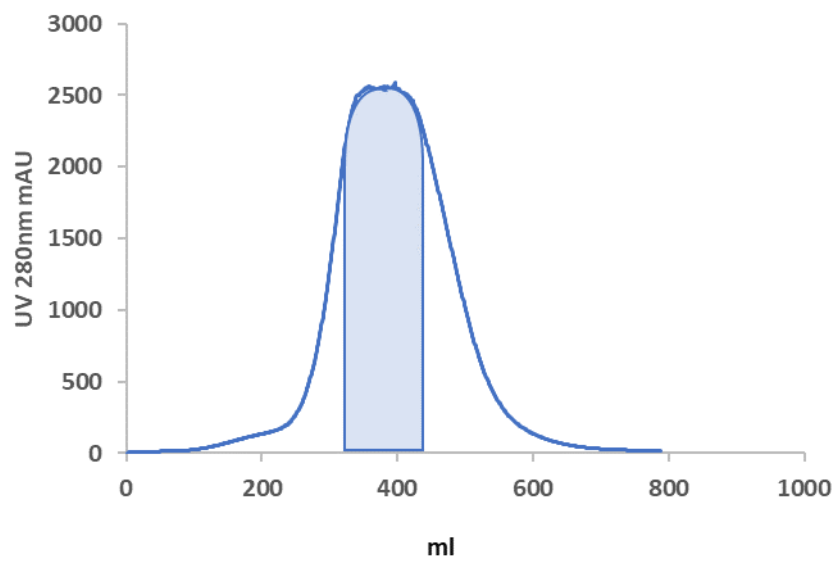
a.

GST EVL-EVH1

b.

GST ENAH EVH1

c.

d.

ADAP$_{WT}$
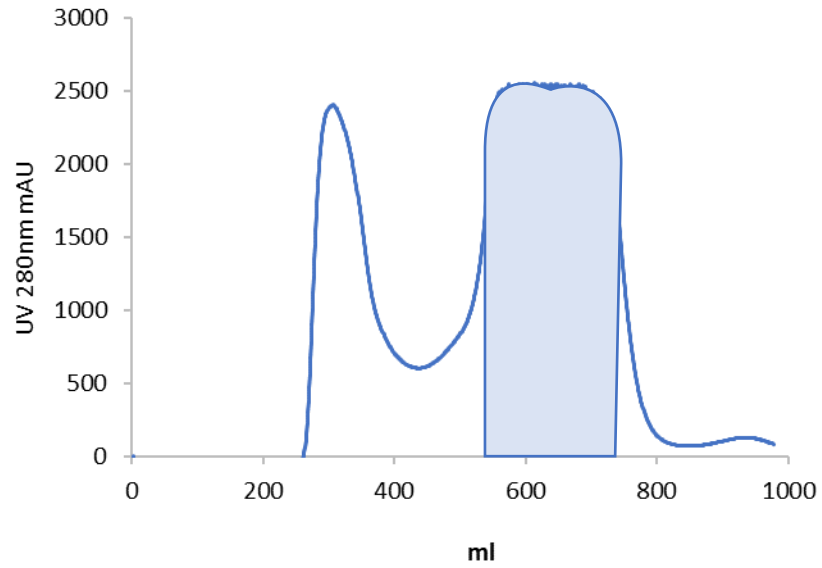
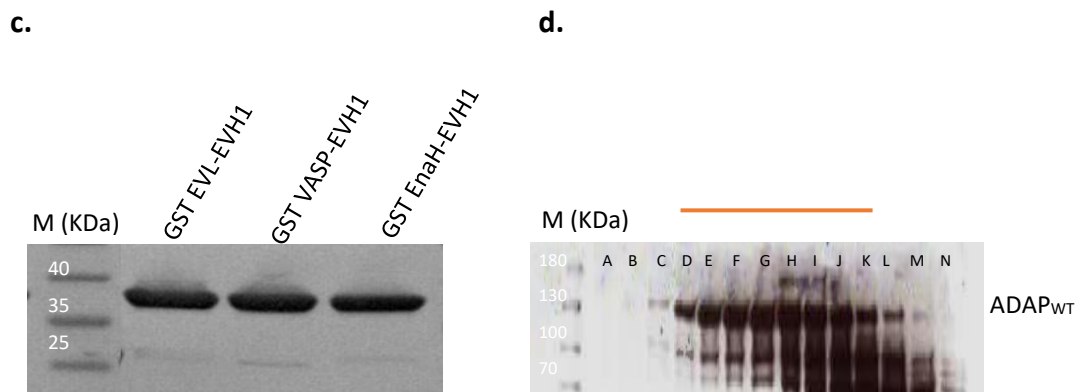**Figure 3.1: Purification of proteins by ÄKTA and analyzing in 15% SDS-gel by coomassie blue staining: a,b:** Chromatogram of recombinant GST-EVH1 domain of EnaH and EVL purified in ÄKTA system. Absorbance of protein was measured at 280 nm. Fractions corresponded to purified peaks (light blue) on histogram were collected and pooled. **c.** 10 µg of purified GST-EVH1 domain of EnaH, VASP and EVL were loaded on 15% SDS-PAGE and stained with Coomassie blue. EVH1 domain detected at the size of about 39 KDa **d.** Recombinantly expressed His-ADAP fl fractions collected after size exclusion chromatography, were loaded on SDS-PAGE followed by coomassie blue staining for the purity analysis. Fractions from D to J were collected and stored at -80^{0}C after shock freeze. ADAP runs at the size of about 120 KDa. M represent pre-stained protein ladder.

3.2. *In-Vitro* displacement of EVH1 domain-mediated interaction partners by EVH1 inhibitors in Jurkat cells:

3.2.1. Mass spectrometric identification of the EVH1 domain-mediated interaction partners in Jurkat cells:

The EVH1 inhibitor replaces key interactors in the MDA-MB-231 cell line (Dr. Matthias Müller). However, to determine the displacement of EVH1 mediated interaction partners specifically in Jurkat cells, I used a mass spectrometric approach. For this purpose, I have used the first-generation EVH1 inhibitor Ac-2 Cl-F-[ProM2]-[ProM1]-NH$_2$. The pull-down experiment was performed with the GST-EVH1 domain as "bait" to pull-down its interaction partners from Jurkat cell lysate. This experiment was conducted with and without EVH1 inhibitor at a concentration of 100 µM predetermined in the MDA-MB 231 cell line. SDS-PAGE separated the final pull-down protein complex. The eluate from pull-down assay (with and without EVH1 inhibitor) were run in adjacent parallel lanes of the SDS-PAGE. The gel was precisely excised at the same level of both lanes and followed by a tryptic in-gel digestion protocol to prepare the final mass spectrometry sample (Fig. 3.2). A label-free quantification approach of mass spectrometry was used in this study. Proteins were sorted based on abundance and ratio of intensities between conditions with and without EVH1 inhibitor. The identified binding partners are presented in Table 3.2 below.

It is known that the EVH1 inhibitor mimics the F/L/PPPP motif necessary for EVH1 binding. Therefore, it must have the ability to displace the number of proteins from the EVH1 domain. In this study, I identified some known EVH1 domain interaction partners like WAVE2, Zyxin, Palladin, RIAM and Lipoma Preferred Partner (LPP), those were completely displaced by EVH1 inhibitor. Interestingly, few T cell-specific interaction partners were also identified that were displaced with EVH1 inhibitors, like Nck, SKAP, ADAP/FYB and Talin. However, among them, only ADAP possessed various PPPP motifs that are necessary for binding to the EVH1 domain. Although, the interaction of ADAP with detected proteins through its different domains had already been established. So, ADAP was assumed to be the primary interaction partner to the EVH1 domain here. ADAP is a T-cell signaling protein that is important in several cellular processes [169].+

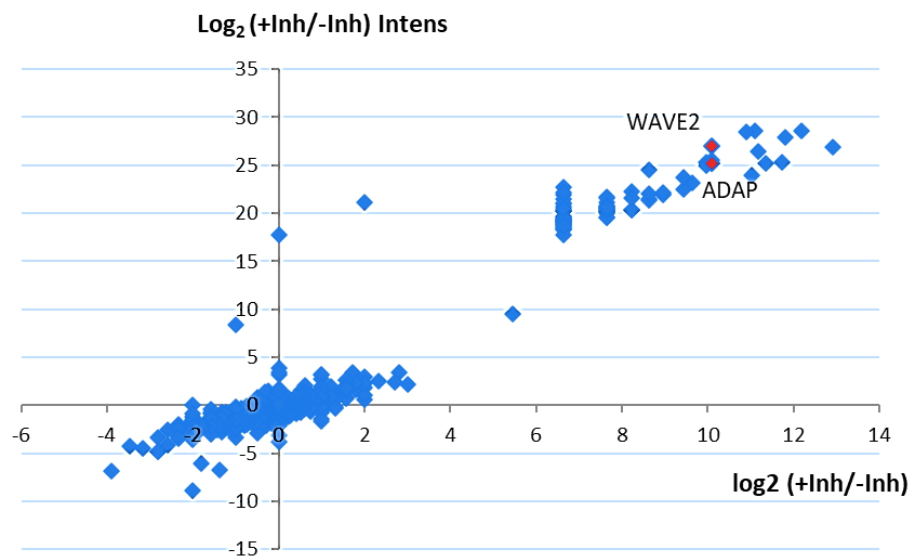**a.**
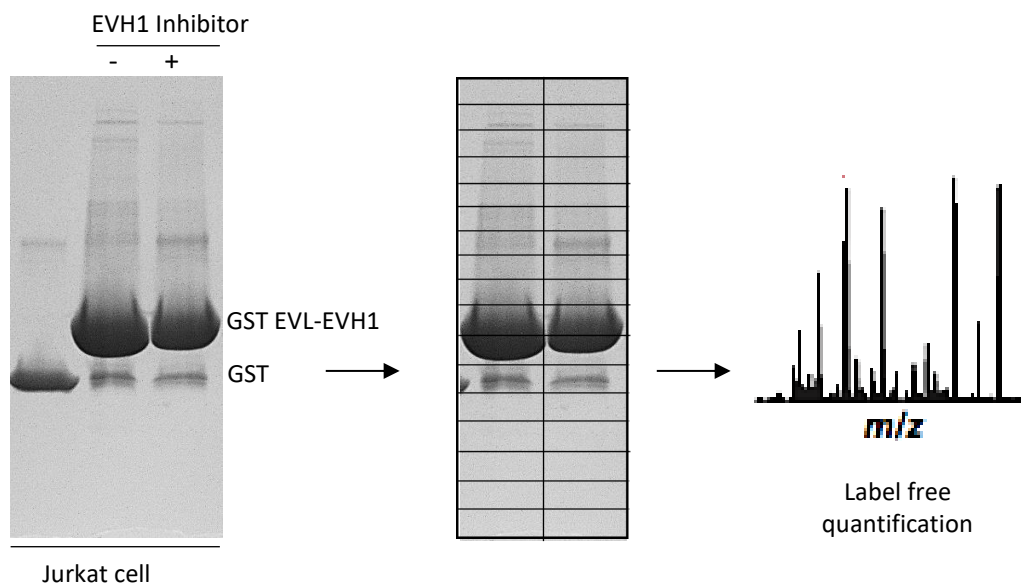
b.

Figure 3.2*: **Identification of displaced EVH1 domain interaction partner with EVH1 inhibitor in Jurkat cells by mass spectrometry analysis: a.** GST pull-down assay was conducted by GST tagged EVH1 domain of Ena/VASP proteins in Jurkat cell lysate, with and without EVH1 inhibitor (+/-). Pull-down assay was resolved by SDS-PAGE (4-20%) and stained with mild coomassie blue (BIO-RAD). SDS-PAGE excised carefully at same level of both lanes. Excised gel fractions, then subjected to trypsin-in-gel digestion and directed to label free mass spectrometric analysis. **b**. Mass spectrometry result for the GST pull-down show number of proteins (including ADAP and WAVE2) displaced by EVH1 inhibitor at concentration of 100μM.

Table 3.1: Identified binding partners of EVH1 domain in Jurkat cells by mass spectrometry:

Binding partners of Ena/VASP-EVH1 domain were identified by pull-down experiments followed by quantitative mass spectrometric analysis using label free quantification method. The MaxQuant software was used for protein identification and quantification. The mass spectrometry analysis was performed by Dr. Eberhard Krause lab.

	PROTEINS
EVH1 binding partners	Protocadherin Fat 1
	Vinculin
	Zyxin
	RAPH1
	Lipoma preferred partner
	Amyloid-beta A4 precursor protein-binding family B member 1-interacting protein
	Proline-rich protein
	La related protein
FORMIN	Protein Diaphanous homolog 1
	Protein Diaphanous homolog 2
LIM DOMAIN	Lipoma preferred partner
	LIM domain only protein
T-CELL RELATED	**FYN-binding protein (ADAP)**
	Nck-associated protein 1
	Src Kinase associated phosphoprotein1
	Talin-1
	Tyrosine-protein kinase ZAP70
WAVE Complex	AbI interactor 1 & 2
	Actin related protein 2/3 complex
	Protein BRICK1
	Wiskott-Aldrich syndrome protein
	Wiscott-Aldrich protein family member 2
	Protoncogene VAV

3.2.2. Determine binding affinity of ADAP with EVH1 domains:

F/Y/L/WPPPP is characterized as EVH1 domain binding core sequence [118]. ADAP also holds multiple similar polyproline motifs in its sequence (Fig. 3.3). To analyze the exact binding motif of ADAP with the EVH1 domain, I map polyproline motifs of ADAP one by one against the EVH1 domain by using the Isothermal titration calorimetry (ITC) technique. The biophysical study aims to determine whether ADAP holds multiple binding motifs to the EVH1 domain and also measure the binding association constant between ADAP and EVH1 domain.

a.

```
MAKYNTGGNP TEDVSVNSRP FRVTGPNSSS GIQARKNLFN NQGNASPPAG
PSNVPKFGSP KPPVAVKPSS EEKPDKEPKP PFLKPTGAGQ RFGTPASLTT
RDPEAKVGFL KPVGPKPINL PKEDSKPTFP WPPGNKPSLH SVNQDHDLKP
LGPKSGPTPP TSENEQKQAF PKLTGVKGKF MSASQDLEPK PLFPKPAFGQ
KPPLSTENSH EDESPMKNVS SSKGSPAPLG VRSKSGPLKP AREDSENKDH
AGEISSLPFP GVVLKPAASR GGPGLSKNGE EKKEDRKIDA AKNTFQSKIN
QEELASGTPP ARFPKAPSKL TVGGPWGQSQ EKEKGDKNSA TPKQKPLPPL
FTLGPPPPKP NRPPNVDLTK FHKTSSGNST SKGQTSYSTT SLPPPPPSHP
ASQPPLPASH PSQPPVPSLP PRNIKPPFDL KSPVNEDNQD GVTHSDGAGN
LDEEQDSEGE TYEDIEASKE REKKREKEEK KRLELEKKEQ KEKEKKEQEI
KKKFKLTGPI QVIHLAKACC DVKGGKNELS FKQGEQIEII RITDNPEGKW
LGRTARGSYG YIKTTAVEID YDSLKLKKDS LGAPSRPIED DQEVYDDVAE
QDDISSHSQS GSGGIFPPPP DDDIYQGIEE EDADDGFPAP PKQLDMGDEV
YDDVDTSDFP VSSAEMSQGT NVGKAKTEEK DLKKLKKQEK EEKDFRKKFK
YDGEIRVLYS TKVTTSITSK KWGTRDLQVK PGESLEVIQT TDDTKVLCRN
EEGKYGYVLR SYLADNDGEI YDDIADGCIY DND
```

b.

ADAP PEPTIDE

1	**Ac-SKPTFPWPPGNKPSL-NH2**
2	**Ac-ARFPKAPSKLTV-NH2**
3	**Ac-SLPPPPPSHP-NH2**
4	**Ac-SGGIFPPPPDDDIY-NH2**
5	**Ac-EDADDGFPAPPKQLDM-NH2**

Figure 3.3: Mapping EVH1 domain binding site in ADAP sequence: a. Amino acid sequence and structural motifs of ADAP/ Fyb (UniProtKB - O15117). Boxes highlighted contain poly-proline rich motifs as putative EVH1 domain–binding sites. **b.** Table represent putative peptide sequence of ADAP that chemically synthesized for mapping the binding affinity with EVH1 domain. Each peptide was titrated against EVH1 domain of Ena/VASP family proteins by isothermal calorimetric (ITC) method.

ITC technique was used to determine the binding association constant of ADAP peptides with the EVH1 domain. In this approach, the ADAP peptide (7.5 mM) was titrated against Ena/VASP-EVH1 domain (500 mM) in the protein chamber. Change in thermodynamics of the ITC system was analyzed and quantified with each 2.5 µl of peptide injected to titrate protein. Each data point in ITC data (Fig. 3.4) represented a single injection. The titration experiment was performed in triplicates and the titration curves described here are the average of 3 replicates expressed in blue and red color. Both ligand and protein buffers were titrated against each other and subtracted the values from the titration to eliminate background noise. The control buffer titration is represented by green color in the ITC graph. The ITC data were processed in R script by Dr. Robert Optiz and presented as a dissociation constant (K_D) and expressed in µM. R script indicated a one-to-one model fit best to describe this binding process.

The ITC measurements showed that only one ADAP-peptide (Ac-SGSGGIFPPPPDDDIY-NH2) was able to bind to the EVH1 domain. As seen in figure 3.4, ADAP peptide bind to all EVL- (70 µM), EnaH- (140 µM), and VASP-EVH1 (200 µM) domains. ITC measurements showed a negative enthalpy change, indicating that ADAP binding to the EVH1 domain is an exothermic process. To prove single binding site for EVH1 domain in ADAP, a point mutation was introduced by PCR in the recombinant construct of full-length ADAP. Two integral proline units in the core motif were substituted by random amino acids, from FPPPP (615-620) to FGSPP. Pull-down assay was performed with GST EVL-EVH1 as bait to validate this finding. Pull-down assay result revealed that the ADAP-EVH1 domain interaction was entirely lost with mutated ADAP (ADAP$_{MUT}$), while in wild-type ADAP (ADAP$_{WT}$) this interaction was presented as shown in (Fig. 3.4 **c**). This data suggested that despite having multiple polyproline-rich motifs, ADAP has only one binding site for the EVH1 domain.
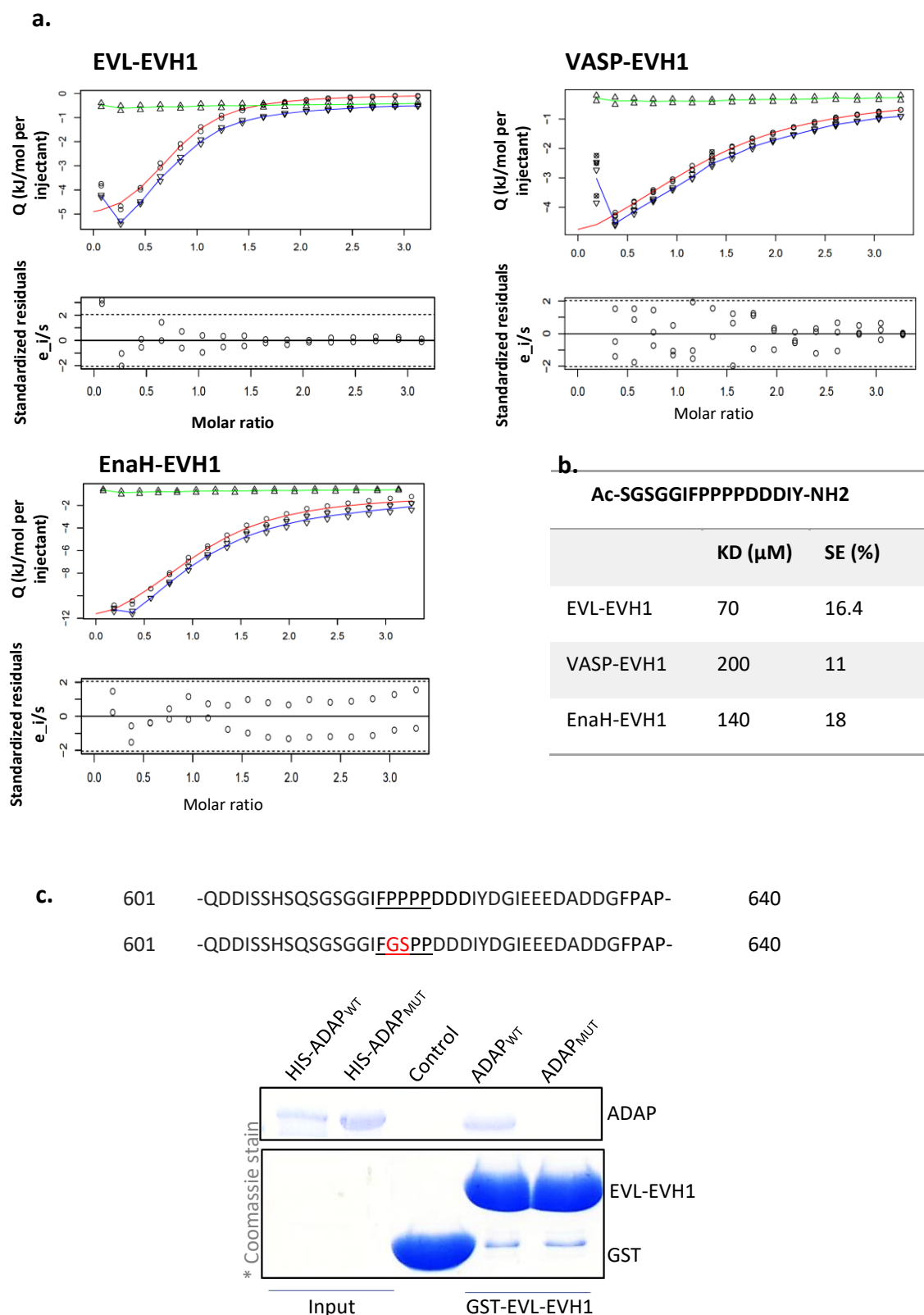
a.

EVL-EVH1

VASP-EVH1

EnaH-EVH1

b.

Ac-SGSGGIFPPPPDDDIY-NH2

	KD (µM)	SE (%)
EVL-EVH1	70	16.4
VASP-EVH1	200	11
EnaH-EVH1	140	18

c.

601   -QDDISSHSQSGSGGI<u>FPPPP</u>DDDIYDGIEEEDADDGFPAP-   640

601   -QDDISSHSQSGSGGIFGSPPDDDIYDGIEEEDADDGFPAP-   640

Figure 3.4: Binding affinity of ADAP ligands with EVH1 domain of Ena/VASP: **a**. ITC titration data of Ac-SGSGGIFPPPPDDDIY-NH2 ligand with EVH1 domain of all Ena/VASP family proteins. **b.** Table represent dissociation constant K_D of ADAP peptide with EnaH-, VASP- and EVL-EVH1 domain, quantified in R script. K_D was expressed in µM. The data suggested relatively strong binding affinity between ADAP and EVL-EVH1 domain. **c.** To validate single binding motif of ADAP by mutating its core FPPPP to FGSPP, the pull-down assay was performed with GST VEL-EVH1 domain as bait. Outcome of pull-down assay was loaded on SDS-PAGE and resolved by coomassie staining. Pull-down data showed by introducing single site mutation in ADAP, its interaction with EVH1 domain is completely lost.

3.2.3. Expression profiling of different proteins in Jurkat cell/U-937:

EnaH, VASP, and EVL share similar functional domains and play important roles in regulating actin dynamics [114]. More than one Ena/VASP paralogue can be expressed in single type of cell [110]. The Ena/VASP paralogues are differ in their ability to promote actin polymerization *in-vitro* . The additional indications suggest paralogue-specific interactions and modes of regulation [170,171]. Therefore, in order to investigate the Ena/VASP-EVH1 domain in immune cell lines, it was necessary to identify the endogenous expression of Ena/VASP paralogues in Jurkat cells and macrophages. Cells were lysed with RIPA buffer at 4^0C, cellular debris were removed, and 25 µg of lysate concentration was loaded on gradient (4-20%) SDS-PAGE followed by western blot. The MDA-MB-231 cell lysate was used as a control. Blot was treated with indicated protein-specific antibodies and revealed by IR scan (Odyssey). Result demonstrated that EVL is the most abundant member of Ena/VASP family expressed in Jurkat cells, whereas in U-937 cells, VASP expression was dominated. Surprisingly, EnaH was detected neither in Jurkat cells nor U-937 cells. ADAP expression was slightly higher in Jurkat cells than in U-937 cells. Compared to the MDA-MB-231 cell line as control in which ADAP was undetected, supporting the fact that ADAP is the immune cell-specific adaptor protein.
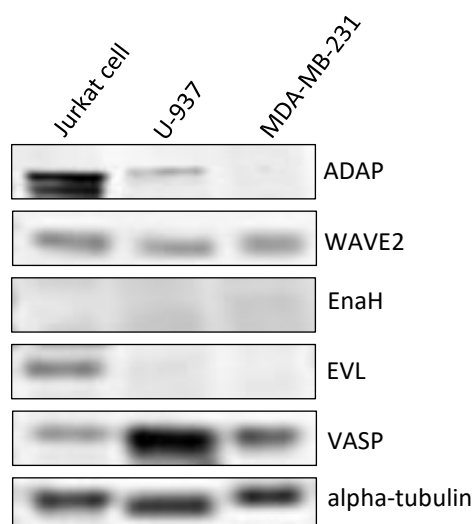

Figure 3.5: Protein expression profile of Jurkat cell/U-937: Immunoblot of total cell lysates (25 µg) of Jurkat cell, U-937 and MDA-MB-231 exhibit differential expression profile of Ena/VASP family proteins. Ena/VASP proteins, ADAP, WAVE2 expression in Jurkat cell and U-937 cells were compared to MDA-MB-231 cell. Alpha-tubulin protein represented as loading control. Two bands of Alpha-tubulin indicated phosphorylated and un-phosphorylated form of protein that could happened by unintended stimulation of cells.

3.2.4. Concentration-dependent inhibition of EVH1 inhibitor in Jurkat cells and U-937 cells:

In-Vitro pull-down data demonstrated direct interaction of the EVL-EVH1 domain with ADAP and WAVE2. To investigate the concentration-dependent inhibition of EVH1 domain-mediated interactions in immune cells, varying concentrations (0, 1, 10, 100 and 200 µM) of EVH1 inhibitors (inhibitor a and b) were used in a pull-down assay. The recombinant GST EVL-EVH1 bound to GST-agarose beads served as "bait" to pull-down all its interaction partners from Jurkat and U-937 cell lysate under different concentrations of Inhibitors. The pull-down complex was resolved by SDS-PAGE followed by a western blot. Blot was probed with antibodies to ADAP, WAVE2, EVL, and GST (Fig. 3.6). The assay result suggested that both inhibitors completely displaced ADAP and WAVE2 from the EVH1 domain at 100 µM concentration in Jurkat cell lysate.

a.
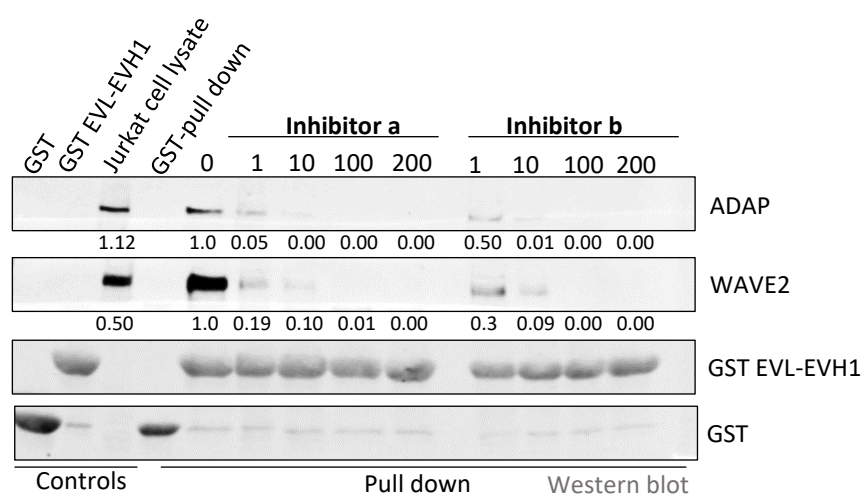
b.
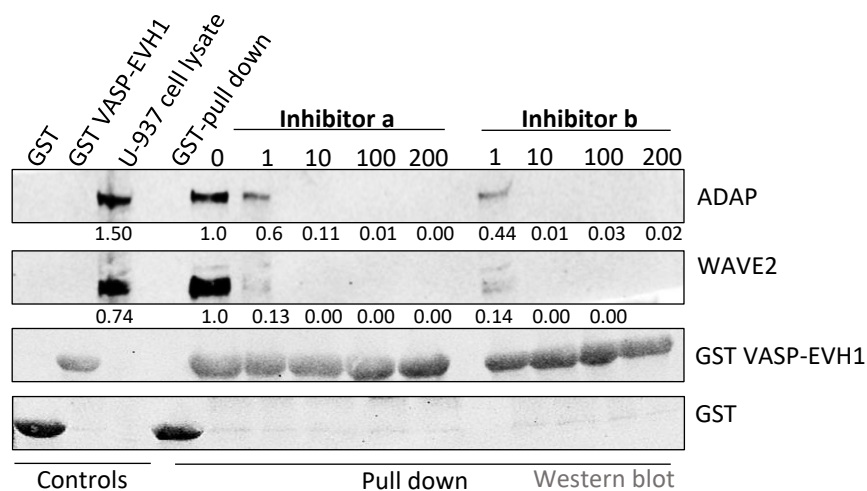
Figure 3.6: Concentration dependent displacement of EVH1-domain interaction partners:
a. Immunoblot from pull-down assay of Jurkat cell showing displacement of ADAP and WAVE2 from EVH1-domain. Inhibitor **a** and **b** were used in 0, 1, 10, 100 and 200 µM concentration. Both inhibitors had showed concentration dependent displacement of EVH1-interaction partners. **b.** Immunoblot from pull-down assay of U-937 cell lines has also showed same concentration dependent displacement of ADAP and WAVE2 from EVH1-domain. Pull-down with recombinant GST protein was held as negative control. Band intensities was quantified by ImageJ, keeping 0 inhibitor concentration as 1.

Inhibitor **a** and **b** were used at 100 µM concentration to verify endogenous inhibition of ADAP, WAVE2 interaction with EVH1-domain. ADAP and WAVE2 were co-immunoprecipitated with EVL antibody-bound magnetic beads from Jurkat cell lysate. Endogenous EVL was bound to EVL antibody and formed a multiprotein complex with its interaction partners in Jurkat cell lysate. The complex was collected using Protein G magnetic beads. Bound proteins were eluted, resolved by SDS-PAGE followed by western blot and probed with ADAP and WAVE2 antibodies. As a negative control, lysates were immunoprecipitated using an IgG antibody that has no antigen-binding site.
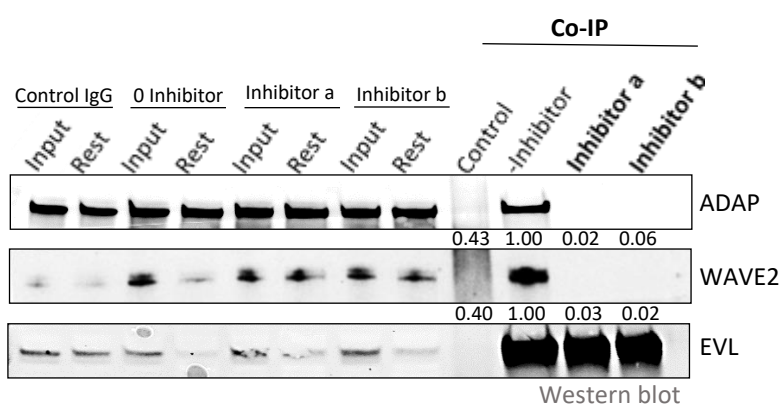
Figure 3.7: Co-Immunoprecipitation of Jurkat cells with EVL antibody and EVH1 inhibitors: EVL protein co-immunoprecipitated its interaction partners from Jurkat cell lysate. Immunoblot was probed with ADAP and WAVE2 antibodies. It was observed from blot that at 100 µM concentration of inhibitor **a** and **b**, ADAP and WAVE2 interactions were completely lost. Cell lysate in Co-IP before and after multiprotein complex formation termed as input and rest, respectively. Antibody IgG served as negative control to elucidate any unspecific binding to beads or antibody. Band intensity scores were quantified using ImageJ keeping 0 inhibitor concentration as 1.

3.3. Lentiviral transduction of WT/MUT-ADAP and WT/MUT-WAVE2 in Jurkat cells:

The interaction of ADAP and WAVE2 with Ena/VASP-EVH1 domain was confirmed *in-vitro* in Jurkat cells. However, to determine the significance of ADAP, WAVE2 interaction with EVH1 domain in Jurkat cells was very important to understand their impact in T-cells responses. To investigate this, a knockdown/re-expression approach was used in this study. The small hairpin RNA (shRNA)-mediated downregulation of endogenous ADAP and WAVE2 was achieved individually in Jurkat cells. shRNA encoded the UTR sequence of human ADAP and WAVE2 transduced in Jurkat cells. Subsequent to knock-down, the vector that encoded mutation at EVH1 binding sequence (WAVE2$_{MUT}$) was delivered in WAVE2$_{KD}$. Similarly, ADAP$_{MUT}$ vector was delivered to ADAP$_{KD}$ Jurkat cells. In parallel, a control over-expression vector encoding wild-type ADAP (ADAP$_{WT}$) and WAVE2 (WAVE2$_{WT}$) were transduced to their relative cells. Cell lysate of stably transduced Jurkat cells of both constructs was analyzed individually by western blot to reveal knock-down/re-expression efficiency. Expression of endogenous ADAP and WAVE2 were reduced >80% with shRNA knockdown, quantified by ImageJ software.

In addition, re-expression vectors allowed the comparable expression of wild-type and mutated proteins in Jurkat cells. As proof of concept, HEK293T cells were co-transfected with Flag-EVL vector, mCherry tagged vector of WAVE2$_{WT,}$ and WAVE2$_{MUT}$. Similarly, on the other hand, HEK293T cells were co-transfected with Flag-EVL vector and GFP-ADAP$_{WT}$ and GFP-ADAP$_{MUT}$. mCherry and GFP antibodies were employed to co-immunoprecipitated EVL from cell lysate. mCherry and GFP empty vectors were used as a negative control. While as assay control IgG antibody without antigen-binding site was used. Co-IP data revealed that ADAP$_{MUT}$ and WAVE2$_{MUT}$ Jurkat cells loss of binding to EVL protein reflecting the significance of their EVH1 binding sequence.
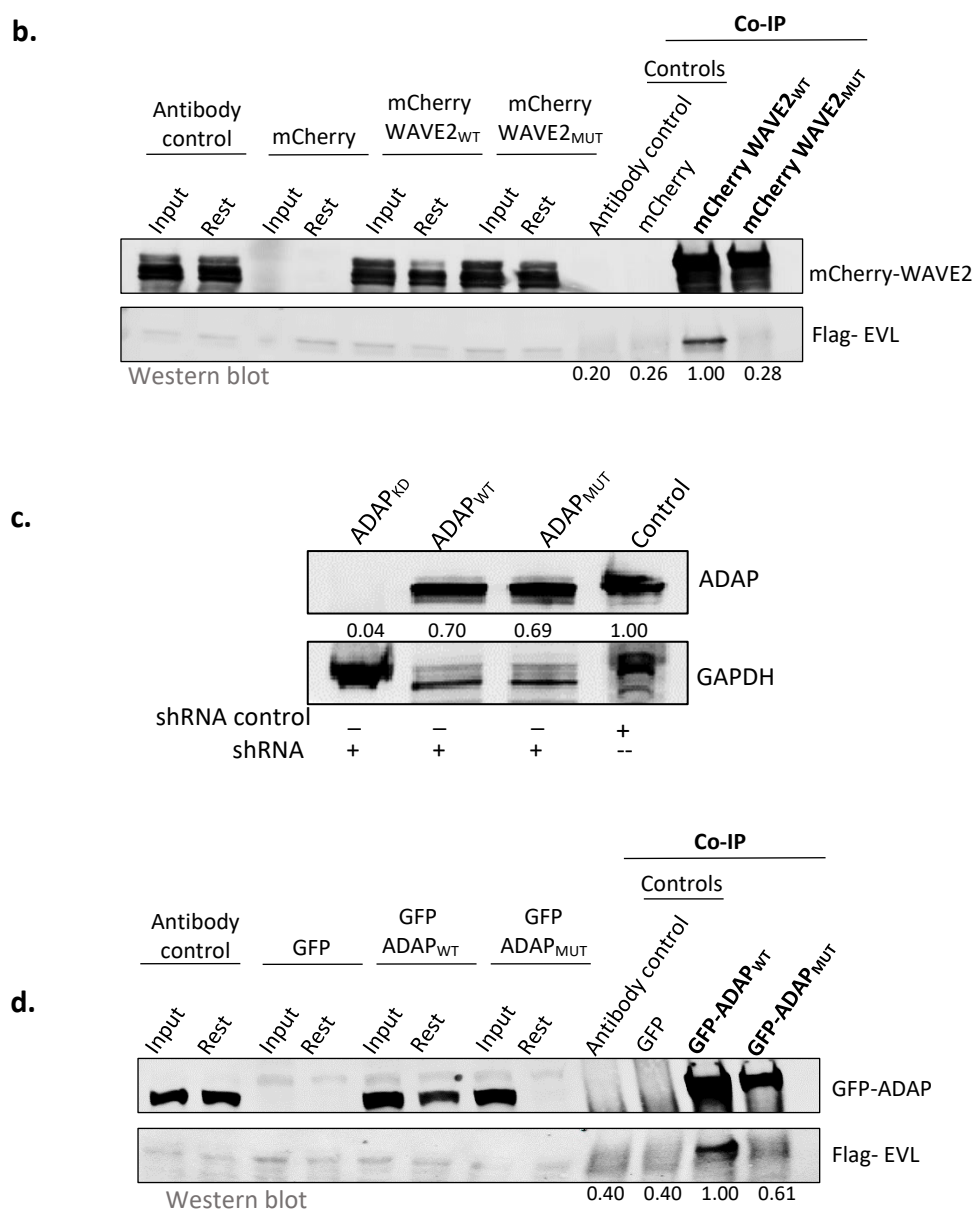
a.

b.

c.

d.
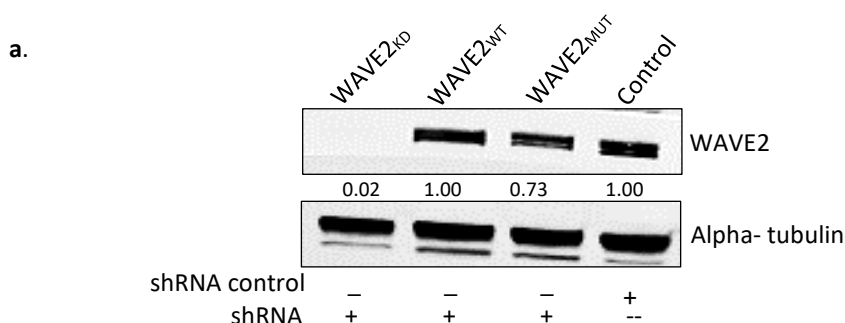
Figure 3.8: Knock-down/re-expression of WAVE2 and ADAP in Jurkat cells: a. Jurkat cells were stably transduced by lentiviral transduction with vector encoding shRNA for WAVE2 knock-down (WAVE2$_{KD}$) and subsequently with re-expression vector for wild-type WAVE2$_{WT}$ and mutated WAVE2$_{MUT}$. Transduced cells were lysed, run on SDS-PAGE, transferred and analyzed by immunoblotting. An empty shRNA vector was used as control. Alpha-tubulin antibody was served as loading control. **b.** HEK293T cells were co-transfected with Flag-EVL vector and mCherry, mCherry-WAVE2$_{WT}$ and mCherry-WAVE2$_{MUT}$ vectors. mCherry antibody was used to co-immunoprecipitated proteins from cell lysate and resolved on SDS-PAGE followed by western blot. Immunoblot was treated with EVL antibody to reveal the protein complex. mCherry empty vector was used as negative control while antibody without antigen binding site was served as assay control. **c.** Stably transfected Jurkat cells with vector encoding shRNA for ADAP knock-down (ADAP$_{KD}$) were generated. Later ADAP$_{KD}$ Jurkat cells were transduced with re-expression vector for wild-type ADAP$_{WT}$ and mutated ADAP$_{MUT}$. Cell lysates were resolved by SDS-PAGE, transferred and analyzed by immunoblotting. An empty shRNA vector was used as control. GAPDH antibody was served as loading control. **d.** Flag-EVL and GFP-ADAP co-transfected in HEK293T cells. GFP antibody co-immunoprecipitated protein complex from cell lysate and Flag-EVL was detected with EVL antibody. GFP empty vector was used as negative control while antibody without antigen binding site was served as assay control. Band intensities were quantified by ImageJ software.

3.4. Liposomal delivery of EVH1 inhibitor to immune cells:

Initial cellular assay data with EVH1 inhibitors expressed poor compliance with *in-vitro* results. Low cell permeability of EVH1 inhibitor was suspected in Jurkat cells. Therefore, we employed a commercially available protein carrier system (Fuse-It-P) to deliver molecules/drugs in the cell. The Fuse-It-P (ibidi) is a fusogenic liposomal carrier system. The lipid bilayer of the liposome simply fuses with the cell membrane and released the encapsulated water-soluble protein/peptide directly into the cytoplasm. In principle, the lipid bilayer of liposomes mimics the natural membrane, thus conveniently fusing with the cell membrane, resulting in the immediate and efficient transfer of molecule/drug. The mechanism of liposomal delivery is entirely based on membrane fusion without the involvement of endocytosis, lysosomal degradation, and mitosis.
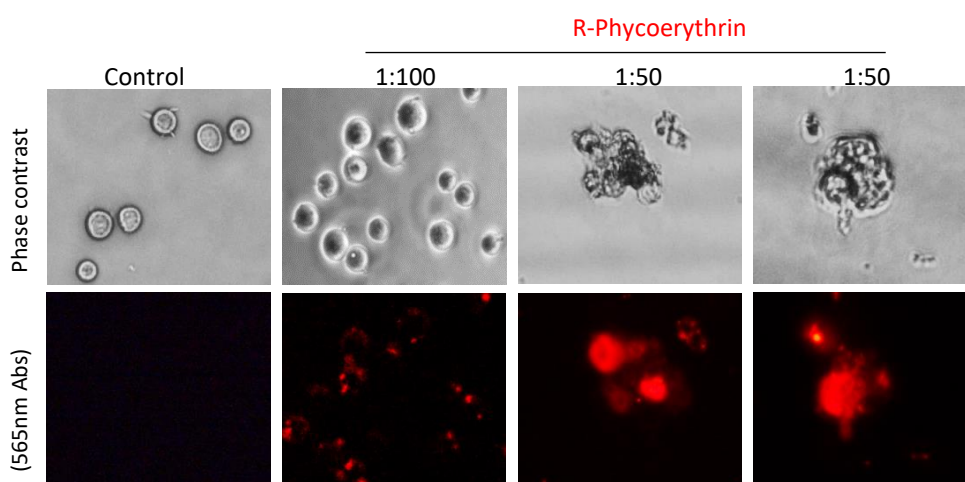

Figure 3.9: Liposomal delivery of R-Phycoerythrin in Jurkat cell: Fluorescent protein (R-Phycoerythrin) was delivered to Jurkat cells by liposomal carrier system. Liposomes were formed as per manufacturer's instructions. Liposomes were allowed to fuse with Jurkat cell membrane in 1:100 and 1:50 ratio. Cells were observed under microscope at 565 nm in 20X objective. It is observed that 1:50 ratio has better delivery of R-Phycoerythrin. Therefore, same ratio was used in Jurkat cell for delivering EVH1 inhibitors.

As a control, I used cell impermeable fluorescent protein (R-phycoerythrin) for transporting in Jurkat cells. R-Phycoerythrin is a large (240 kDa) protein that is unable to pass through mammalian cell membranes without molecular carriers. Liposomes loaded with R-phycoerythrin were prepared according to supplier instructions. To fuse the liposomes, Jurkat cells 1 X10^6 cells/ml were taken in 15ml falcon. Media was removed, and

cells were washed with PBS. Two different concentrations of liposomes were added to Jurkat cells (1:100, 1:50) in order to observe the optimal effect. Jurkat cells were incubated in the water bath at 37 ^{0}C for 3-5 min. Add 9 ml media to stop the fusion process in cells. Centrifuged the cells and replaced the media with fresh media. Cells were observed under a confocal microscope to check the fluorescent protein uptake in the cytoplasm. Liposomes loaded with only protein buffer served as a negative control.

3.5. Significance of ADAP/WAVE2-EVH1 domain interactions in Jurkat cell and U-937 phenotypes:

3.5.1. Role of EVH1 domain-mediated interactions in integrin activation:

Upon activation of TCR or chemokine receptor, the protein complex formed that initiates inside out signaling leads to a conformational change in surface-integrin and makes it highly affine to its ligand. Integrin activation leads to T-cell adhesion and conjugate formation with APC [131]. Both adhesion and APC interaction sites are rich in actin cytoskeletal polymerization. Therefore, it is assumed that actin cytoskeletal machinery is linked to the integrin activation process. ADAP and WAVE2 both are directly related to integrin activation and actin polymerization. Therefore, I aimed to investigate the role of the EVH1 mediated interaction with ADAP and WAVE2 in the activation of integrin (β_1 integrin). For this purpose, **EVH1 inhibitor a and b** were used to understand the effect of inhibition of EVH1 mediated interactions with these proteins on activation of β_1 (CD29) integrin. Further the effects of $ADAP_{MUT}$ and $WAVE2_{MUT}$ constructs in integrin activation were also examined.

PE-conjugated CD29 antibody was used as a marker of β1 (CD29) integrin activation. CD29 antibody binds only to activated integrins, as in the low-affinity conformation of Integrin the antibody binding site is hindered [172]. Solely on activation, the antibody binding site is exposed. Jurkat cells were activated with PMA 100 ng/ml for 10 min at room temp. Cells were washed twice with PBS then labeled with 1:100 PE-conjugated CD29 (β1 integrin) antibody and 200 µM MnCl$_2$ for 30 min at room temperature. Cells were washed and resuspended in FACS buffer and observed in flow cytometry at 561-578 nm. The displayed histogram profiles were representative of four independent experiments. Data obtained by FACS analysis explained that inhibition of EVH1 domain by EVH1 inhibitor had no significant impact on integrin activation. However, integrin activation has markedly declined in $ADAP_{KD}$

as a comparison to WAVE2$_{KD}$ which exhibited no effect. While on the other hand, both ADAP$_{MUT}$ and WAVE2$_{MUT}$ apparently have no altered integrin activation.
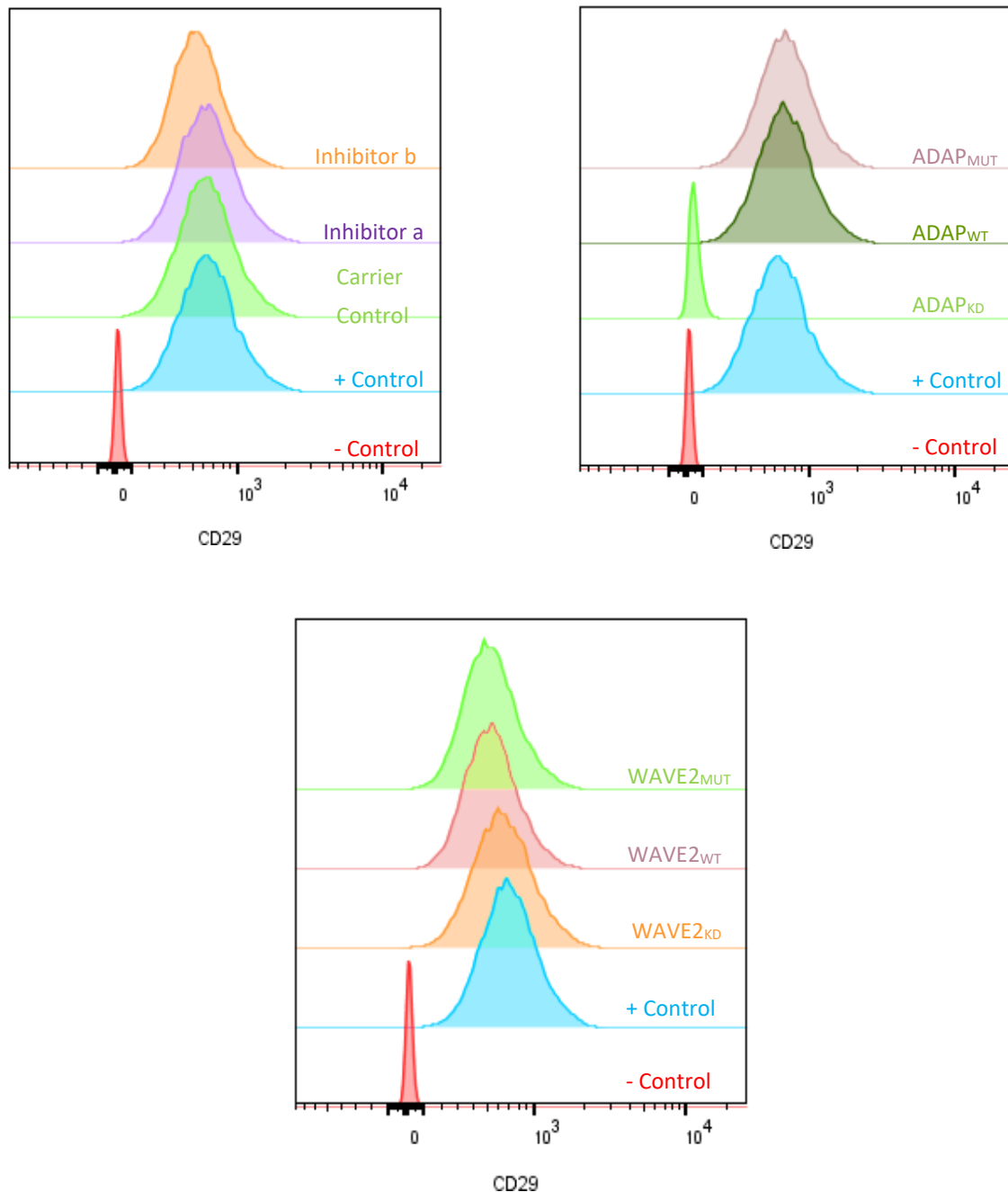

Figure 3.10*: CD29 (β$_1$) activation detected by FACS analysis after stimulation with phorbol myristate acetate (PMA):* Jurkat cells were stimulated by PMA (100 ng/ml) to activate integrin **(β$_1$).** Integrin activation was analyzed by FACS analysis. Jurkat cells were labelled with PE conjugated CD29 antibody to detect β$_1$ activation. Activated Jurkat cells unravel the binding site for CD29 antibody. Jurkat cells without PMA stimulation (-PMA) served as negative control. While the β$_1$ activation were compared to the Jurkat cells stimulated with PMA (+PMA) as positive control. In case of **Inhibitor a** and **inhibitor b** carrier mediated delivery, additional carrier control was taken. Each histogram representing mean of 4 independent measurements.

3.5.2. Inhibition of EVH1 domain-mediated interactions alter the Jurkat cell spreading:

Integrin activation proceeds to the anchoring to its ligand on the surface of endothelial cells or ECM. At this point cells firmly adhere to its counter surface and in order to get maximum contact with the cell surface/ECM, cells initiate spreading. This cellular spreading is the vital initial response of the cell to elicit migration or endothelial invasion. The process of cell spreading involves highly dynamic actin machinery. Therefore, the effect of inhibition of EVH1 mediated interactions specifically with ADAP and WAVE2 on actin cytoskeletal-based cell spreading was primarily focused.

Cell spreading was analyzed by TIRF microscopy. The analysis was performed in GFP-lifeact transiently transfected Jurkat cells plated on ICAM-1 and VCAM-1 coated glass slide. Cell spreading is illustrated by the cell aspect ratio quantified by ImageJ software. Cell spreading data revealed that **inhibitor a** and **b** treated cells were able to adhere to the surface, but they were not efficiently spread over the surface. Similarly, $ADAP_{KD}$ and $WAVE2_{KD}$ showed a significant decrease in cell spreading compared to their wild-types. Interestingly, $WAVE2_{MUT}$ cells showed a substantial loss in cell spreading as compared to $ADAP_{MUT}$. Three independent experiments were performed, the data were pooled and subjected to statistical analysis.
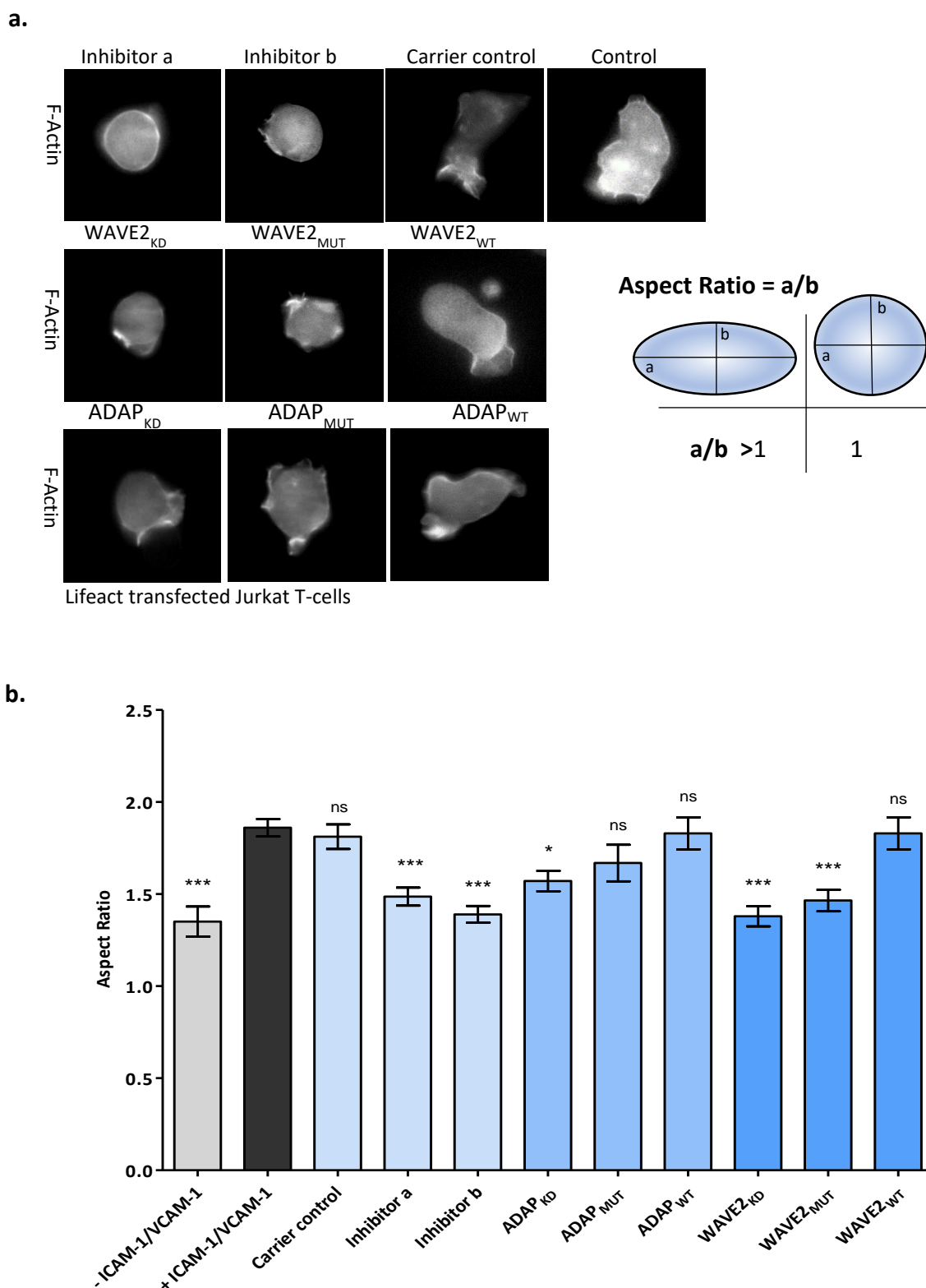
a.

Lifeact transfected Jurkat T-cells

b.

Figure 3.11: Effect of EVH1 domain inhibition on Jurkat cell spreading: a. Jurkat cells were transiently transfected with LifeAct and allowed to spread over ICAM-1/VCAM-1 coated surface for 30 min. Suspended cells were removed and adhered cells were observed under EPI-TIRF (488 nm) and aspect ratio was quantified by imageJ software. **b.** Bar graph represented aspect ratio of the cells from 3 independent experiments. Data was subjected to On-way ANOVA followed by Dunnett multiple comparison test to determine statistical significance. Data was considered significant when *$p < 0.05$, ***$p < 0.001$, n = 3.

3.5.3. Effect of EVH1 domain inhibition in transendothelial migration of Jurkat cells and U-937:

Jurkat cell migration across the endothelial cell barrier requires highly dynamic actin cytoskeletal polymerization. The chemokine gradient triggers transendothelial migration. The chemokine gradient was provided to cells by CXCL12 (100 ng/ml). Cells migrate towards the chemokine gradient and in order to cross transendothelial barrier, the Jurkat cell tends to squeeze through a small space between endothelial cells. This conformational change in Jurkat cells resulted as an outcome of actin cytoskeletal remodeling.

Human umbilical vein endothelial cells (HUVECs) were confluent on the basal side of the transwell insert membrane of 24 well plates. Jurkat cells and U-937 cells were labeled with cytoplasmic cell staining dye CFSE prior to subjecting into the transwell chamber. Cells were allowed to migrate through HUVECs barrier for 2.5-hours. Fluorescent intensity was analyzed at 488 nm by microplate TECAN reader. The following figure reflected the experimental setup for transendothelial migration (Fig. 3.12). The analyzed data represented four independent experiments. The data was normalized, keeping positive control as 100%. Statistical analysis was performed using one-way ANOVA, followed by Dunnett's multiple comparison test.
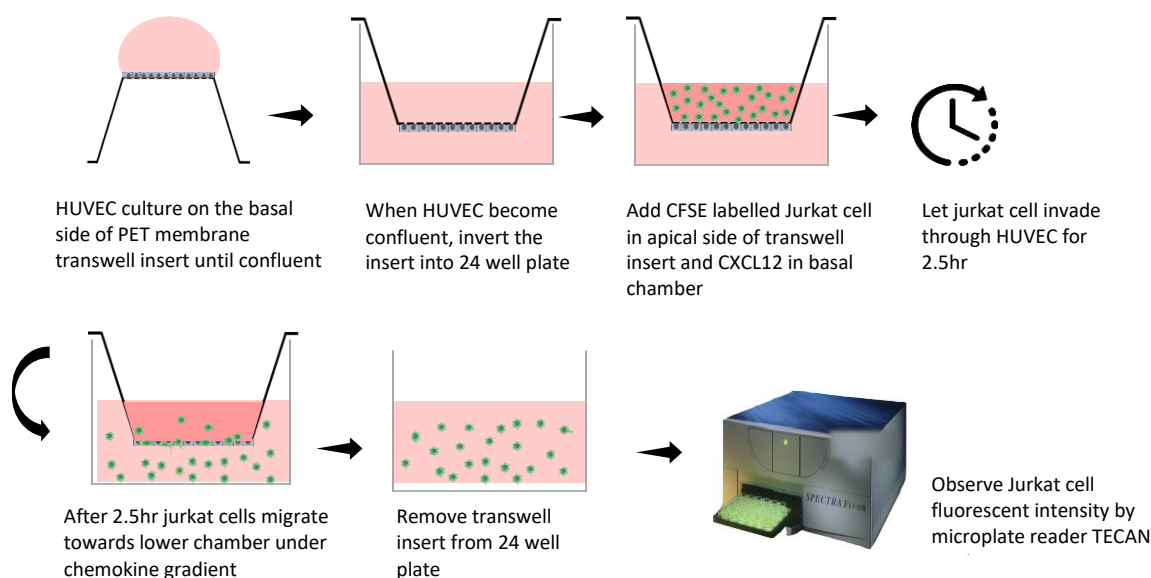

HUVEC culture on the basal side of PET membrane transwell insert until confluent

When HUVEC become confluent, invert the insert into 24 well plate

Add CFSE labelled Jurkat cell in apical side of transwell insert and CXCL12 in basal chamber

Let jurkat cell invade through HUVEC for 2.5hr

After 2.5hr jurkat cells migrate towards lower chamber under chemokine gradient

Remove transwell insert from 24 well plate

Observe Jurkat cell fluorescent intensity by microplate reader TECAN

Figure 3.12: Experimental setup for transendothelial Jurkat cell migration
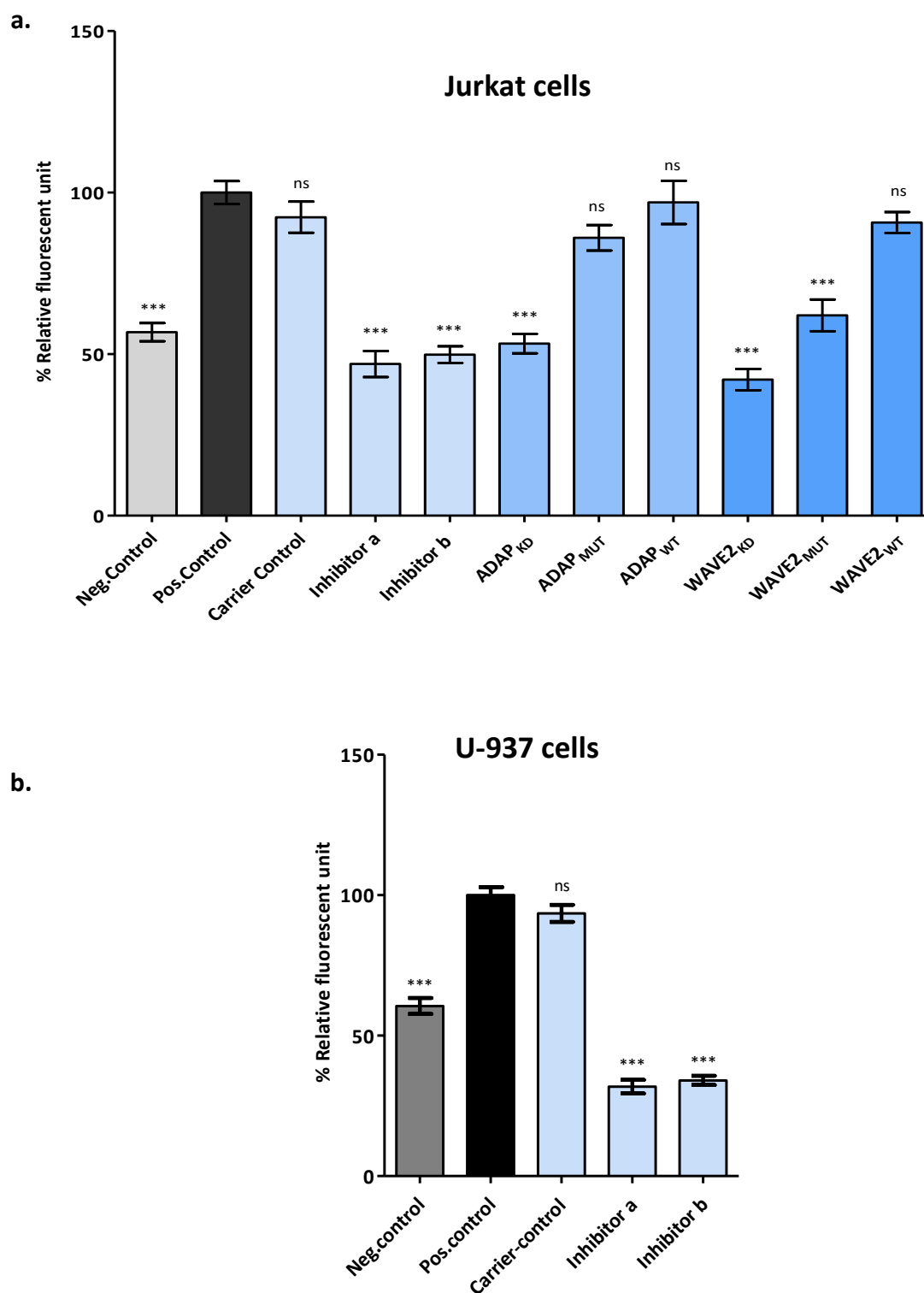
a.

Jurkat cells

b.

U-937 cells

Figure 3.13: Transendothelial migration impairs due to inhibition of EVH1 domain mediated interactions: a. Fluorescently labelled Jurkat cells were allowed to migrate through transwell membrane confluent with HUVECs. 100 ng/ml CXCL12 gradient was provided to lower chamber. The data was normalized to positive control. Condition without provision of chemokine gradient served as negative control. **b**. Graph represented transendothelial migration in U-937 cells under similar conditions. Data obtained from 4 independent experiments was normalized keeping positive control as 100%. On-way ANOVA followed by Dunnett multiple comparison test was applied for determining statistical significance. Data was considered significant when ***$p<0.001$, n = 4.

3.5.4. Effect of EVH1 inhibitor, ADAP and WAVE2-EVH1 binding site mutation in immune synapse formation:

An immune synapse formation between the T-cell and antigen-presenting cell (APC) is a crucial step for the activation of T-cells [37]. With the initial contact formed between T-cell and APC, the cell began spreading around the contact site. Various studies claimed that actin cytoskeletal reorganization at the immune synapse site is indispensable for T-cell activation and recognition of antigen [173]. Actin cytoskeletal polymerization is believed to provide firm contact sites between ligated cells and is involved in reorganizing proteins for T-cell activation [174]. Therefore, the significance of actin polymerization is well established at the immune synapse site.

Jurkat cell-B-cells conjugate formation was observed by dual-color flow cytometry. The mean percent population was noticed in each quadrant of the FACS histogram. Conjugated cells in quadrant Q2 were observed. The FACS analysis revealed EVH1 **inhibitor a** and **b** significantly reduced conjugate population as compared to the control group. Interestingly ADAP$_{MUT}$ expressed substantial loss in immune synapse formation while WAVE2$_{MUT}$ showed no significant effect. A significant decrease in the conjugation of Jurkat cells and B-cells was observed in ADAP$_{KD}$ and WAVE2$_{KD}$ groups. The data represented (Fig 3. 14) from 3 independent experiments and subjected to statistical analysis.
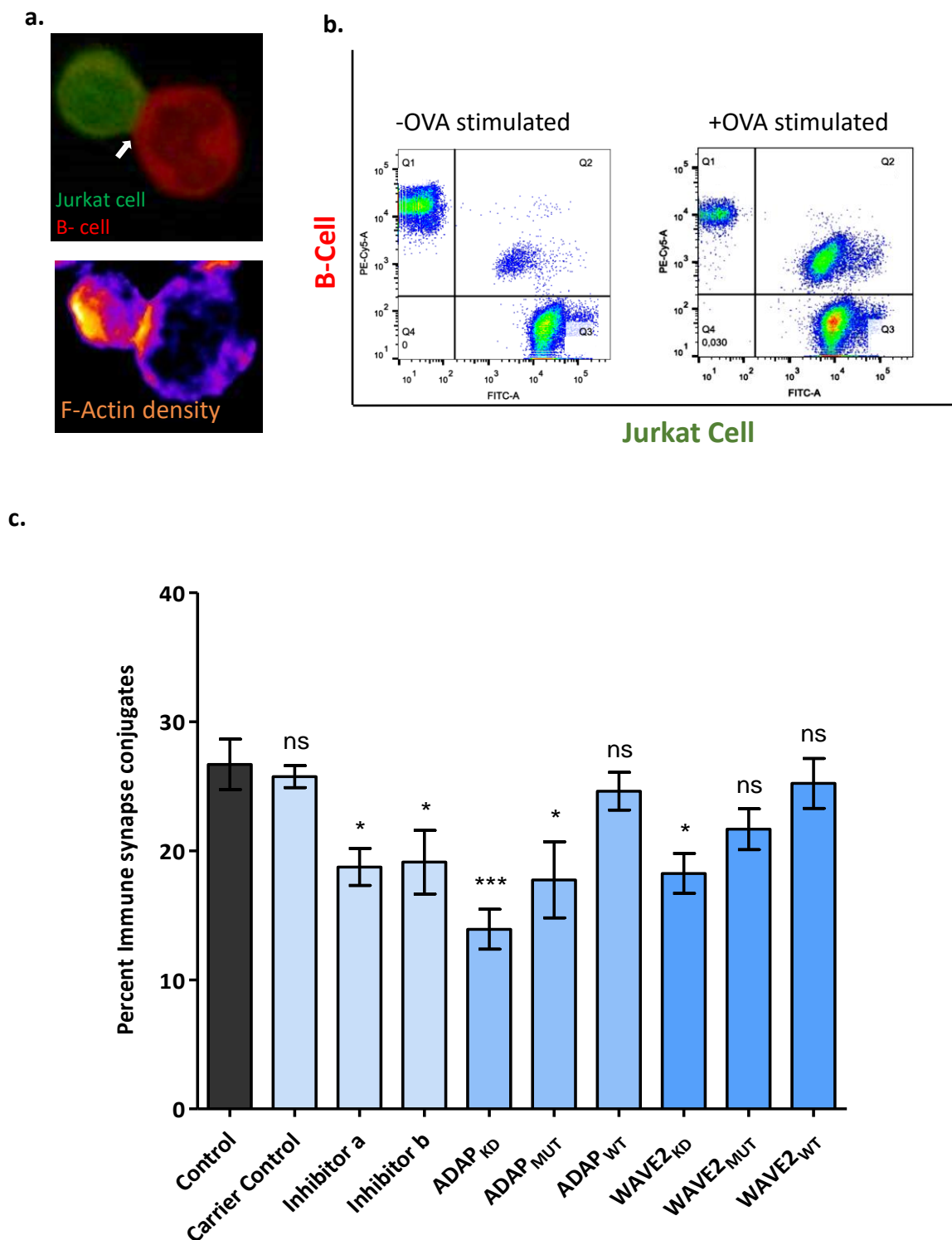
Figure 3.14: Effect of EVH1 domain inhibition in immune synapse formation: a. Represented figure of the immune synapse formation between T-cell (green) and B-cell (red) by confocal laser scanning microscopy. Cells were stained with lifeact dye to visualize actin. Bright yellow color represents actin filament density around contact site. b. Representation of the FACS analysis for the quantification of cell population in different quadrants. Cell population in Q2 quadrant represents conjugate formation. **c.** Bar graphs represent percent conjugated cell population in Q2 quadrant measured from three replicates. The data was subjected to one-way ANOVA with Dunnett's multiple comparison test was applied as post-test to compare all conditions with respect to positive control where $*p < 0.05$, $***p < 0.001$.

3.5.5. EVH1-mediated interactions inhibition affects chemotaxis migration in Jurkat cell:

3.5.5.1. 2D chemotaxis migration:

To observe chemotaxis migration in Jurkat cells, 2D *in-vitro* setup from ibidi μ-slide was used. This setup provided a chemokine gradient while migrating Jurkat cells were tracked over time under video microscopy. **Inhibitor a** and **b** in liposomal preparation were given to Jurkat cells according to the method described in the previous section. Liposomes containing the only buffer were used as carrier control in this experiment. Cells were observed under a brightfield microscope with 4X objective and 1.5X zoom. Cells were recorded over a period of 2 hours with 1 min time interval between each recording. Migration of cells along chemokine gradient was quantified by automatic tracking in ImageJ software. The data from three independent replicates were combined and subjected to statistical analysis. Cell trajectories were representing 50 cells from each condition. The average speed and directionality of migrating cells were measured from the pooled set of populations. The result revealed (in Fig. 3.15) that **inhibitor a** and **b** significantly reduced chemokine-directed migration in Jurkat cells. Both speed and directionality of cells were declined considerably as compared to the positive control.
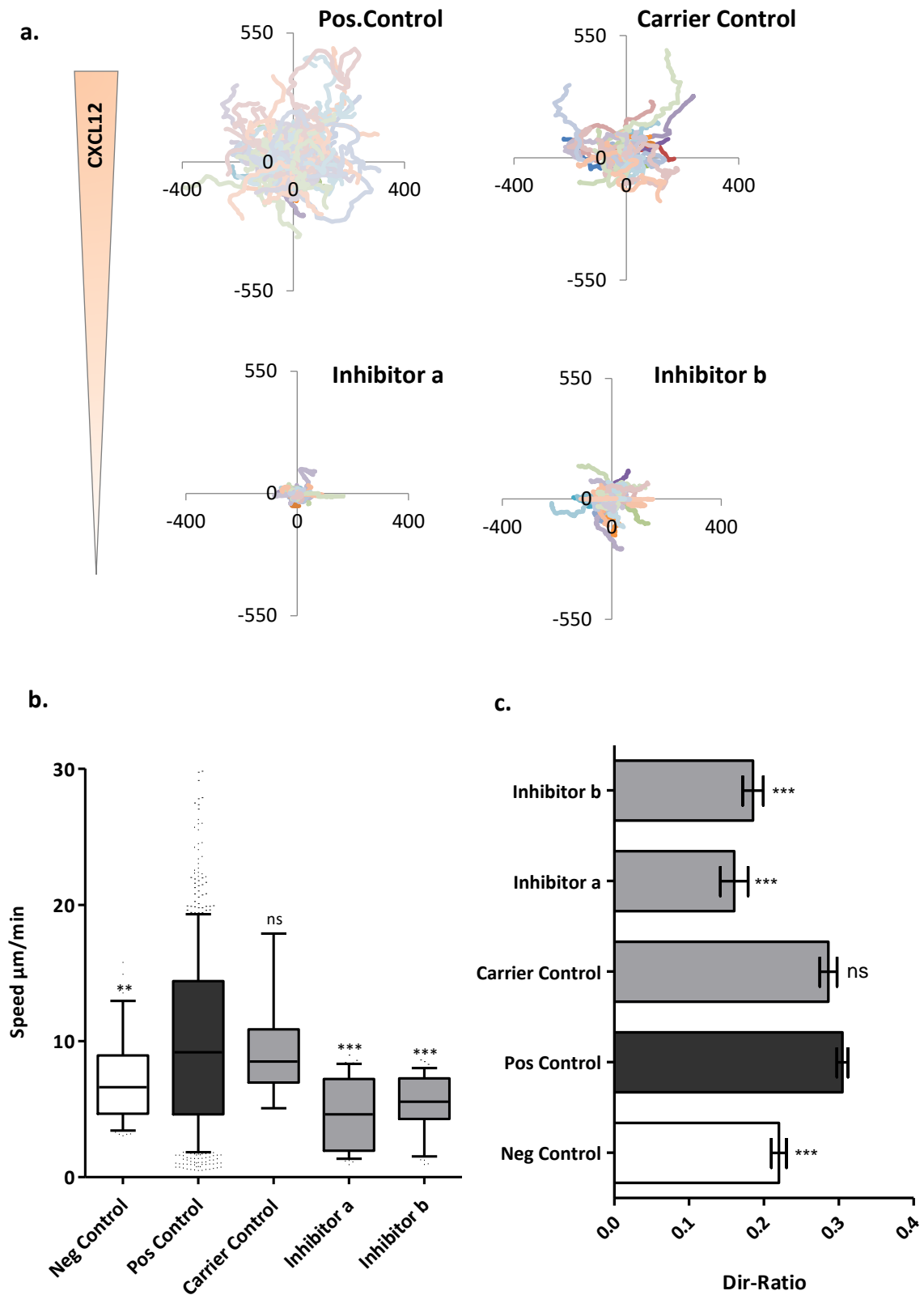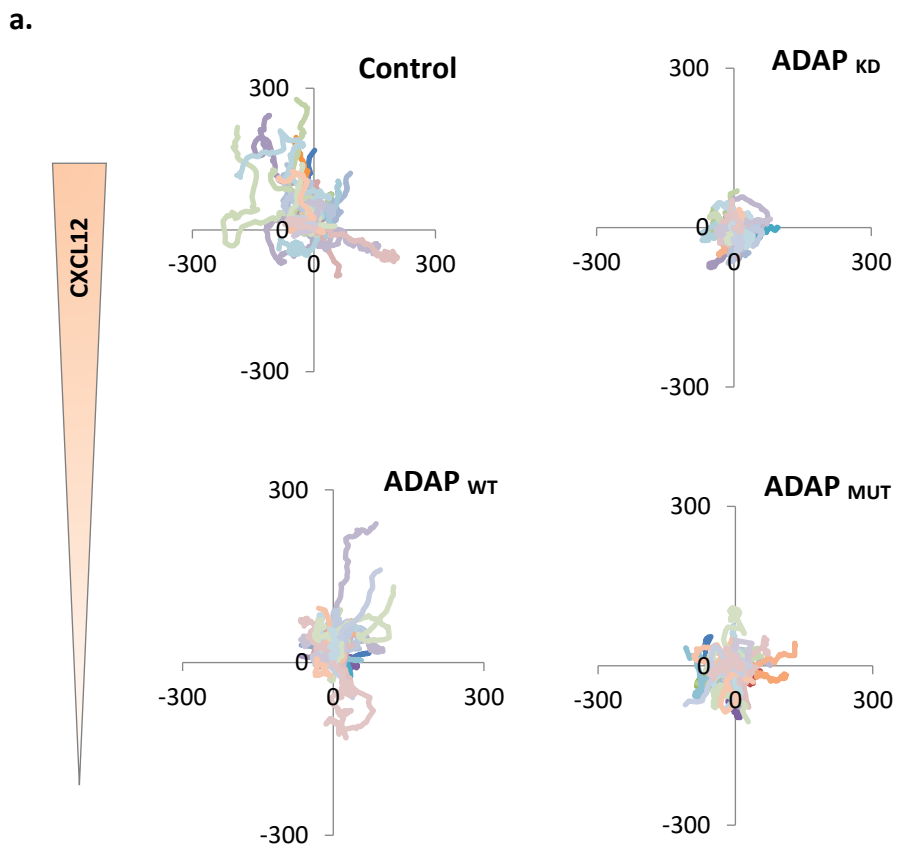
Figure 3.15: 2D chemotaxis migration in Jurkat cell with inhibitor a and b: a. Cell trajectories of Jurkat cells migrating towards chemokine (CXCL12 100ng/ml) gradient were graphed by automatic tracking in ImageJ software. **b and c.** Bar graphs represent speed and directionality of the cells measured from three replicates. The data was subjected to one-way ANOVA with Dunnett's multiple comparison test was applied as post-test to compare all conditions with respect to positive control where $*p < 0.005$. $**p < 0.01$.

Chemotaxis results expressed in figure 3.16 and 3.17 revealed a significant decrease in chemotaxis migration with $ADAP_{KD}$ and $WAVE2_{KD}$. In parallel, Jurkat cells with re-expression of $ADAP_{WT}$ and $WAVE2_{WT}$ showed a non-significant difference with respect to controls. However, $WAVE2_{MUT}$ Jurkat cells have significantly reduced speed and directionality whereas $ADAP_{MUT}$ had a significant reduction in speed, but directionality did not expressively alter in chemokine mediated migration.
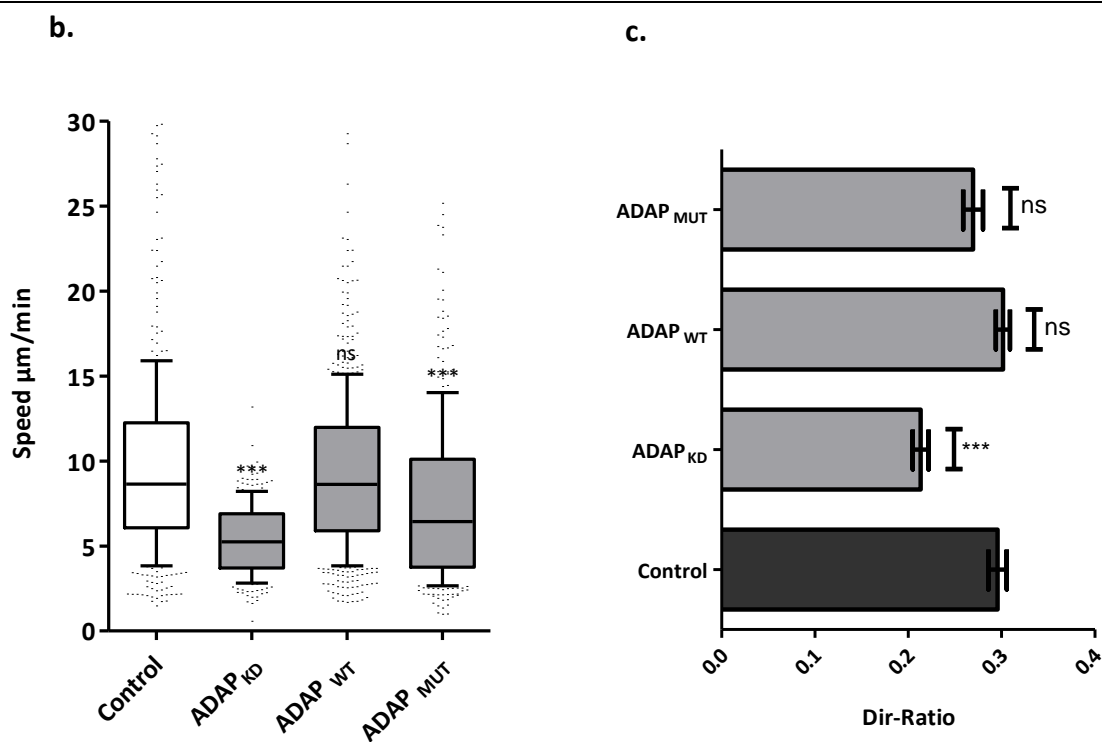
a.

b.

c.

Figure 3.16: 2D chemotaxis migration of ADAP variant in Jurkat cells along CXCL12 gradient:
a. Cell trajectories in graph represent cell migration towards chemokine gradient (CXCL12-100 ng/ml). **b and c:** Cell speed and directionality were quantified by automatic tracking script. Data was analyzed in GraphPad Prism and statistical significance was pronounced after applying one-way ANOVA with Dunnett's multiple comparison post-test to compare all conditions with respect to control. Where ***$p < 0.001$.
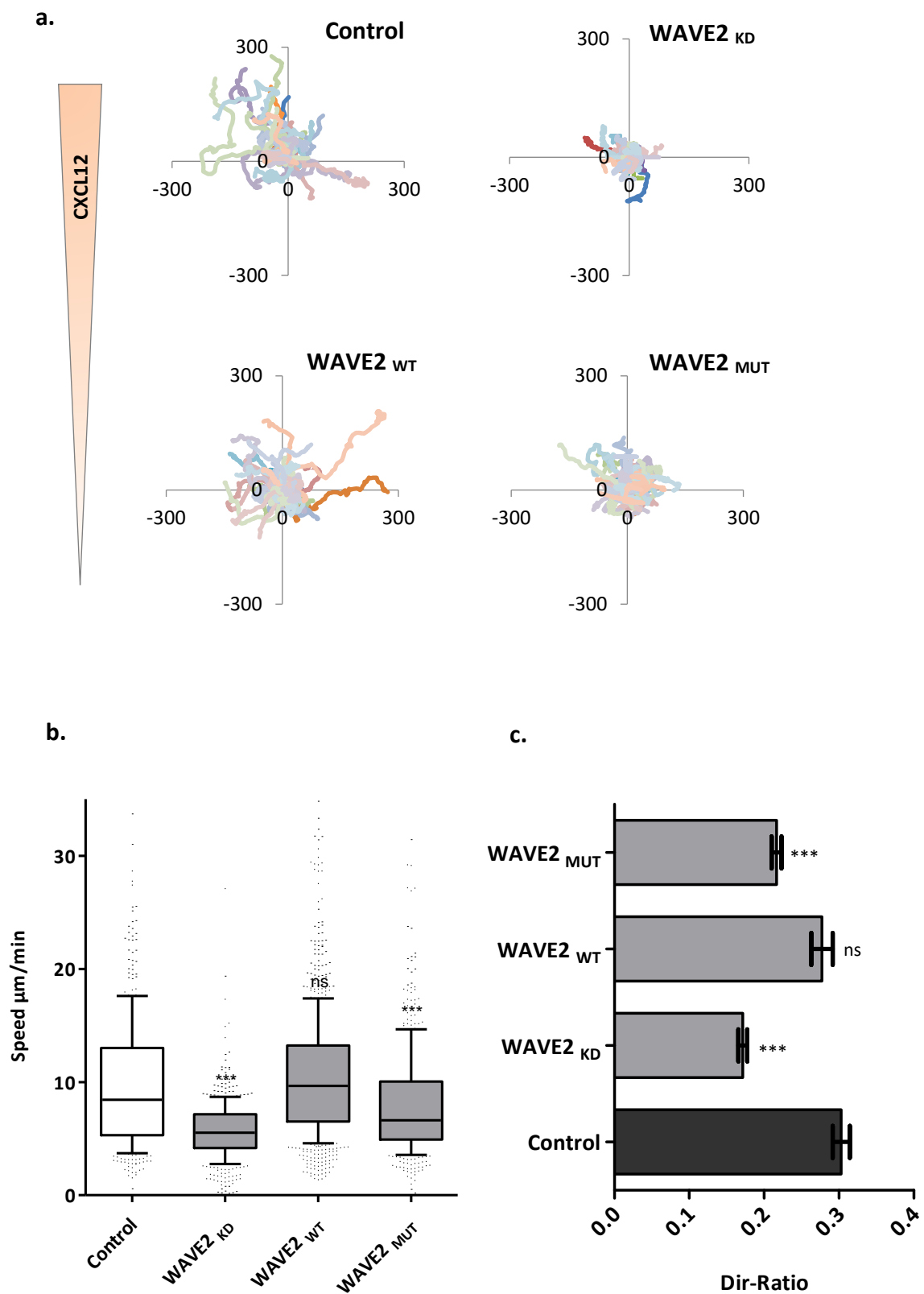
Figure 3.17: 2D chemotaxis migration of WAVE2 variants in Jurkat cells along CXCL12 gradient: a. Cell trajectories in graph represent cell migration in chemokine CXCL12 gradient (100 ng/ml). **b and c:** Cell speed and directionality were quantified by automatic tracking script. The data was analyzed in GraphPad Prism and statistical significance was pronounced after applying one-way ANOVA with Dunnett's multiple comparison post-test to compare all conditions with respect to control. Where ***$p < 0.001$.

3.5.5.2. Loss of chemotaxis migration in 3D collagen environment:

In-Vivo T-cells migrate in a dense extracellular matrix (ECM) and to mimic physiological tissue environment 3D chemotaxis setup was generated, as described in the previous section (2.2.6.4). Jurkat cells were analyzed in time-lapse microscopy. The migration of Jurkat cells along the chemokine gradient was observed in a brightfield microscope with a 10X objective. Migrating cells were captured every 2 min and observed for 4 hours. The data obtained from three replicates were pooled down and subjected to statistical analysis. Results showed in figure 3.18 unveiled no significant difference between positive control and carrier control. However, there was a significant reduction in the average cell speed of the cells with both **inhibitors a** and **b** as compared to the positive control. Jurkat cells also significantly lose directionality with **inhibitors a** and **b**. This suggested that inhibitor has the tendency to inhibit chemokine-mediated cell migration in Jurkat cells by influencing the speed and directionality of cells.
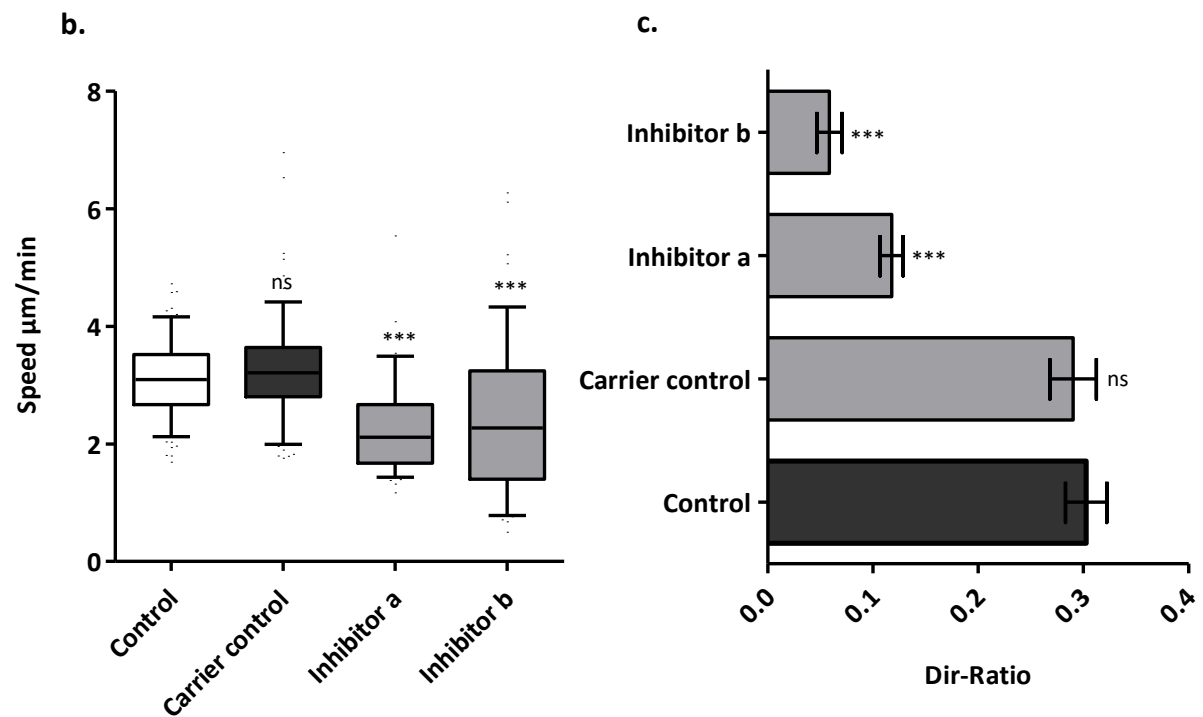
a.

b.

c.
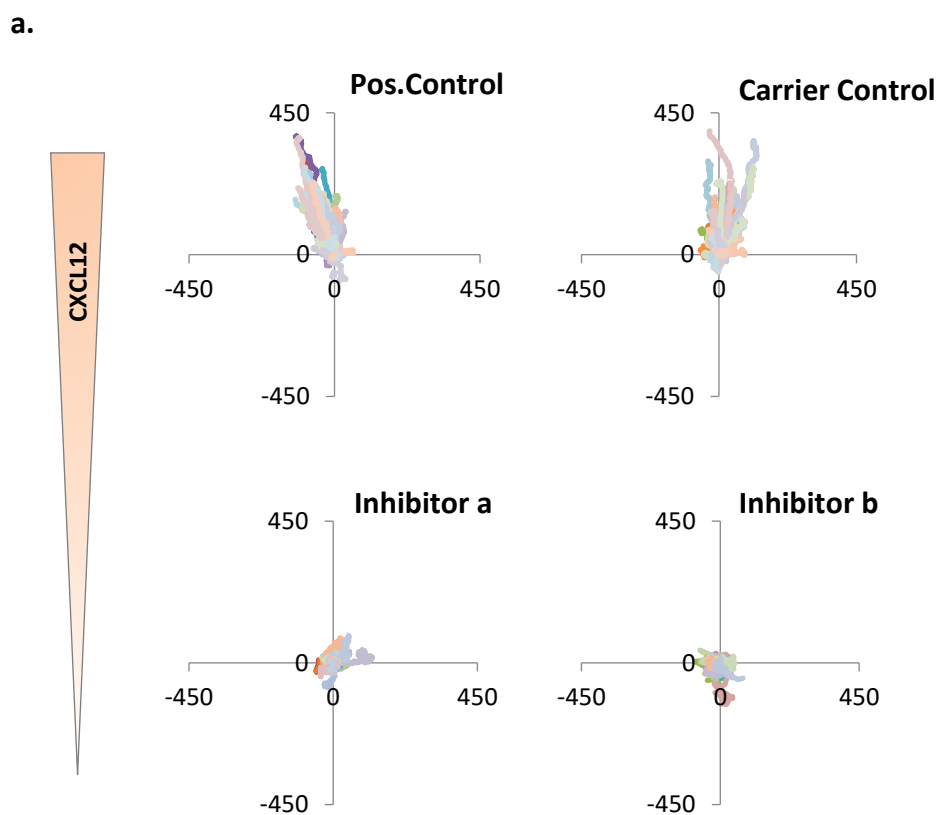
Figure 3.18: Effect of EVH1 inhibitors in Jurkat cell migration in 3D collagen matrix: a. Cell trajectories represent cell migration in CXCL12 100 ng/ml gradient. Cells were treated with **Inhibitor a** and **b** in liposomal preparation. Carrier control cells served as assay control. **b and c:** Cell speed and directionality were quantified by automatic tracking in ImageJ software. The data was analyzed in GraphPad Prism and statistical significance was pronounced after applying one-way ANOVA with Dunnett's multiple comparison post-test to compare all conditions with respect to control. Where *** $p < 0.001$.

IV: DISCUSSION

4: Discussion

To elicit a normal immune response, immune cells undergo activation, differentiation, proliferation, and migration. The actin cytoskeletal system provides the dynamic cellular framework necessary to orchestrate these processes and ultimately regulate immune responses [38]. Thereby, the significance of actin cytoskeletal polymerization in various cellular processes turn it into a promising target in controlling immune cell responses. In this study, the effects of actin cytoskeletal remodeling disruption in integrin-mediated T-cell adhesion, migration, and immunological synapse formation were investigated. In this regard, EVH1 mediated interactions of Ena/VASP proteins were mainly focused. In response to upstream signals, effector proteins bind to the EVH1 domain for recruiting actin machinery to the site of action. Dr. Kühne's lab has designed and developed a small molecular inhibitor that can displace interaction partners from the EVH1 domain [120]. ADAP and WAVE2, the important interaction partners of the EVH1 domain in T-cells, are displaced by these EVH1 inhibitors. ADAP is one of the immune cell-specific adaptor protein that play crucial part in integrin mediated adhesion and migration. While WAVE2 is a member of the WASP family which is involved in the actin-mediated cellular processes like lamellipodia formation, cell spreading, and migration. In Jurkat cells, the expression of endogenous ADAP and WAVE2 was downregulated by using the small hairpin RNA (shRNA) targeting UTR of their sequences. EVH1 binding sites of ADAP and WAVE2 were mutated by PCR with suitable primers. $ADAP_{WT}$/$ADAP_{MUT}$ and $WAVE2_{WT}$/$WAVE2_{MUT}$ were then over-expressed in Knock-down Jurkat cells.

In the first part of my study, I investigated the *in-vitro* binding affinity of the EVH1 domain to putative binding sites of ADAP. Further, the concentration-dependent inhibition of EVH1 inhibitor was examined. In the second part, I focused on uncovering the functional importance of targeting the EVH1 binding sites of ADAP and WAVE2 in immune cells (T-cells, macrophages). In this regard phenotypes like cell adhesion, spreading, migration, and immune synapse formation were closely monitored.

4.1. Identification of EVH1 binding partners in Jurkat cells:

Identification of protein interaction partners is an essential step toward understanding protein functions and determining relevant biological pathways. The mass spectrometric analysis aimed to identify new interaction partners of the Ena/VASP-EVH1 domain in T-cells. Pull-down assay was performed with GST tag Ena/VASP-EVH1 domain attached to glutathione beads, followed by mass spectrometry (MS). Mass spectrometry (MS/MS) is the classical method for the quantitative analysis of protein interaction partners [175]. In mass spectrometry analysis labeling-based quantification approaches were commonly used. Labeling-based quantitation approaches use stable isotope labels that are incorporated within peptides, that introduce an expectable mass difference between two or more experimental conditions. However, this method has potential limitations including increased time and complexity of sample preparation, high-cost reagents, and the requirement of specific quantification software. Therefore, to ward off the issues of labeling methods and achieve faster cleaner, and simpler quantification results there is increased interest in label-free shotgun proteomics techniques now a day. Label-free quantitative proteomics is the mass spectrometry-based method that provides fast and low-cost identification of proteins. Protein quantification is commonly based on two kinds of measurements. The first one is based on changes in chromatographic ion intensity such as peptide peak areas or peak heights while the second one is based on spectral counting of identified proteins with MS analysis [176]. Peptide peak intensity or spectral count is quantified for individual LC-MS/MS runs and changes in protein abundance are calculated via a direct comparison between different analysis.

In this study label-free mass spectrometry approach was used. EVH1 inhibitor was implied as a structural analog of ActA peptide to verify EVH1 domain-mediated interactomes. The protein intensity was used to determine the quantity of a particular protein in control and sample. Mass spectrometry analysis revealed that pull-down complexes from all EnaH, VASP, and EVL-EVH1 domains were enriched with zyxin, vinculin, RIAM, AbI, Arp2/3, WAVE2, ADAP, Nck, and SKAP55. Most of these proteins are known to bind with the EVH1 domain via their proline-rich sequence. Vinculin and Zyxin are known to localize with Ena/VASP at focal adhesions, cell-cell contacts, and along stress fibers where they are suggested to play a fundamental role through regulation of actin dynamics [114,176].

RIAM (Rap1-interacting adaptor molecule) possesses multiple binding sites for the EVH1 domain [151,179]. Various studies reported the colocalization of RIAM with Ena/VASP proteins at the tips of lamellipodia [152,180]. RIAM is involved in the signal transduction pathways like Ras activation to actin cytoskeletal remodeling and inside-out integrin signaling in T-cells. The role of RIAM in cytoskeletal reorganization and integrin activation has implications in cell migration and trafficking. A study by Chen *et al.*, 2014 revealed that the interaction between the Ena/VASP EVH1 domain with components of WAVE regulatory complex (WRC) stimulates Arp2/3 complex-mediated actin assembly in the presence of Rac [177]. This association between EVH1 and WRC increases lamellipodia formation, cell spreading, and migration [181]. The EVH1 domain interacts with an extended proline-rich binding site in human Abi. This binding significantly enhanced Rac to activate WRC-mediated actin polymerization via the Arp2/3 complex. However, it has been discovered that the loss of interaction between Abi mutant and Ena/VASP did not disrupt the ENA/VASP localization at lamellipodia and leading edge [177]. Another component of WRC, WAVE2 has consistently appeared in mass spectrometric analysis. WAVE2 is associated with multiple signaling pathways due to the presence of verprolin-homology cofilin- homology acidic (VCA) domain at their C-terminus. VCA domain binds both actin monomers (via the V region) and the Arp 2/3 complex (via the CA region) [90] for actin nucleation and polymerization. The VCA domain of WAVE2 binds to activate the Arp2/3 complex by inducing conformational changes and delivering the first actin monomer of the daughter filament [155]. The Arp2/3 complex nucleates de novo actin polymerization on the sides of preexisting actin filaments to yield branched structures [182]. WAVE2 was colocalized with Ena/VASP at lamellipodial tips. Chen *et al.,* 2014 revealed direct binding of WAVE2 with EVH1 domain by virtue of carrying $LPPPP_{267-271}$ motif. This binding motif was confirmed by epitope mapping of the proline-rich segment of the WAVE2 by a colleague from our lab Dr. Matthias Müller. Although not much information is available about this interaction, yet it is believed that the WAVE2-EVH1 domain interaction is necessary to stabilize Ena/VASP and WRC interaction and enhance the Arp2/3-based actin polymerization [177,183].

In this study, T-cell-specific EVH1 interactomes identified were ADAP, SKAP55, and Nck. ADAP is a T-cell specific adaptor protein involved in various signaling pathways in T-cells, including integrin inside-out and outside-in signaling, the activation of NF-kB pathway

for subsequent production of proinflammatory cytokines (e.g., IFN-g and IL-2), T-cell trafficking, and in the formation of the immunological synapse [40,184,185]. As an adaptor protein, ADAP bears multiple modular domains that mediate protein-protein interactions. Nck binds via its SH2-domain to the phosphorylated tyrosine $Y_{595}DDV$ and $Y_{651}DDV$ residues of ADAP as shown in figure 1.9. ADAP/Nck cooperatively facilitates integrin-mediated adhesion [186]. Nck and SKAP55 structural analysis revealed both proteins do not possess an EVH1 binding motif. Hence it is proposed these can be secondary binding partners to the EVH1 domain. Whereas, ADAP harbors four proline-rich motifs analogous to EVH1 binding core motif [118,125]. However, only two of them contain the adjacent acidic residues that are essential for binding to the EVH1 domain. At 100 µM concentration EVH1 inhibitor, a significant reduction in peak intensity of ADAP was observed. This corresponds to the findings by Krause *et al.,* 2000 who had indicated the direct interaction of ADAP with VASP. However, it it remains unclear whether that ADAP contains a single or more than one EVH1 binding site. This question was addressed in this study while analyzing the binding affinity between ADAP peptides and EVH1 domains.

4.2. Recognition of EVH1 binding site in ADAP and its binding affinity to the EVH1 domain:

Quantification of protein-protein association is necessary for the biological understanding of the mechanistic model of proteins/signal transduction pathways. The dissociation constant 240 µM between VASP-EVH1 and detected WAVE2 peptide (Ac-SEDNLPPPPAEF-NH2) was already determined by one of my colleagues (Section 3.2.2). ADAP contains multiple putative proline-rich sites (PRS) for Ena/VASP-EVH1 domain recognition [40,187]. Nevertheless, these binding sites of ADAP and ADAP-EVH1 binding dissociation constant were never investigated. Therefore, all putative PRS of ADAP were studied independently for EVH1 binding and the dissociation constant was determined by Isothermal titration calorimetry (ITC). ITC is a useful tool that allows the determination of the binding affinity and the binding enthalpy simultaneously, providing a complete thermodynamic characterization of the ligand binding in one experiment [188].

ITC data revealed that despite multiple PRS, only a single $ADAP_{612-625}$ peptide Ac-SGGIFPPPPDDDIY-NH2 binds to the EVH1 domain. The ADAP-peptide Ac-SGGIFPPPPDDDIY-NH2 exhibits binding affinity with EVH1 domain in the molecular range of KD 70-140 µM. This is likely explained by the fact, that the Ac-SGGIFPPPPDDDIY-NH2 peptide along with the FPPPP motif contains charged core flanking residues necessary to boost the specificity and affinity to the EVH1 domain [121]. The ITC data demonstrated at 25^0C, negative heat pulses indicating exothermic binding, decreasing to baseline levels at higher ligand concentrations. The differential binding curve showed the best fit to the data using a single-site binding model. The finding was consistent with all members of the Ena/VASP family. This result coincides with the previous findings that the proposed C-terminal of ADAP has a binding site for EVH1 domain [40,175]. To verify the single binding site for EVH1 interaction, a mutation was introduced at this specific site of $ADAP_{612-625}$ and mutant ADAP was recombinantly expressed. Spot array analysis of the core motif has revealed the first conserved proline cannot be substituted without the loss of affinity [120]. Thus, the first two prolines of the core motif were replaced in full-length ADAP with random amino acids FPPPP to FGSPP, which resulted in the complete loss of binding to EVH1 domain as shown in the figure 3.4. The cumulative evidence concluded that ADAP has a single binding site at its C-terminal for the EVH1 domain.

4.3. Liposomes enhanced cellular uptake of EVH1 inhibitors:

The *in-vitro* data suggested complete displacement of EVH1 domain interaction partners by the EVH1 inhibitors used in this study. The study in MDA-MB 231 also confirmed the efficiency of the EVH1 inhibitor. Contrary to the *in-vitro* data, initial cellular assays depict the unresponsiveness of EVH1 inhibitos that suspect the bioavailability of the drug. In new drug development, efficient delivery of biologically active molecules into the cell is one of the crucial factors. Initial pharmacokinetic profiling of EVH1 inhibitors by Pharmacelsus GmbH revealed, high metabolic stability, low protein binding, first-order excretion, and suboptimal cell permeation of EVH1 inhibitors. Many developing therapeutics exhibit inadequate pharmacokinetic properties that restrain their use [189]. The plasma membrane serves as the first barrier in transmembrane drug delivery. Generally, small molecular hydrophilic drugs show poor permeability that limits their clinic application because of reduced bioavailability. Thus, it was expected that EVH1 inhibitor possesses sub-optimal cell-permeability.

To improve the therapeutic acceptability of poor cell-permeable drugs, the implication of a carrier-based system is an ideal approach. Therefore, I decided to employ a liposomal drug delivery system for EVH1 inhibitor cell permeation. The advantage of this approach is, delivering inhibitors successfully across the cell membrane without any structural or chemical modification. Liposomes are small cholesterol and natural non-toxic phospholipids vesicles that are artificially synthesized. Mostly liposomes are non-toxic, flexible, biocompatible, biodegradable, non-immunogenic preparations that are intended for systemic and non-systemic administrations [190]. Liposomes mimic natural cell membranes and are widely accepted as drug carriers due to their excellent entrapment capacity. They have been used to improve the therapeutic index of a drug by modifying drug uptake, absorption, reducing metabolism, prolonging biological half-life, or reducing toxicity [191,192]. Various studies describe the feasibility of encapsulation of a wide range of drugs, including anti-cancer, antimicrobial agents, peptides, hormones, enzymes, vaccines, and genetic materials [191,193]. Conventional techniques for the preparation of liposomes do not require sophisticated equipment. Therefore, in this study commercially available liposomal system Fuse-It P by ibidi was utilized. Fuse-It P delivers drug receptor-independently and the delivery was based entirely on fusion mediated across the cell

membrane. Fusion is exclusively driven by physicochemical-attractive interactions between the PM and the lipid bilayer of fusogenic liposomes [194].

Kamalesh *et al.,* 2014 explained how commercially available liposomal formulations for therapeutics like Ketoprofen, furosemide, amphotericin B, doxorubicin, vincristine, and hormones exhibit improvement in their pharmacokinetic parameters. A recent study on ketoprofen encapsulated inside liposome showed 93.3% enhancement in its *in-vitro* dissolution compared to that of free ketoprofen which was 49.77% based on analytical measurements. Similar to that, liposomal preparation of furosemide liposomes has increased the permeability of the encapsulated drug by 28% when compared to free furosemide in *in-vitro* studies [195]. The 30-fold increase in bioavailability of vitamins, minerals, and plant substances was observed when encapsulated in liposomes [190]. EVH1 inhibitors, when encapsulated in fusogenic liposomes, exhibit alteration in Jurkat cells phenotypes. The data depicted that PBS-loaded Jurkat cells have similar results compared to the cells without liposomal exposure. It ascertains the fact that EVH1 inhibitors exhibit poor cell permeability. However, there are some limitations of this delivery system. It is not possible to control the intracellular concentration of EVH1 inhibitors due to the distinct fusion of liposomes to the cell surface. The intracellular concentration of EVH1 inhibitor cannot be controlled thus, cells do not have the homogenous concentration of drug intracellularly. Despite this fact, the liposomal drug delivery system is the best available tool to investigate the effect of EVH1 inhibitors in Jurkat cells. Hence the overall effect in the phenotype of the cell is considered to evaluate the effect of EVH1 inhibitor in T-cell functionality. Based on these, further investigations can be carried out with improved drug modification to make sure homogenous drug delivery.
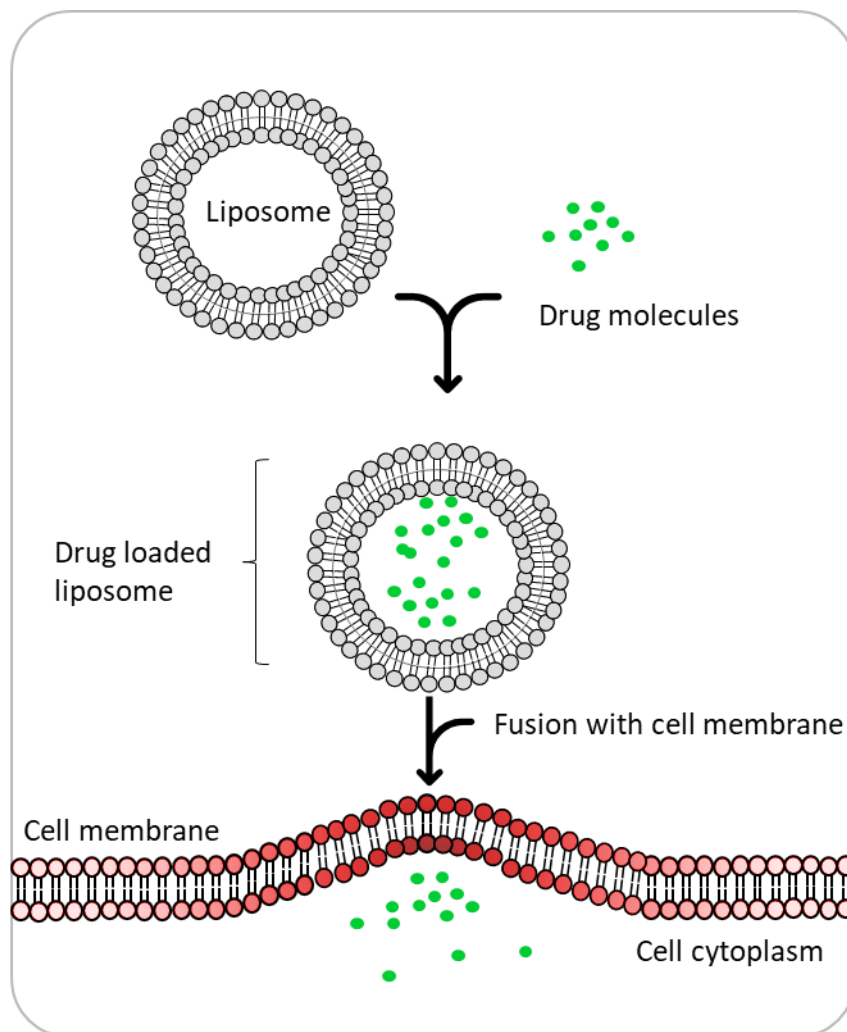
Figure 4.1: Model describing fusogenic liposomal drug delivery across cell membrane: Liposomes deliver drug molecule through fusion to lipidbilyer cell membrane.

4.4. Functional role of targeting EVH1 mediated interactions in Jurkat cell phenotype:

4.4.1. Integrin activation is independent of EVH1 mediated interactions in Jurkat cells:

T-cells regulate integrin activation and function by manipulating the affinity of integrin ligand spatially and temporally. Structural and functional analysis suggest varied ligand affinity states of integrin from low, intermediate to high. Crystal structure uncovered the inactive form of integrin present in folded V-shaped structure with the head of the integrin heterodimer bent close to the proximal regions of the extracellular base of integrin (Fig. 4.2). Integrin undergoes reversible conformation transition from low affinity bent form to high ligand affinity. The integrin extended-open state has 5,000-fold higher ligand affinity than the bent-closed and extended-closed states [196]. Integrin activation leads to various signaling pathways necessary for cell functionals such as adhesion, spreading, migration to lymph node, site of inflammation, and generation of the immunological synapse. In addition to these, integrins also serve as a costimulatory molecule in antigen recognition [197]. Mechanisms for regulating T-cell adhesion include (i) enhanced affinity of cell surface integrin receptors for their extracellular ligands and (ii) modification of cellular actin cytoskeletal network following post-receptor occupancy [167]. Thus, integrin activation is a prerequisite for firm adhesion, necessary not only in transmigration but also in the formation of the immunologic synapse during the contact between naïve T-cells and APCs.

FACS analysis data for integrin activation revealed that ADAP$_{KD}$ Jurkat cells exhibited a significant reduction in CD29 (integrin) activation (Fig. 3.10). This can be explained by the fact, that ADAP is an adaptor protein that is involved in several signaling pathways for integrin activation [198,199]. In T-cells, SKAP55 expression is well controlled as a positive regulator for integrin activation, T-cell adhesion, and conjugate formation with APC. ADAP/SKAP55 signaling module also strongly attenuated activation of integrins [33,43]. Structure-function analysis of the ADAP/SKAP55 signaling module revealed that a mutation which hinders the binding of ADAP and SKAP55 strongly reduces integrin activation [33,150]. It is identified that the disruption in the ADAP/SKAP55 interaction results in the small GTPase Rap1 displacement from the PM without influencing its GTPase activity [132]. The further analysis revealed SKAP55 as an essential binder of RIAM. SKAP55/RIAM complex associated

with active Rap1 localization. SKAP55/RIAM interaction disruption diminished T-cell adhesion to fibronectin and ICAM-1 as well as the ability of the T-cell to form an immunological synapse with APCs [152]. This suggests the potential function of ADAP and SKAP55 as a scaffold that is indirectly involved in active Rap1 recruitment. Further, loss of ADAP in Jurkat cells destabilizes SKAP55 and induces its degradation [150]. A study in ADAP-deficient mice revealed that its primary peripheral blood T-cells concomitantly lack the expression of SKAP55, while SKAP55 mRNA expression is readily detectable. While SKAP55-deficient T-cells express normal ADAP levels and exhibit no major alterations in T-cell phenotype [33]. The data suggested that the loss of SKAP55 might be compensated by SKAP-HOM, which is expressed in T-cells as well.

ADAP also interacts with EVL/VASP proteins, which consider facilitating integrin activation. However, based on the data of our study, it appeared that ADAP-EVH1 binding does not play part in the change of integrin affinity. This effect is further confirmed by using the EVH1 inhibitors that presented similar results. Jurkat cells treated with EVH1 inhibitors also exhibited no alteration in integrin activation. Thus, it is suggested that the ADAP-EVH1 interaction might facilitate integrin linkage to F-actin however, this interaction is not implicated in integrin conformational changes or activation.

The actin regulatory protein WAVE2 is considered as an essential component of the "inside-out" signaling required for TCR-mediated integrin activation [154]. VCA-Arp2/3 complex links WAVE2 to the integrin scaffolding proteins vinculin and talin. The formation of a WAVE2-Arp2/3-vinculin complex leads to talin recruitment to the PM and its high-affinity binding to the integrin tail [200]. In contrast to that, no significant on integrin activation effect was observed by WAVE2$_{KD}$ cells. It is assumed that actin polymerization is not involved in the integrin conformational shift. Integrin activation can be differentiated into two parts. Upon suitable signals, the initial change in conformation of integrin subunits enhance its affinity. Then high-affinity integrin binds to its ligand to convey outside-in signaling that links integrin tail to cellular actin cytoskeletal network [34]. The limitation in our FACS analysis is that it entirely focuses on determining integrin activation based on its conformation. Therefore, based on the FACS observations it is suggested that WAVE2 does not contribute in the change of integrin conformation. Similarly, ADAP plays an important role in the activation of integrin signaling pathways however its link to Ena/VASP via the

EVH1 domain did not exhibit any contribution to this process. Further, **EVH1 inhibitor a** and **b** data confirms that EVH1 mediated interactions are not involved in the integrin receptor conformational shift. In conclusion, ADAP and WAVE2 are important players in the integrin signaling but their EVH1 mediated interactions do not implicate in the initial step of integrin activation. It is assumed that actin polymerization machinery that is linked to integrin activation is involved in affinity maturation and integrin-mediated adhesion/protrusion formation. The further investigations are necessary to validate this conclusion. However, the next section can explain the effect of actin-based cell spreading mediated by firm integrin adhesion.
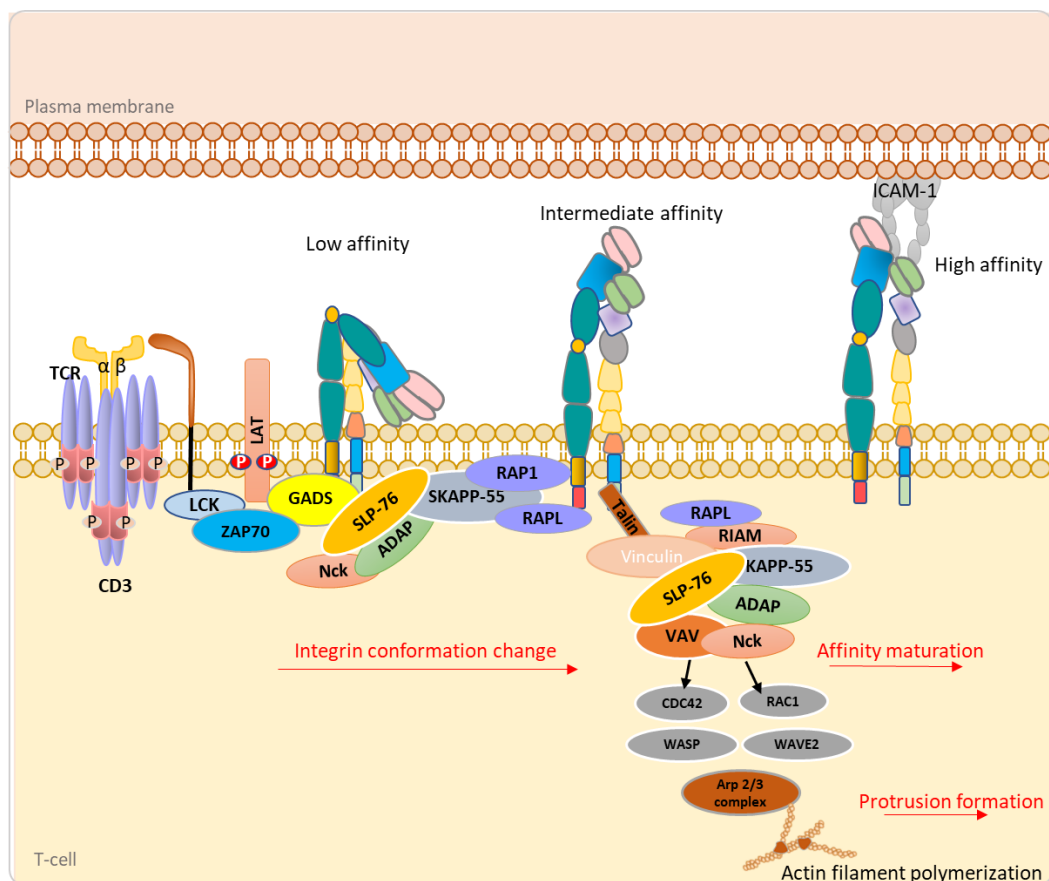
Figure 4.2: Proposed model of T-cell signaling in Integrin conformational changes: SLP76/ADAP/SKAP55 signalosome alter low-affinity bend form of integrin to active. Integrin with intermediate affinity linked to its counter ligand ICAM-1. While WAVE2/Arp2/3 mediated actin polymerization is involved in affinity maturation and T-cell spreading.

4.4.2. T-cell spreading dependant on WAVE2-Ena/VASP interaction:

Integrin receptors not only act as an adhesion molecule but also serve as a signaling receptor by actively regulating the F-actin reorganization that is essential for T-cell-dependent processes [201]. Integrin-mediated adhesion is a prerequisite for cell spreading, migration, and immunological synapse formation during the contact between naive T-cells and APCs. Integrin-dependent cell spreading is characterized by the extension of the cell membranes with underlying cytoskeletal structure, where integrin ligand adherent cells extend outward membrane protrusion towards chemokine signals to form new integrin-dependent adhesions. Cell spreading involves distinct morphological modification of cell membranes including the formation of protrusions, filopodial extensions, and lamellipodia [29]. Lamellipodia are thin actin protrusions at the very leading edge of migrating cells and are enriched with branched-chain actin filaments nucleated by the Arp2/3 complex. In the lamellipodia, rapid actin treadmilling mediated by the Arp2/3 complex is considered essential for chemokine directed cell migration. While forward propulsive forces are created by the actin machinery situated near focal adhesion sites [35].

The WAVE complex plays the main role in the Arp2/3 complex activation for actin filament nucleation and their assembly in migrating cell lamellipodia. Other important participants in lamellipodial protrusion formation are Ena/VASP proteins, which enhance actin filament elongation. WAVE2 an important subunit of the WAVE complex also holds direct interaction with Ena/VASP proteins via its EVH1 domain [183]. The significance of the EVH1 mediated interactions in cell spreading was investigated in this study using TIRF microscopy. The change in cell morphology from round to stretched was analyzed and cell aspect ratio was quantified. The significant loss in the aspect ratio of WAVE2$_{KD}$ and WAVE2$_{MUT}$ Jurkat cells was observed (Fig. 3.11). The substantial loss of WAVE2$_{KD}$ cell spreading data is more likely to be associated with disruption of WRC. However, Jurkat cell aspect ratio in WAVE2$_{MUT}$ cells appears difficult to understand. As RIAM is an important regulator of cell protrusion formation. Direct binding of RIAM to Ena/VASP-EVH1 domain, helps in delivering it to the growing barbed ends, where Ena/VASP exhibited its actin polymerization activity [179]. Moreover, RIAM also colocalizes with the WAVE complex at the very edge of lamellipodia and directly interacts with this complex by binding to the Abi-SH3 domain. Hence, RIAM is assumed to acts as a platform to link Ena/VASP and the WAVE

complex at the leading edge of cells to regulate lamellipodium formation and cell migration [202]. However, despite the presence of intact RIAM, and Ena/VASP, the decrease in cell aspect ratio in WAVE2$_{MUT}$ cells cannot be explained. Law A. *et al.,* 2013 showed in his study that EVH1 binding site deletion in RIAM does not affect lamellipodia formation. It is suggested that the function of RIAM in T-cell migration is not mediated by Ena/VASP proteins but is predominantly facilitated by the WAVE complex [202]. The other possible explanation is, at cell leading-edge highly branched actin filaments are formed by the Arp2/3 complex. WAVE2 coordinates molecular collaboration between the Arp2/3 complex and Ena/VASP via direct binding to them. WAVE2 in membrane-bound WRC, activates the Arp2/3 complex with its VCA domain, which then shortly dissociates to allow a new branch to grow. While WAVE2 also recruits Ena/VASP in addition to binding and activating the Arp2/3 complex. This colocalization increase surface-directed polymerization on its own, and also provide new filament primers for subsequent rounds of Arp2/3 complex–based branching [183]. This finding is consistent with transendothelial migration assay, where WAVE2$_{MUT}$ cells showed reduced invasion through HUVEC cell layer barrier (Fig. 3.13). Thus, based on available data it can be concluded that WAVE2-EVH1 direct binding is required for potentiating Arp2/3 complex activity and lamellipodial actin assembly. In the absence of WAVE2-EVH1 binding, the process of lamellipodia formation may slows down. Although there is not sufficient data available in the favor of this explanation. As in cell spreading and transendothelial migration assay, only endpoint readings were taken after a given time. Time-lapse observation can give a better insight to this process. The EVH1 inhibitors data of Jurkat cell spreading confirmed this further. Although significant reduction in cell aspect ratio seen by the EVH1 inhibitors is not only linked to the reduced lamellipodia formation. The loss of Zyxin-Ena/VASP at focal adhesion points that provide traction forces for the cells to extend forward is also involved [178]. Therefore, it is believed that inhibition of EVH1 mediated interactions can reduce cell spreading process which is a prerequisite to migration and invasion.

A significant loss of cell aspect ratio in ADAP$_{KD}$ was quite expected. As described in previous chapter, ADAP is an important adaptor protein bearing binding sites for various crucial signaling proteins/molecules for inside-out and outside-in signaling. Integrin mediated adhesion is an initial step in cell spreading and migration. Therefore, in ADAP defiecient cells, integrin activation is impaired and thus the cell spreading. This finding was

consistent with the transendothelial migration assay data in which ADAP-deficient T-cells interact with the endothelial cells was analyzed. ADAP-deficient T-cells exhibit reduced contact times with the endothelial cells [43]. On the other hand, ADAP$_{MUT}$ does not show a noticeable difference in cell spreading as compared to ADAP$_{WT}$. It is believed that RIAM is associated with the ADAP-SKAP55 module, upon chemokine receptor signaling. Hence, the RAPL/Mst1/Rap1 and RIAM/Rap1/Kindlin/Talin complex are recruited to the PM where RIAM activates Ap2/3 mediated actin polymerization via WRC [144,152]. Hence, ADAP's direct link to Ena/VASP via EVH1 domain does not specifically imply in cell spreading or invasion.

4.4.3. EVH1 domain-mediated interactions affect chemotaxis migration in Jurkat cells:

Cell migration is a very complex and highly regulated process, in which intracellular and extracellular signals are interconnected to generate a coordinated response. The migration process comprises precise and inter-related steps that involve front-to-back actin polarization in response to extracellular cues. The integration of migratory signals into coordinated cell shape remodeling is achieved by the actin cytoskeleton. Rapid and dynamic remodeling of the actin network provides the physical force for the formation of the protrusions that allow complex motility tasks such as cell body translation, environment probing, and invasion through tissue barriers [127]. Actin is the fundamental molecular machinery that manages protrusions and adopts different organizations in lamellipodia and filopodia. Lamellipodia are the thin widely spread structure at the front or leading edge of the cell. It is made of dense filament meshwork that is composed of highly branched actin fibers [109]. The other structure formed at the leading edge is characterized by the presence of long, thin, and linear protrusions of various lengths called filopodia. Filopodia are the parallel bundles of cross-linked actin fibers which carry out an exploratory function. Filopodia can either be embedded within the lamellipodium or emitted independently [28]. For lamellipodial formation, the small GTPases Cdc42 and Rac activate adaptor and signaling molecules of the Wiskott-Aldrich syndrome protein family such as WASP and WAVE, which ultimately activate the Arp2/3 complex. This complex nucleates actin-filament branches, and results in a broad dendritic-like actin network [161,200]. In filopodia, Cdc42 promotes linear actin polymerization via formins and Ena/VASP [108]. The physical structure of filopodia and lamellipodia is characterized by dynamic actin remodeling, which allows accomplishing complex cell motility steps such as directed migration, invasion, and interaction with other cells. T-cells excel in these motility steps to ensure their role during immune surveillance.

Jurkat cells were exposed in this study to a chemokine gradient in the chemotaxis microchamber in order to monitor their migration characteristics for two hours over one min. intervals. Parameters like chemotaxis migration, average speed and directionality ratio were focused. As expected, Jurkat cells deprived of WAVE2 exhibit defective chemotaxis migration and a significant reduction in average speed was observed. In addition to that,

the directionality ratio was also declined significantly. The WAVE2 in WRC is the main Arp2/3 complex activator for nucleation and assembly of the actin filaments in the migrating cell lamellipodia. Our findings have intriguingly resembled the study in megakaryocytes where WAVE2-/- exhibited defective peripheral lamellipodia formation on fibrinogen, indicating WAVE2 is required for the integrin-mediated cell spreading [203].

Chemotaxis migratory data of WAVE2$_{MUT}$ in this work have shown a comparable decrease in chemotaxis migration and parameters like average speed and directionality. This can be explained as WAVE2 in WRC activates the Arp2/3 complex via its VCA domain which then shortly dissociates from the activated Arp2/3 complex to allow a new branch to grow. WAVE2 also recruits VASP via its EVH1 domain in addition to binding and activating the Arp2/3 complex. Thus, the Ena/VASP provides a link between the Arp2/3 complex and the actin network while it enhances the growth of new barbed ends. This could not only increase surface-directed polymerization on its own, but it could also contribute to providing new filament primers for subsequent rounds of Arp2/3 complex–based branching [183]. Therefore, based on our chemotaxis data there is a possibility that WAVE2-EVH1 direct binding is required for potentiating Arp2/3 complex activity and lamellipodial actin assembly. Thus, it can be assumed that in the absence of WAVE2-Ena/VASP binding, the process of lamellipodia formation slows down. The data from the EVH1 inhibitors **a** and **b** further confirms these findings. The 2D and 3D chemotaxis migration data of the EVH1 inhibitors is comparable. Collectively the data revealed a significant reduction in average speed and directionality ratio during chemotaxis migration. The decrease in directionality ratio by WAVE2$_{MUT}$ Jurkat cells was unclear. Barzik *et al.,* 2014 have shown mDia1/2 initiated filopodia formation with Ena/VASP to probe the surface for chemokine signals. Despite the intact mDia1/2-Ena/VASP assembly, a decrease in directionality ratio can be elucidated as directionality ratio d/D measures the deviation between path distance (D) and linear distance (d) from start to end point. Whereas in WAVE2$_{MUT,}$ the delayed process of lamellipodial formation might influence the overall directionality ratio of the cells. When critically examined EVH1 inhibitors data of directionality, a potential decrease in directionality ratio is seen comparable to WAVE2$_{MUT}$. Collectively, EVH1 inhibitor data demonstrate that EVH1 mediated interactions are necessary for the recruitment of actin machinery at the effector site. EVH1 domain inhibition negatively impacts all parameters of

Jurkat cell migration. These findings are in line with the data from MDA-MB231 cells in which EVH1 inhibitors significantly reduce breast cancer invasion and migration [120,204].

ADAP knock-down Jurkat cells expressed a reduction in speed and directionality ratio as seen in figure 3.16. This can be explained as adhesion is the fundamental step for the initiation of migration. Geng, L. *et al.,* 2001 have already shown that ADAP-deficient T-cells defects in integrin-mediated cell adhesion [184]. Secondly, actin filaments forming protrusions are linked to the adhesion assembly [35]. On the other hand, ADAP$_{MUT}$ Jurkat cell data depicted a noticeable change in average speed of the cell however, directionality is unaltered. The effect on the average velocity was unusual and cannot be explained as integrin activation data did not show any defect in ADAP$_{MUT}$ Jurkat cells. These ADAP$_{MUT}$ findings were also not in line with our Jurkat cell spreading data. It is assumed that ADAP-Ena/VASP interaction may play a partial role in outside-in signaling linking the actin network to adhesion assembly during chemokine-directed migration. Therefore, when ADAP-Ena/VASP assembly is disrupted the process of migration slows down. This can then explain our ADAP$_{MUT}$ cell spreading data where end point measurements were taken. However, a detailed investigation of ADAP-EVH1 binding is required to uncover its role during the cell migration. Overall, the potential role of EVH1 mediated interactions in chemokine directed migration predicted as a promising target for regulating cell migration. Future studies should extend to animal models to carefully examine the effect of EVH1 mediated interactions in cell migration.

4.4.4. EVH1 mediated interactions interfere in immune synapsis formation:

T-cells and antigen-presenting cells conjugation is the determinative event in the initiation of an adaptive immune response. The immunological synapse (IS) acts as a platform for signaling complexes leading to proliferation, differentiation, and effector function of the T-cells. The differentiation of naïve T-cells into specialized effector cells is initiated from signals triggered by the T-cell receptor (TCR) following engagement with specific peptide antigen associated with the MHC on antigen-presenting cells (APC) surface. The TCR–MHC engagement is not sufficient to induce activation of naïve T-cells hence, additional costimulatory signals facilitate the process to lower the threshold dose of antigen to achieve T-cell activation. The TCRs, integrins, and co-stimulatory receptors work in coordination. The TCR-MHC along with costimulatory signals are integrated to elicit both short-term effects such as the dynamic reorganization of the actin and tubulin cytoskeleton for firm engagement and initiate gene expression cascade that will produce effector or memory T-cells [205]. In addition, to provide cell-cell adhesion, LFA-1-ICAM-1 engagement delivers specific intracellular signals (outside-in signaling) that lower the threshold dose of antigen required to achieve T-cell activation. Actin network exerts a special centripetal force on LFA-1, encouraging the conformational changes needed for high-affinity ligand binding. Moreover, the actin network facilitates costimulatory signaling and organizes its spatial arrangement at the IS [206].

The three-dimensional contact domains in T-cell and APC interface at IS due to receptor clustering, and intracellular proteins rearrangement appeared to contain distinct surface molecules, named 'supramolecular activation clusters' (SMACs). In the mature IS, centripetal force relocates TCR/MHC complexes to the center of SMAC (cSMAC) together with their co-stimulatory molecules, intracellular kinases, and adaptor proteins. Whereas LFA-1-ICAM-1 complexes are distributed to the integrin-enriched peripheral SMAC (pSMAC). In pSMAC, LFA-1 initiates T-cell activation by accumulating TCR/MHC complexes in the cSMAC and other signaling molecules to the pSMAC. Outside the pSMAC is an actin and CD45-rich ring called the distal-SMAC (dSMAC) [207]. Evidence provided by live-cell microscopy revealed actin network flow from the outer edge of the synapse inward, sweeping in TCR microcluster and providing force to activate LFA-1 [38,208]. Despite the

contribution from myosin motors, actin polymerization is the main force driving the actin flow [209].

WASP is associated with dynamic actin-mediated cellular events such as membrane protrusion formation, endocytosis, and vesicular trafficking. WASP recruitment to the T-cell -APC contact site and its functional activation are triggered by the Rho GTPase, Cdc42, and phosphorylation on Y291 [148,210]. WASP is considered to be predominantly involved in the stabilization of the IS. Unlike WASP, the dynamic molecular interactions regulating WAVE2 recruitment to the PM specifically in the TCR signaling complex are largely unknown. Recent studies revealed the role of WAVE2 as the main regulator of F-actin polymerization downstream to the T-cell receptor (TCR). WAVE2 complex is required for TCR-mediated Rap1 activation. It was shown that RNAi-mediated depletion of WAVE2 inhibits TCR-induced spreading and F-actin polymerization at the IS [211,212]. In this study, FACS analysis of WAVE2$_{KD}$ in Jurkat cells exhibits impaired ability to form a conjugate with B-cells. This demonstrates that the WAVE2 dependent Arp2/3 complex assists in forming a branched actin network around the engagement site to form sustained TCR-APC conjugate. However, the prime question was to investigate the disruption of WAVE2-EVH1 interaction in TCR-APC conjugation. The WAVE2$_{MUT}$ data exhibit unaltered TCR-APC conjugation which contradicts the statement that WAVE2-EVH1 mediated actin polymerization is involved in cell spreading at the IS. A study by Lettau, M. *et al.,* 2014 demonstrates that WASP, WAVE2 recruitment to the TCR site depends on the protein-tyrosine kinase, and the adaptor proteins LAT, SLP76, Nck, and ADAP [186]. Like WASP, WAVE2 is recruited to the TCR site upon its engagement to MHC, and forms signaling clusters. However, in contrast to WASP, WAVE2 leaves this signaling complex and migrates peripherally together with vinculin and talin to the membrane leading edge [153]. Thus, based on available data, it can be proposed that WAVE2-EVH1 interaction plays an essential role in cell spreading and lamellipodia formation during migration. However, during IS formation, the WAVE2-EVH1 complex is not involved in PM spreading around APC. Rather other players are participating in actin-based cell membrane extension at IS site.

The role of ADAP in integrin activation, inside-out, and outside-in signaling has been explored in detail. However, its direct involvement in actin cytoskeleton reorganization mediated by Ena/VASP-EVH1 specifically was unclear. Therefore, in this work, I addressed

it using an ADAP$_{MUT}$ variant of ADAP. ADAP$_{KD}$ exhibited a significant reduction in T-cell conjugate formation as shown in figure 3.14. This can be explained as ADAP is well known to be involved in integrin activation and adhesion. Precise alignment of the T-cell and APC membrane at 15 nm is essential for efficient conjugate formation. The integrin LFA-1 and its major immunoglobulin superfamily ligand ICAM-1 interact to span this distance and initiate costimulatory signals for sustained TCR-APC conjugation. Thus, the process of integrin activation by ADAP is further linked to the cytoskeletal network to trigger the expansion of cell contact area around APC [213]. A link between TCR and the actin network may be formed by ADAP-Ena/VASP interaction. Interestingly, a significant reduction in T-cell-APC conjugate formation by ADAP$_{MUT}$ revealed the implication of ADAP-EVH1 interaction in the process of antigen recognition. Previous studies have suggested that activation of Fcγ receptors triggers VASP and profilin recruitment to the membrane via direct interaction with ADAP. According to one of the studies, ADAP-Ena/VASP complex regulates the assembly of actin structures essential for the process of phagocytosis [185].

It was reported in activated T-cells that inhibition of ADAP and Ena/VASP binding impairs TCR-dependent actin rearrangement, suggesting that these interactions play a key role in linking T-cell signaling to the actin cytoskeleton remodeling [40]. Further, in murine cells, removal of the C-terminal ~400 AA of ADAP (426–819) containing EVH1 domain-binding motif showed restricted conjugate formation, indicating that the C terminus of ADAP is also essential for efficient conjugate formation [214]. Based on available data I suggest a model of TCR-APC signaling as follows in figure 4.3. According to this, ADAP plays a dual role in TCR activation by initiating integrin-mediated adhesion and linking actin machinery to the TCR complex for plasma membrane expansion over APC. It is assumed that due to the proximity of ADAP at the TCR complex, it recruits Ena/VASP through its EVH1 domain to the APC contact site. This is further confirmed by EVH1 inhibitors that exhibit a substantial reduction in TCR conjugate with APC as expressed by our FACS data. It is considered that EVH1 inhibitor displaced ADAP from the EVH1 domain thus restricting the Ena/VASP recruitment to the membrane that is necessary for sustained conjugation. However, overall inhibition of EVH1 mediated interactions by EVH1 inhibitors is projected to affect the conjugate formation. These findings are considered as a promising aspect for addressing unrestrained activation and differentiation of cytotoxic T-cells in various autoimmune

diseases. EVH1 inhibitor is considered to be a potential drug substance to inhibit excessive differentiation of T-cells at tumor microenvironment to restrict metastasis. Further work is certainly required to access the EVH1 inhibitor as a potential drug molecule for autoimmune diseases and metastasis in animal models.
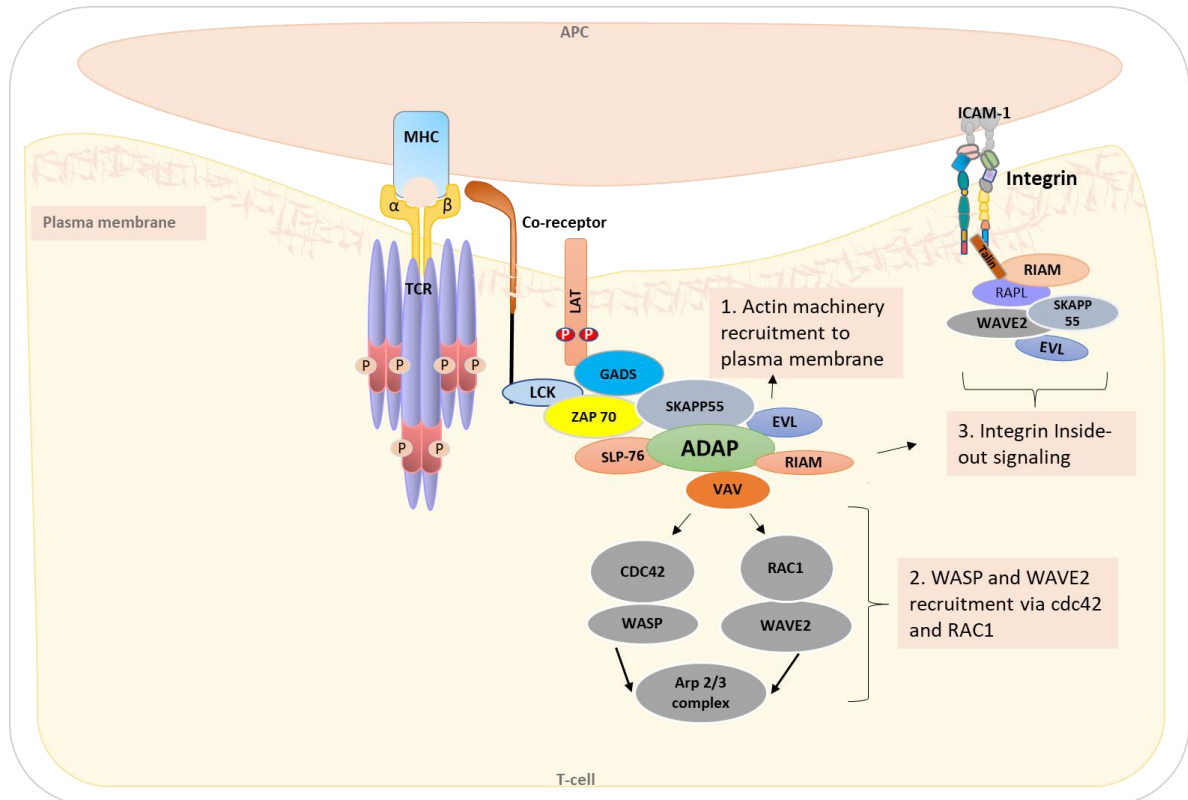

Figure 4.3: Proposed model explains how ADAP is linked to actin machinery during immune synapse formation. 1. Downstream of TCR a signaling complex formed in which ADAP regulates actin machinery by binding to Ena/VASP via its EVH1 domain. Ena/VASP recruitment to the plasma membrane facilitates membrane expansion around APC necessary for sustained TCR-APC conjugation. 2. ADAP in association with VAV and NCK, recruits WASP and WAVE2 downstream of the complex. 3. Moreover, ADAP is one of the main players of inside-out integrin activation. Collectively, multiple interactions of ADAP contribute to TCR-APC conjugate formation.

Summary

The immune system is an extremely complicated system that is continuously evolving to maintain homeostasis. The intact immune responses, such as immune surveillance or immunoediting are mandatory for maintaining intrinsic physiological functions of the immune system. The fundamental characteristics that enable immune cells to perform efficient immune surveillance include Integrin-mediated adhesion, antigen recognition, activation, and motility. However, a slight discrepancy in these fundamental characteristics or their components leads to a pathological condition. Autoimmune disorders, chronic inflammation, and tumor evasion are the manifestations of extravagant T-cell responses 3. Chronic inflammation is a critical hallmark of cancer. Various studies support that the diverse immune cells infiltration plays a central role in smoldering inflammation in the tumor microenvironment. The dynamic tumor-immune cell interplay gives rise to excessive production of chemokines and growth factors that are not only encouraging tumor growth but also help in tumor cell evasion from its primary site [158,204]. Similarly, autoimmune disorder studies have shown enhanced embracement of migratory attributes by immune cells in some cases. Chemokines and chemokine receptors upregulation in blood and cerebrospinal fluid of MS patients is a well-known phenomenon [76,77]. Further, overexpression of adhesion molecule responsible for enhanced macrophage migration and activation in active SLE patients, which is associated with its uncontrolled tissue recruitment and excessive inflammatory cytokine production [52]. Collectively, excessive T-cell activation and migration are related to autoimmune diseases, chronic inflammation, and tumor evasion. In the case of multiple inflammatory disorders, extravagant tissue infiltration of immune cells leads to significant pathogenesis, hence pharmacological inhibition of immune cell motility can be of prime therapeutic value. There are inadequate target-specific and potent therapies available against the chronicity of such diseases. Eventually, immunosuppressants including corticosteroids are used for the long term but they are also associated with potential adverse effects. Thus, a definitive targeted therapy is required that can control actin-based immune cell responses for the regulation of autoimmune diseases and tumor progression. Ena/VASP proteins are key actin regulators and their EVH1 domain is responsible for the localization of actin machinery within the cells.

A small-molecule inhibitor targeting the Ena/VASP-EVH1 domain has been designed in order to inhibit the proline-mediated protein-protein interactions. EVH1 inhibitor data in Jurkat cells and macrophages interpreted that by targeting the EVH1 domain of Ena/VASP, actin-rich structure lamellipodia formation is hindered, and therefore migration is interrupted. Moreover, the EVH1 inhibitors have shown a significant reduction in effective antigen recognition in T cells. Thus, based on our findings, I concluded that inhibition of the EVH1 domain by a small molecular inhibitor can be a promising approach to regulate immune cell responses. Jurkat cells data provide a promising starting point for the characterization of EVH1 inhibitors in *in-vivo* models as a promising therapy for various autoimmune diseases and metastasis. However, EVH1 inhibitors need modification to enhance their cell permeation, which ultimately increases the bioavailability and efficiency.

Furthermore, the importance of WAVE2 and ADAP in T-cells actin cytoskeletal related processes was unveiled. These are two important interaction partners of the EVH1 domain in T-cells that are displaced by EVH1 inhibitors. WAVE2 is an actin regulatory protein, and ADAP is an immune cell-specific adaptor protein that mainly regulates immune-specific functions. Here, we found that in Jurkat cells, WAVE2-EVH1 interaction is necessary for lamellipodia formation, cell spreading, and migration. Whereas ADAP with Ena/VASP direct link is necessary for the formation of immune synapse. In conclusion, the Ena/VASP-EVH1 mediated interaction of both proteins holds an important place in T-cell functionality.

Zusammenfassung:

Das Immunsystem ist ein extrem komplexes System, das sich kontinuierlich entwickelt, um die natürliche Homöostase aufrechzuerthalten. Die intakten Immunreaktionen, wie die Immunüberwachung oder die Immunaufbereitung, sind zur Aufrechterhaltung der körpereigenen physiologischen Funktionen des Immunsystems zwingend erforderlich. Integrin-vermittelte Adhäsion, Antigenerkennung, Aktivierung und Motilität sind die grundlegenden Eigenschaften, die es Immunzellen ermöglichen, eine effiziente Immunüberwachung durchzuführen. Eine geringfügige Diskrepanz in diesen Eigenschaften oder auch in Bestandteilen davon führt jedoch zu einem pathologischen Zustand. Autoimmunerkrankungen, chronische Entzündungen und entkommen von Tumorzellen sind die Manifestation extravaganter T-Zell-Reaktionen 3. Chronische Entzündungen sind ein kritisches merkmal von Krebs. Verschiedene Studien belegen, dass die vielfältige Infiltration von Immunzellen eine zentrale Rolle bei der schwelenden Entzündung in der Tumormikroumgebung spielt. Das dynamische Zusammenspiel von Tumor-Immunzellen führt zu einer übermäßigen Produktion von Chemokinen und Wachstumsfaktoren, die nicht nur das Tumorwachstum fördern, sondern auch bei der Ausweichung von Tumorzellen von ihrem primären Standort aus helfen.158,204 Zusätzlich haben studien zu Autoimmunerkrankungen gezeigt, dass die Aufnahme von wandernden Attributen durch Immunzellen in einigen Fällen verstärkt ist/wird. Die Tatsache, dass Chemokine und Chemokinrezeptoren im Blut hochreguliert sind und die existenz von Cerebrospinalflüssigkeit bei MS-Patienten ist bereits bekannt 76,77. Darüber hinaus trägt die Überexpression von Adhäsionsmolekülen auch zu einer verstärkten Makrophagen-Migration und Aktivierung bei aktiven SLE-Patienten, die mit Gewebsrekrutierung und entzündlicher Cytokin-Produktion verbunden ist 20. Insgesamt sind übermäßige T-Zell-Aktivierung und Migrationsstörungen von Immunzellen sind mit Autoimmunerkrankungen, chronischer Entzündung und Tumorflucht verbunden. Eine pharmakologische Hemmung der Motilität von Immunzellen kann bei einer Vielzahl von entzündlichen Erkrankungen, bei denen eine übermäßige Gewebeeinfiltration erhebliche Schäden verursachen kann, sehr vorteilhaft sein. Der Mangel an wirksamen und selektiven Therapien für solche Krankheiten konnte ihre Chronizität nicht auflösen und erfordert daher die weitere Anwendung immunsuppressiver Behandlungen wie Kortikosteroide mit potenziellen Nebenwirkungen.

Daher ist eine definitive gezielte Therapie notwendig, um aktinbasierte Immunzellreaktionen und Autoimmunerkrankungen zu kontrollieren, und die Krebszellprogression zu bekämpfen. Ena/VASP-Proteine sind wichtige Aktinregulatoren und ihre EVH1-Domäne ist für die aktinmaschinelle Lokalisierung innerhalb der Zellen verantwortlich. Ein kleiner molekularer Inhibitor der Ena/VASP-EVH1-Domäne wurde entwickelt, um die Prolin-vermittelte Protein-Protein-Wechselwirkung zu inhibieren.

Jurkat-Zell- und Makrophagendaten demonstrieren, dass durch das Targeting der EVH1-Domäne von Ena/VASP die Bildung von Lamellipodien mit aktinreicher Struktur behindert wird und daher die Migration unterbrochen wird. Darüber hinaus haben die EVH1-Inhibitoren eine signifikante Verringerung der effektiven Antigenerkennung in T-Zellen gezeigt. Basierend auf unseren Ergebnissen kam ich zu dem Schluss, dass die Hemmung der EVH1-Domäne durch einen kleinmolekularen Inhibitor ein vielversprechender Ansatz zur Regulierung von Immunzellantworten sein kann. Jurkat-Zelldaten bieten einen hervorragenden Ausgangspunkt für die Charakterisierung von EVH1-Inhibitoren in In-vivo-Modellen als potenzielle Therapie für verschiedene Autoimmunerkrankungen und Metastasen. EVH1-Inhibitoren müssen jedoch hinsichtlich ihrer Zellpermeabilität modifiziert werden, um letztendlich die Bioverfügbarkeit und Effizienz zu verbessern.

Außerdem wurde die Bedeutung von WAVE2 und ADAP in T-Zellen-Aktin-Zytoskelett-bezogenen Prozessen enthüllt. Dies sind zwei wichtige Interaktionspartner der EVH1-Domäne in T-Zellen, die durch EVH1-Inhibitoren verdrängt werden. WAVE2 ist ein aktinregulierendes Protein, und ADAP ist ein immunzellspezifisches Adapterprotein, das hauptsächlich immunspezifische Funktionen reguliert. Hier fanden wir heraus, dass in Jurkat-Zellen die WAVE2-EVH1-Interaktion für die Lamellipodienbildung, Zellausbreitung und Migration notwendig ist während ADAP mit Ena/VASP-Direktverbindung für die Bildung von Immunsynapsen erforderlich ist. Zusammenfassend nimmt die Ena/VASP-EVH1-vermittelte Interaktion beider Proteine einen wichtigen Platz in der T-Zell-Funktionalität ein.

Bibliography

1. Pandya, P. H., Murray, M. E., Pollok, K. E. & Renbarger, J. L. The Immune System in Cancer Pathogenesis : Potential Therapeutic Approaches. *J. Immunol. Res.* **2016**, 1–13 (2016).

2. Gonzalez, H., Hagerling, C. & Werb, Z. Roles of the immune system in cancer : from tumor initiation to metastatic progression. *GENES Dev. 321267–1284* **32**, 1267–1284 (2018).

3. Navegantes, K. C., Gomes, R. D. S., Aparecida, P. & Pereira, T. Immune modulation of some autoimmune diseases : the critical role of macrophages and neutrophils in the innate and adaptive immunity. *J. Transl. Med.* **15**, 1–21 (2017).

4. Chen, L. *et al.* Inflammatory responses and inflammation-associated diseases in organs. *Oncotarget* **9**, 7204–7218 (2018).

5. Nowarski, R., Gagliani, N., Huber, S. & Flavell, R. A. Innate Immune Cells in Inflammation and Cancer. *Cancer Immunol Res* **1**, 77–85 (2013).

6. Moser, B. & Willimann, K. Chemokines: Role in inflammation and immune surveillance. *Ann. Rheum. Dis.* **63**, 84–90 (2004).

7. Cruz-Adalia, A. *et al.* Conventional CD4 + T cells present bacterial antigens to induce cytotoxic and memory CD8 + T cell responses. *Nat. Commun.* **8**, 1–11 (2017).

8. Hivroz, C. & Saitakis, M. Biophysical aspects of T lymphocyte activation at the immune synapse. *Front. Immunol.* **7**, 1–12 (2016).

9. Pagès, F. *et al.* Effector Memory T Cells, Early Metastasis, and Survival in Colorectal Cancer. *N. Engl. J. Med.* **353**, 2654–2666 (2005).

10. Hansson, G. K., Libby, P., Schönbeck, U. & Yan, Z. Innate and Adaptive Immunity in the Pathogenesis of Atherosclerosis. *Circ. Res.* **91**, 281–291 (2002).

11. Huse, M. The T-cell-receptor signalling network. *J. Cell Sci.* **122**, 1269–1273 (2009).

12. Lima, H. R., Gasparoto, T. H., Salles, T., Malaspina, D. S. & Campanelli, A. P. Immune Checkpoints in Leprosy: Immunotherapy As a Feasible Approach to Control Disease Progression. *Front Immunol.* **8**, 1–9 (2017).

13. Acuto, O., Bartolo, V. Di & Michel, F. Tailoring T-cell receptor signals by proximal negative feedback mechanisms. *Nat. Rev. Immunol.* **8**, 699–712 (2008).

14. Wieczorek, M. *et al.* Major histocompatibility complex (MHC) class I and MHC class II proteins: Conformational plasticity in antigen presentation. *Front. Immunol.* **8**, 1–16 (2017).

15. Luckheeram, R. V., Zhou, R., Verma, A. D. & Xia, B. CD4 + T Cells : Differentiation and Functions. *Clin. Dev. Immunol.* **2012**, 1–12 (2012).

16. Masopust, D. & Schenkel, J. M. The integration of T cell migration, differentiation and function. *Nat. Rev. Immunol.* **13**, 309–320 (2013).

17. Andrea Facciabene, Gregory T. Motz, and G. C. T Regulatory Cells: Key Players in Tumor

Immune Escape and Angiogenesis. *Cancer Res.* **72**, 2162–2171 (2013).

18. Halle, S. *et al.* In Vivo Killing Capacity of Cytotoxic T Cells Is Limited and Involves Dynamic Interactions and T Cell Article In Vivo Killing Capacity of Cytotoxic T Cells Is Limited and Involves Dynamic Interactions and T Cell Cooperativity. *Immunity* **44**, 1–13 (2016).

19. Hosoya, T. *et al.* Induction of oligoclonal CD8 T cell responses against pulmonary metastatic cancer by a phospholipid- conjugated TLR7 agonist. *PNAS* **115**, 6836–6844 (2018).

20. Bettelli, E., Korn, T., Oukka, M. & Kuchroo, V. K. Induction and effector functions of TH 17 cells. *Nature* **453**, 1051–1057 (2008).

21. Skapenko, A., Leipe, J., Lipsky, P. E. & Schulze-koops, H. The role of the T cell in autoimmune inflammation. *Arthritis Res. Ther.* **7**, 1–11 (2005).

22. Téllez, C. N., Siachoque, J. J., Siachoque, S. J., Alejandra, J. M. & Siachoque, M. H. Review article T-cell activation , alterations in systemic lupus erythematosus : A narrative review ⚥. *Rev. Colomb. Reumatol.* **25**, 38–54 (2018).

23. Emamaullee, J. A. *et al.* Inhibition of Th17 Cells Regulates Autoimmune Diabetes in NOD Mice. *Diabetes* **58**, 1302–1311 (2009).

24. Kaur, A. *et al.* Remodeling of the collagen matrix in aging skin promotes melanoma metastasis and affects immune cell motility. *Cancer Discov.* **9**, 64–81 (2019).

25. Vijayan, D., Young, A., Teng, M. W. L. & Smyth, M. J. Targeting immunosuppressive adenosine in cancer. *Nat. Rev. Cancer* **17**, 709–724 (2017).

26. Comerford, I. *et al.* A myriad of functions and complex regulation of the CCR7/CCL19/CCL21 chemokine axis in the adaptive immune system. *Cytokine Growth Factor Rev.* **24**, 269–283 (2013).

27. Cernuda-Morollón, E., Millán, J., Shipman, M., Marelli-Berg, F. M. & Ridley, A. J. Rac activation by the T-cell receptor inhibits T cell migration. *PLoS One* **5**, 1–13 (2010).

28. Dupré, L., Houmadi, R., Tang, C. & Rey-Barroso, J. T Lymphocyte Migration : An Action Movie Starring the Actin and Associated Actors. *Front Immunol.* **6**, 1–18 (2015).

29. Izdebska, M., N, W. Z., Grzanka, D. & Gagat, M. The Role of Actin Dynamics and Actin-Binding Proteins Expression in Epithelial-to-Mesenchymal Transition and Its Association with Cancer Progression and Evaluation of Possible Therapeutic Targets. *Biomed Res. Int.* **2018**, 1–13 (2018).

30. Verma, N. K. & Kelleher, D. Adaptor regulation of LFA-1 signaling in T lymphocyte migration: Potential druggable targets for immunotherapies? *Eur. J. Immunol.* **44**, 3484–3499 (2014).

31. Guo, J., Wang, W., Yu, D. & Wu, Y. Spinoculation Triggers Dynamic Actin and Cofilin Activity That Facilitates HIV-1 Infection of Transformed and Resting CD4 T Cells. *J. Virol.* **85**, 9824–9833 (2011).

32. Shao, J. *et al.* Inhibition of CXCL12-mediated chemotaxis of Jurkat cells by direct immunotoxicants. *Arch. Toxicol.* **90**, 1685–1694 (2016).

33. Kliche, S. *et al.* The ADAP / SKAP55 Signaling Module Regulates T-Cell Receptor-Mediated Integrin Activation through Plasma Membrane Targeting of Rap1 †. *Mol. Cell. Biol.* **26**, 7130–7144 (2006).

34. Zhang, Y. & Wang, H. Integrin signalling and function in immune cells. *Immunology* **135**, 268–275 (2012).

35. Le Clainche, C. & Carlier, M. F. Regulation of actin assembly associated with protrusion and adhesion in cell migration. *Physiol. Rev.* **88**, 489–513 (2008).

36. Na, B., Jun, C. & Synapse, I. In vitro Assessment of Immunological Synapse Formation by Flow Cytometry. *Bio-protocol* **6**, 1–7 (2016).

37. Kuokkanen, E., Šuštar, V. & Mattila, P. K. Molecular control of B cell activation and immunological synapse formation. *Traffic* **16**, 311–326 (2015).

38. Comrie, W. A. & Burkhardt, J. K. Action and Traction : Cytoskeletal Control of Receptor Triggering at the immunological Synapse. *Front Immunol.* **7**, 1–25 (2016).

39. Samstag, Y., Eibert, S. M., Klemke, M. & Wabnitz, G. H. Actin cytoskeletal dynamics in T lymphocyte activation and migration of the immunological synapse at the interface be-. *J. Leukoc. Biol.* **73**, 30–48 (2003).

40. Krause, M. *et al.* Fyn-binding protein (Fyb)/SLP-76-associated protein (SLAP), ena/vasodilator-stimulated phosphoprotein (VASP) proteins and the Arp2/3 complex link T cell receptor (TCR) signaling to the actin cytoskeleton. *J. Cell Biol.* **149**, 181–194 (2000).

41. Zeng, R. *et al.* SLP-76 Coordinates Nck-Dependent Wiskott-Aldrich Syndrome Protein Recruitment with Vav-1/Cdc42-Dependent Wiskott-Aldrich Syndrome Protein Activation at the T Cell-APC Contact Site. *J. Immunol. Immunol.* **171**, 1360–1368 (2003).

42. Wang, H. & Rudd, C. E. SKAP-55, SKAP-55-related and ADAP adaptors modulate integrin-mediated immune-cell adhesion. *Trends Cell Biol.* **18**, 486–493 (2008).

43. Witte, A. *et al.* Emerging Roles of ADAP , SKAP55 , and SKAP-HOM for Integrin and NF- κ B Signaling in T cells. *J. Clin. Cell. Immunol.* **S12**, 1–8 (2012).

44. Kumari, S., Curado, S., Mayya, V., Dustin, M. L. & All, E. B. V. Biochimica et Biophysica Acta T cell antigen receptor activation and actin cytoskeleton remodeling. *BBA - Biomembr.* **1838**, 546–556 (2014).

45. Gordon, S. & Plu, A. Role of Macrophages in Autoimmunity. in *The Autoimmune Diseases* 161–174 (2014). doi:10.1016/B978-0-12-384929-8.00011-3.

46. Palomino, D. C. T. & Marti, L. C. Chemokines and immunity. *Einstein* **13**, 469–473 (2015).

47. Shalapour, S. & Karin, M. Immunity , inflammation , and cancer : an eternal fight between good and evil. *J. Clin. Invest.* **125**, 3347–3355 (2015).

48. Ushio, A. *et al.* Crucial roles of macrophages in the pathogenesis of autoimmune disease. *World J. Immunol.* **7**, 1–8 (2017).

49. Janssen, L. M. E., Ramsay, E. E., Logsdon, C. D. & Overwijk, W. W. The immune system in

cancer metastasis : friend or foe ? *J. Immunother. Cancer* **5**, 1–14 (2017).

50.   Davis, M. J. *et al.* Macrophage M1 / M2 Polarization Dynamically Adapts to Changes in Cytokine Microenvironments in Cryptococcus neoformans Infection. *MBio* **4**, 1–10 (2013).

51.   Russo, V. & Martelli, A. M1 and M2 macrophage recruitment during tendon regeneration induced by amniotic epithelial cell allotransplantation in ovine. *Res. Vet. Sci.* **105**, 92–102 (2016).

52.   Sasaki, K. *et al.* Modulation of autoimmune pathogenesis. *Nat. Commun.* **10**, 1–16 (2019).

53.   Nielsen, S. R. & Schmid, M. C. Macrophages as Key Drivers of Cancer Progression and Metastasis. *Mediators Inflamm.* **2017**, 1–11 (2017).

54.   Tam, W. L. & Weinberg, R. A. The epigenetics of epithelial-mesenchymal plasticity in cancer. *Nat Med* **19**, 1438–1449 (2013).

55.   Lim, B., Woodward, W. A., Wang, X., Reuben, J. M. & Ueno, N. T. Inflammatory breast cancer biology: the tumour microenvironment is key. *Nat. Rev. Cancer* **18**, 485–499 (2018).

56.   Spano, D. & Zollo, M. Tumor microenvironment : a main actor in the metastasis process. 381–395 (2012) doi:10.1007/s10585-012-9457-5.

57.   Kruger, S. *et al.* Advances in cancer immunotherapy 2019 - Latest trends. *J. Exp. Clin. Cancer Res.* **38**, 1–11 (2019).

58.   Brilot, F., Pilli, D., Zou1, A., Tea, F. & Dale, R. C. Expanding Role of T Cells in Human Autoimmune Diseases of the Central Nervous System. *Front Immunol.* **8**, 1–17 (2017).

59.   Marshall, J. S., Warrington, R., Watson, W. & Kim, H. L. An introduction to immunology and immunopathology. *Allergy, Asthma Clin. Immunol.* **14**, 1–10 (2018).

60.   Shirdel, S. Autoimmune diseases & the pathogenic mechanism.

61.   Sudres, M. *et al.* Pathophysiological mechanisms of autoimmunity. *Ann. N. Y. Acad. Sci.* **1413**, 59–68 (2018).

62.   Yamamoto, K. Mechanisms of Autoimmunity: Recent concept. *J. Japan Med. Assoc.* **47**, 403–406 (2004).

63.   Jun, B. H., Yoon, C., Zbytnuik, L., Rooijen, N. Van & Yoon, J. The Role of Macrophages in T Cell – mediated Autoimmune Diabetes in Nonobese Diabetic Mice. *J. Exp. Med.* **189**, 347–358 (1999).

64.   Zhang, Y. & Wang, H. Integrin signalling and function in immune cells. *Immunology* **135**, 268–275 (2012).

65.   Bluestone, J. A. *et al.* T cells in the control of organ-specific autoimmunity. *J. Clin. Invest.* **125**, 2250–2260 (2015).

66.   Ma, W., Gao, F., Gu, K. & Chen, D. The Role of Monocytes and Macrophages in Autoimmune Diseases : A Comprehensive Review. *Front Immunol.* **10**, 1–24 (2019).

67. Ballotti, S., Chiarelli, F. & Martino, M. de. Autoimmunity : Basic Mechanisms and Implications in Endocrine Diseases. *Horm. Res.* **66**, 132–141 (2006).

68. Chang, M. H. & Nigrovic, P. A. Antibody-dependent and -independent mechanisms of inflammatory arthritis. *JCI insight* **4**, 1–15 (2019).

69. Esensten, J. H., Wofsy, D. & Bluestone, J. A. Regulatory T cells as therapeutic targets in rheumatoid arthritis. *Nat Rev Rheumatol.* **5**, 560–565 (2009).

70. York, M. R., Nagai, T., Mangini, A. J., Seventer, J. M. Van & Lafyatis, R. A Macrophage Marker , Siglec-1 , Is Increased on Circulating Monocytes in Patients With Systemic Sclerosis and Induced by Type I Interferons and Toll-like Receptor Agonists. *Arthritis Rheum.* **56**, 1010–1020 (2007).

71. Suárez-fueyo, A., Bradley, S. J. & Tsokos, G. C. T cells in Systemic Lupus Erythematosus. *Curr Opin Immunol* **43**, 32–38 (2017).

72. Mak, A. & Kow, N. Y. The Pathology of T Cells in Systemic Lupus Erythematosus. *J. Immunol. Res.* **2014**, 1–8 (2014).

73. Estin, M. L. *et al.* Ena/VASP proteins regulate activated T-cell trafficking by promoting diapedesis during transendothelial migration. *Proc. Natl. Acad. Sci. U. S. A.* **114**, E2901–E2910 (2017).

74. Comte, D. *et al.* T cells as a therapeutic target in SLE. *Lupus* **24**, 351–363 (2016).

75. D'Ambrosio, D., Mariani, M., Panina-Bordignon, P. & Sinigaglia, F. Chemokines and their receptors guiding T lymphocyte recruitment in lung inflammation. *Am. J. Respir. Crit. Care Med.* **164**, 1266–1275 (2001).

76. Cheng, W. & Chen, G. Chemokines and Chemokine Receptors in Multiple Sclerosis. *Mediat. Inflamm.* **2014**, (2014).

77. Cui, L., Chu, S. & Chen, N. The role of chemokines and chemokine receptors in multiple sclerosis. *Int. Immunopharmacol.* **83**, 1–11 (2020).

78. Kong, D., Kim, Y. K., Kim, M. R., Jang, J. H. & Lee, S. Emerging Roles of Vascular Cell Adhesion Molecule-1 (VCAM-1) in Immunological Disorders and Cancer. *Int. J. Mol. Sci.* **19**, 1.16 (2018).

79. Warnke, D. C. *et al.* Natalizumab and Progressive Multifocal Leukoencephalopathy: What are the causal factors? Can it be avoided? *Arch Neurol* **67**, 923–930 (2010).

80. Spano, D., Heck, C., De Antonellis, P., Christofori, G. & Zollo, M. Molecular networks that regulate cancer metastasis. *Semin. Cancer Biol.* **22**, 234–249 (2012).

81. Qian, C. N., Mei, Y. & Zhang, J. Cancer metastasis: Issues and challenges. *Chin. J. Cancer* **36**, 1–4 (2017).

82. Guan, X. Cancer metastases: Challenges and opportunities. *Acta Pharm. Sin. B* **5**, 402–418 (2015).

83. Steeg, P. S. Targeting metastasis. *Nat. Rev. Cancer* **16**, 201–218 (2016).

84. American Cancer Society. Cancer Facts & Figures 2019, Special Section: Cancer in the Oldest Old. **2019**, 1–6 (2019).

85. Chin, A. R. & Wang, S. E. Cancer tills the premetastatic field: Mechanistic basis and clinical implications. *Clin. Cancer Res.* **22**, 3725–3733 (2016).

86. Welch, D. R. & Hurst, D. R. Defining the Hallmarks of Metastasis. *Cancer Res.* **79**, 3011–3027 (2019).

87. Arvelo, F., Sojo, F. & Cotte, C. Tumour progression and metastasis. *ecancer 2016,* **10**, 1–25 (2016).

88. Chaffer, C. L., San Juan, B. P., Lim, E. & Weinberg, R. A. EMT, cell plasticity and metastasis. *Cancer Metastasis Rev.* **35**, 645–654 (2016).

89. Larue, L. & Bellacosa, A. Epithelial – mesenchymal transition in development and cancer : role of phosphatidylinositol 3 0 kinase / AKT pathways. *Oncogene* **24**, 7443–7454 (2005).

90. Morris, H. T. & Machesky, L. M. Actin cytoskeletal control during epithelial to mesenchymal transition : focus on the pancreas and intestinal tract. *Br. J. Cancer* **112**, 613–620 (2015).

91. Pignatelli, J. *et al.* Invasive breast carcinoma cells from patients exhibit MenaINV- and macrophage-dependent transendothelial migration. *Sci. Signal* **7**, 1–25 (2014).

92. Roussos, E. T. *et al.* Mena invasive (MenaINV) promotes multicellular streaming motility and transendothelial migration in a mouse model of breast cancer. *J. Cell Sci.* **124**, 2120–2131 (2011).

93. Wang, M. *et al.* Role of tumor microenvironment in tumorigenesis. *J. cancer* **8**, 761–773 (2017).

94. Peltanova, B., Raudenska, M. & Masarik, M. Effect of tumor microenvironment on pathogenesis of the head and neck squamous cell carcinoma: A systematic review. *Molecular Cancer* vol. 18 1–24 (2019).

95. Agarwal, S. *et al.* Quantitative assessment of invasive mena isoforms (Mena calc) as an independent prognostic marker in breast cancer. *Breast Cancer Res.* **14**, 1–8 (2012).

96. Qian Binzhi and Jeffrey W. Pollard. Macrophage Diversity Enhances Tumor Progression and Metastasis. *Cell* **141**, 39–51 (2010).

97. Grivennikov, S. I., Greten, F. R. & Karin, M. Immunity, Inflammation, and Cancer. *Cell* **140**, 883–899 (2010).

98. Oudin, M. J. *et al.* MENA confers resistance to paclitaxel in triple-negative breast cancer. *Mol Cancer Ther* **16**, 143–155 (2018).

99. Conniot, J. *et al.* Cancer immunotherapy: Nanodelivery approaches for immune cell targeting and tracking. *Front. Chem. Rev. Artic.* **2**, 1–27 (2014).

100. Gao, J. *et al.* VISTA is an inhibitory immune checkpoint that is increased after ipilimumab therapy in patients with prostate cancer Jianjun. *Nat Med* **23**, 1–14 (2017).

101. Li, B., Chan, H. L. & Chen, P. Immune Checkpoint Inhibitors : Basics and Challenges. *Curr. Med. Chem.* **24**, 1–15 (2017).

102. Sambi, M., Bagheri, L. & Szewczuk, M. R. Current challenges in cancer immunotherapy: Multimodal approaches to improve efficacy and patient response rates. *J. Oncol.* **2019**, 1–12 (2019).

103. Harbeck, N. *et al. Breast cancer*. *Nature reviews. Disease primers* vol. 5 (2019).

104. Gandalovičová, A. *et al.* Migrastatics—Anti-metastatic and Anti-invasion Drugs: Promises and Challenges. *Trends in Cancer* **3**, 391–406 (2017).

105. Chen, D. *et al.* Enah overexpression is correlated with poor survival and aggressive phenotype in gastric cancer. *Cell Death Dis.* **9**, 1–15 (2018).

106. Menzies, A. S. *et al.* Mena and vasodilator-stimulated phosphoprotein are required for multiple actin-dependent processes that shape the vertebrate nervous system. *J. Neurosci.* **24**, 8029–8038 (2004).

107. Peterson, F. C. & Volkman, B. F. Diversity of polyproline recognition by EVH1 domains. *Front. Biosci.* **14**, 833–846 (2009).

108. Barzik, M., McClain, L. M., Gupton, S. L. & Gertler, F. B. Ena/VASP regulates mDia2-initiated filopodial length, dynamics, and function. *Mol. Biol. Cell* **25**, 2604–2619 (2014).

109. Krause, M. *et al.* Lamellipodin, an Ena/VASP Ligand , Is Implicated in the Regulation of Lamellipodial Dynamics. *Dev. Cell* **7**, 571–583 (2004).

110. Riquelme, D. N., Meyer, A. S., Barzik, M., Keating, A. & Gertler, F. B. Selectivity in subunit composition of Ena / VASP tetramers. *Biosci Rep.* **35**, 1–15 (2015).

111. Bachmann, C., Fischer, L., Walter, U. & Reinhard, M. The EVH2 domain of the vasodilator-stimulated phosphoprotein mediates tetramerization, F-actin binding, and actin bundle formation. *J. Biol. Chem.* **274**, 23549–23557 (1999).

112. Harker, A. J. *et al.* Ena / VASP processive elongation is modulated by avidity on actin filaments bundled by the filopodia cross-linker fascin. *MBoC* **30**, 851–862 (2019).

113. Brühmann, S. *et al.* Distinct VASP tetramers synergize in the processive elongation of individual actin filaments from clustered arrays. *PNAS* **114**, 5815–5824 (2017).

114. Ball, L. J., Jarchau, T., Oschkinat, H. & Walter, U. EVH1 domains : structure , function and interactions. *FEBS* **513**, 45–52 (2002).

115. Volkman, B. F., Prehoda, K. E., Scott, J. A., Peterson, F. C. & Lim, W. A. Structure of the N-WASP EVH1 Domain-WIP Complex : Insight into the Molecular Basis of Wiskott-Aldrich Syndrome. *Cell* **111**, 565–576 (2002).

116. Auerbuch, V., Loureiro, J. J., Gertler, F. B., Theriot, J. A. & Portnoy, D. A. Ena/VASP proteins contribute to Listeria monocytogenes pathogenesis by controlling temporal and spatial persistence of bacterial actin-based motility. *Mol. Microbiol.* **49**, 1361–1375 (2003).

117. Chakraborty, T. *et al.* A focal adhesion factor directly linking intracellularly motile Listeria

monocytogenes and Listeria ivanovii to the actin-based cytoskeleton of mammalian cells. *EMBO J.* **14**, 1314–1321 (1995).

118. Niebuhr, K. *et al.* A novel proline-rich motif present in ActA of Listeria monocytogenes and cytoskeletal proteins is the ligand for the EVH1 domain, a protein module present in the Ena/VASP family. *EMBO J.* **16**, 5433–5444 (1997).

119. Fedorov, A. A., Fedorov, E., Gertler, F. & Almo, S. C. Structure of EVH1, a novel proline-rich ligand-binding module involved in cytoskeletal dynamics and neural function. *Nat. Struct. Biol.* **6**, 661–665 (1999).

120. Opitz, R. *et al.* A modular toolkit to inhibit proline-rich motif-mediated protein-protein interactions. *PNAS* **112**, 5011–5016 (2015).

121. Ball Linda J. *et al.* Dual epitope recognition by the VASP EVH1 domain modulates polyproline ligand specificity and binding affinity. *EMBO J.* **19**, 4903–4914 (2000).

122. Krause, M.-5793(98)01541-5. pdfia. *Role of Ena / VASP Proteins in Homeostasis and Disease This review article is published as a chapter in the Springer handbook : Protein-Protein Interactions as New Drug Targets Handbook of Experimental Pharmacology Volume 186 , 2008 , pp 39-65 The final p*. (2014). doi:10.1007/978-3-540-72843-6.

123. Bear, J. E. & Gertler, F. B. Ena/VASP: Towards resolving a pointed controversy at the barbed end. *J. Cell Sci.* **122**, 1947–1953 (2009).

124. Chereau, D. & Dominguez, R. Understanding the role of the G-actin-binding domain of Ena/VASP in actin assembly. *J. Struct. Biol.* **155**, 195–201 (2006).

125. Laurent, V. *et al.* Role of proteins of the Ena/VASP family in actin-based motility of Listeria monocytogenes. *J. Cell Biol.* **144**, 1245–1258 (1999).

126. Margaret P Quinlan. Suppression of Epithelial Cell Transformation and Induction of Actin Dependent Differentiation by Dominant Negative Rac1 , but not Ras , Rho or Cdc42. *Cancer Biol. Ther.* **3**, 65–70 (2004).

127. Lambrechts, A., Troys, M. Van & Ampe, C. The actin cytoskeleton in normal and pathological cell motility. *Int. J. Biochem. Cell Biol. 36* **36**, 1890–1909 (2004).

128. Dertsiz, L. *et al.* Differential expression of VASP in normal lung tissue and lung adenocarcinomas. *Thorax* **60**, 576–581 (2005).

129. Di Modugno, F. *et al.* Human MENA protein , a serex-defined antigen overexpressed in breast cancer eliciting both humoral and CD8+ T-cell immune response. *Int. J. Cancer* **109**, 909–918 (2004).

130. Hu, L. De, Zou, H. F., Zhan, S. X. & Cao, K. M. EVL (Ena/VASP-like) expression is up-regulated in human breast cancer and its relative expression level is correlated with clinical stages. *Oncol. Rep.* **19**, 1015–1020 (2008).

131. Peterson, E. J. *et al.* Coupling of the TCR to integrin activation by SLAP-130/Fyb. *Science (80-.).* **293**, 2263–2265 (2001).

132. Raab, M. *et al.* T Cell Receptor '" Inside-Out "' Pathway via Signaling Module SKAP1-RapL

Regulates T Cell Motility and Interactions in Lymph Nodes. *Immunity* **32**, 541–556 (2010).

133. Mueller, K. L. *et al.* Adhesion and Degranulation-Promoting Adapter Protein (ADAP) Positively Regulates T Cell Sensitivity to Antigen and T Cell Survival. *J. Immunol.* **179**, 3559–3569 (2007).

134. Veale, M. *et al.* Novel Isoform of Lymphoid Adaptor FYN-T-binding Protein (FYB-130) Interacts with SLP-76 and Up-regulates Interleukin 2 Production *. *J. Biol. Chem.* **274**, 28427–28435 (1999).

135. Sylvester, M. *et al.* Adhesion and Degranulation Promoting Adapter Protein (ADAP) Is a Central Hub for Phosphotyrosine-Mediated Interactions in T Cells. *PLoS One* **5**, 1–11 (2010).

136. Wang, H., Lim, D. & Rudd, C. E. Immunopathologies linked to integrin signalling. *Semin Immunopathol* **32**, 173–182 (2010).

137. Heuer, K., Kofler, M., Langdon, G., Thiemke, K. & Freund, C. Structure of a Helically Extended SH3 Domain of the T Cell Adapter Protein ADAP. **12**, 603–610 (2004).

138. Heuer, K. *et al.* Lipid-binding hSH3 Domains in Immune Cell Adapter Proteins. *J. Mol. Biol* **361**, 94–104 (2006).

139. Blau, A. Current Opinion in Colloid & Interface Science Cell adhesion promotion strategies for signal transduction enhancement in microelectrode array in vitro electrophysiology : An introductory overview and critical discussion. *Curr. Opin. Colloid Interface Sci.* **18**, 481–492 (2013).

140. Krause, M., Bear, J. E., Loureiro, J. J. & Gertler, F. B. The Ena / VASP enigma. *J. Cell Sci.* **115**, 4721–4726 (2002).

141. Hogg, N., Laschinger, M., Giles, K. & Mcdowall, A. T-cell integrins : more than just sticking points. *J. Cell Sci.* **116**, 4695–4705 (2003).

142. Harburger, D. S. *et al.* Integrin signalling at a glance. *J. Cell Sci.* **122**, 159–163 (2009).

143. Evans, R. *et al.* Integrins in immunity. *J. Cell Sci.* **122**, 215–225 (2009).

144. Gael Menasche, Kliche, S., Bezman, N. & Schraven, B. Regulation of T-cell antigen receptor-mediated inside-out signaling by cytosolic adapter proteins and Rap1 effector molecules. *Immunol. Rev.* **218**, 82–91 (2007).

145. Smith, A., Bracke, M., Leitinger, B., Porter, J. C. & Hogg, N. LFA-1-induced T cell migration on ICAM-1 involves regulation of MLCK-mediated attachment and ROCK- dependent detachment. *J. Cell Sci. Cell Sci.* **116**, 3123–3133 (2003).

146. Hogg, N., Patzak, I. & Willenbrock, F. The insider ' s guide to leukocyte integrin signalling and function. *Nat. Rev* **11**, 416–426 (2011).

147. Kuropka, B., Schraven, B., Kliche, S., Krause, E. & Freund, C. Tyrosine-phosphorylation of the scaffold protein ADAP and its role in T cell signaling. *Expert Rev. Proteomics* **13**, 545–554 (2016).

148. Reicher, B., Perl, O., Matalon, O. & Barda-saad, M. WASp and WAVE Proteins : From Structure , Through Function , to Clinical Aspects. *J. Clin. Cell. Immunol. Reicher* **S12**, 1–11 (2012).

149. Kuropka, B. *et al.* Analysis of phosphorylation-dependent protein interactions of ADAP reveals novel interaction. 1–30 (2015).

150. Huang, Y. *et al.* Deficiency of ADAP / Fyb / SLAP-130 Destabilizes SKAP55 in Jurkat T Cells *. *J. Biol. Chem.* **280**, 23576–23583 (2005).

151. Ménasché, G. *et al.* RIAM Links the ADAP/SKAP-55 Signaling Module to Rap1, Facilitating T-Cell-Receptor-Mediated Integrin Activation. *Mol. Cell. Biol.* **27**, 4070–4081 (2007).

152. Lee, H. S., Anekal, P., Lim, C. J., Liu, C. C. & Ginsberg, M. H. Two modes of integrin activation form a binary molecular switch in adhesion maturation. *Mol. Biol. Cell* **24**, 1354–1362 (2013).

153. Pauker, M. H. *et al.* WASp Family Verprolin-homologous Protein-2 (WAVE2) and Wiskott-Aldrich Syndrome Protein (WASp) Engage in Distinct Downstream Signaling Interactions at the T Cell Antigen Receptor Site * □. *J. Biol. Chem.* **289**, 34503–34519 (2014).

154. Jia, S. *et al.* Down-regulation of WAVE2 , WASP Family Verprolin- Homologous Protein 2 , in Gastric Cancer Indicates Lymph Node Metastasis and Cell Migration. *Anticancer Res.* **34**, 2185–2194 (2014).

155. Pollitt, A. Y. & Robert, H. WASP and SCAR / WAVE proteins : the drivers of actin assembly. *J. Cell Sci.* **122**, 2575–2578 (2009).

156. Kurisu, S. & Takenawa, T. WASP and WAVE family proteins : Friends or foes in cancer invasion. *Cancer Sci.* **101**, 2093–2104 (2010).

157. Nolz, J. C. *et al.* The WAVE2 complex regulates T cell receptor signaling to integrins via Abl- and CrkL – C3G- mediated activation of Rap1. *J. Cell Biol.* **182**, 1231–1244 (2008).

158. Humphreys, D., Singh, V. & Koronakis, V. Inhibition of WAVE Regulatory Complex Activation by a Bacterial Virulence Effector Counteracts Pathogen Phagocytosis. *Cell Rep.* **17**, 697–707 (2016).

159. JANE, L., TRACEY MARTIN, WEEKS, H. P. & JIANG, W. G. Structure and Role of WASP and WAVE in Rho GTPase Signalling in Cancer. *Cancer Genomics Proteomics* **11**, 155–165 (2014).

160. Reuter, C. *et al.* Design and stereoselective synthesis of ProM-2: A spirocyclic diproline mimetic with polyproline type II (PPII) helix conformation. *Chem. - A Eur. J.* **21**, 8464–8470 (2015).

161. Golemi-Kotra, D. *et al.* High Affinity, Paralog-Specific Recognition of the Mena EVH1 Domain by a Miniature Protein. *J. Am. Chem. Soc.* **126**, 4–5 (2004).

162. Burkhardt, J. K. Cytoskeletal function in the immune system. *Immunol. Rev.* **256**, 5–9 (2013).

163. Elegheert, J. *et al.* Lentiviral transduction of mammalian cells for fast , scalable and high-level production of soluble and membrane proteins. *Nat Protoc.* **13**, 2991–3017 (2018).

164. Free, R. B., Hazelwood, L. A. & Sibley, D. R. Identifying novel protein-protein interactions using co-immunoprecipitation and mass spectroscopy. *Curr. Protoc. Neurosci.* 1–19 (2009) doi:10.1002/0471142301.ns0528s46.

165. Luque, A. *et al.* Activated Conformations of Very Late Activation Integrins Detected by a

Group of Antibodies (HUTS) Specific for a Novel Regulatory Region (355 − 425) of the Common ⬚ 1 Chain *. *J. Biol. Chem.* **271**, 11067–11075 (1996).

166. Mitjans, F. *et al.* An anti- α v-integrin antibody that blocks integrin function inhibits the development of a human melanoma in nude mice. *J. Cell Sci.* **108**, 2825–2838 (1995).

167. Chigaev, A. & Sklar, L. A. Overview : assays for studying integrin-dependent cell adhesion. *Methods Mol Biol.* **757**, 1–14 (2012).

168. Deng, Y., Herbert, J. A., Smith, C. M. & Smyth, R. L. An in vitro transepithelial migration assay to evaluate the role of neutrophils in Respiratory Syncytial Virus (RSV) induced epithelial damage. *Sci. Rep.* **8**, 1–12 (2018).

169. Parzmair, G. P. *et al.* ADAP plays a pivotal role in CD4 + T cell activation but is only marginally involved in CD8 + T cell activation, differentiation, and immunity to pathogens . *J. Leukoc. Biol.* **101**, 407–419 (2017).

170. Benz, P. M. *et al.* Differential VASP phosphorylation controls remodeling of the actin cytoskeleton. *J. Cell Sci.* **122**, 3954–3965 (2009).

171. Ahern-Djamali, S. M. *et al.* Mutations in Drosophila enabled and rescue by human vasodilator- stimulated phosphoprotein (VASP) indicate important functional roles for Ena/VASP homology domain 1 (EVH1) and EVH2 domains. *Mol. Biol. Cell* **9**, 2157–2171 (1998).

172. Sambrano, J. *et al.* Evaluating integrin activation with time-resolved flow cytometry. *J. Biomed. Opt.* **23**, 1–10 (2018).

173. Su, X., Ditlev, J. A., Rosen, M. K. & Vale, R. D. The Immune Synapse: Methods and Protocols; Reconstitution of TCR Signaling Using Supported Lipid Bilayers. *Methods Mol Biol* **1584**, 65–76 (2017).

174. Gomez, T. S. & Billadeau, D. D. T Cell Activation and the Cytoskeleton: You Can't Have One Without the Other. *Adv. Immunol.* **97**, 1–64 (2008).

175. Lehmann, R., Meyer, J., Schuemann, M., Krause, E. & Freund, C. A novel S3S-TAP-tag for the isolation of T-cell interaction partners of adhesion and degranulation promoting adaptor protein. *Proteomics* **9**, 5288–5295 (2009).

176. Nukala, S. B., Baron, G., Aldini, G., Carini, M. & D'Amato, A. Mass Spectrometry-based Label-free Quantitative Proteomics to Study the Effect of 3PO Drug at Cellular Level. *ACS Med. Chem. Lett.* **10**, 577–583 (2019).

177. Chen, X. J. *et al.* Ena/VASP proteins cooperate with the WAVE complex to regulate the actin cytoskeleton. *Dev. Cell* **30**, 569–584 (2014).

178. Legerstee, K., Geverts, B., Slotman, J. A. & Houtsmuller, A. B. Dynamics and distribution of paxillin , vinculin , zyxin and VASP depend on focal adhesion location and orientation. *Nat. Sci. Reports* **9**, 1–18 (2019).

179. Lafuente, E. M. *et al.* RIAM, an Ena/VASP and profilin ligand, interacts with Rap1-GTP and mediates Rap1-induced adhesion. *Dev. Cell* **7**, 585–595 (2004).

180. Hansen, S. D. & Mullins, R. D. Lamellipodin promotes actin assembly by clustering Ena/VASP proteins and tethering them to actin filaments. *Elife* **4**, 1–29 (2015).

181. Kurisu, S., Suetsugu, S., Yamazaki, D., Yamaguchi, H. & Takenawa, T. Rac-WAVE2 signaling is involved in the invasive and metastatic phenotypes of murine melanoma cells. *Oncogene* **24**, 1309–1319 (2005).

182. Padrick, S. B., Doolittle, L. K., Brautigam, C. A., King, D. S. & Rosen, M. K. Arp2 / 3 complex is bound and activated by two WASP proteins. *PNAS* **108**, 472–479 (2011).

183. Havrylenko, S., Noguera, P., Abou-ghali, M., Manzi, J. & Pollard, T. D. WAVE binds Ena / VASP for enhanced Arp2 / 3 complex – based actin assembly. *Mol Biol Cell* **26**, 55–65 (2015).

184. Geng, L., Pfister, S., Kraeft, S. & Rudd, C. E. Adaptor FYB (Fyn-binding protein) regulates integrin- mediated adhesion and mediator release : Differential involvement of the FYB SH3 domain. *PNAS* **98**, 11527–11532 (2001).

185. Coppolino, M. G., Krause, M., Hagendorff, P., Monner, D. A. & Trimble, W. Evidence for a molecular complex consisting of Fyb / SLAP , SLP-76 , Nck , VASP and WASP that links the actin cytoskeleton to Fc γ receptor signalling during phagocytosis. *J. Cell Sci.* **114**, 4307–18 (2002).

186. Lettau, M. *et al.* The adapter proteins ADAP and Nck cooperate in T cell adhesion. *Mol. Immunol.* **60**, 72–79 (2014).

187. Lehmann, R., Meyer, J., Schuemann, M. & Krause, E. A novel S3S-TAP-tag for the isolation of T-cell interaction partners of adhesion and degranulation promoting adaptor protein. *Proteomics* **9**, 5288–5295 (2009).

188. Velazquez-Campoy, A. & Freire, E. Isothermal titration calorimetry to determine association constants for high-affinity ligands. *Nat. Protoc.* **1**, 186–191 (2006).

189. Gracia, B. *et al. Nanomedicine review : clinical developments in liposomal applications*. *Cancer Nanotechnology* (Springer Vienna, 2019). doi:10.1186/s12645-019-0055-y.

190. Sarfraz, M. *et al.* Development of dual drug loaded nanosized liposomal formulation by a reengineered ethanolic injection method and its pre-clinical pharmacokinetic studies. *Pharmaceutics* **10**, 1–22 (2018).

191. Veloso, D. F. M. C. *et al.* Intravenous delivery of a liposomal formulation of voriconazole improves drug pharmacokinetics, tissue distribution, and enhances antifungal activity. *Drug Deliv.* **25**, 1585–1594 (2018).

192. Lee, M. Liposomes for Enhanced Bioavailability of Water-Insoluble Drugs : In Vivo Evidence and Recent Approaches. *Pharm. Rev.* **12**, 1–30 (2020).

193. Sadozai, H. & Saeidi, D. Recent Developments in Liposome-Based Veterinary Therapeutics. *ISRN Vet. Sci.* **2013**, 1–8 (2013).

194. He, H. *et al.* Adapting liposomes for oral drug delivery $. *Acta Pharm. Sin. B* **9**, 36–48 (2019).

195. Yang, J. *et al.* Drug Delivery via Cell Membrane Fusion Using Lipopeptide Modi fi ed Liposomes. *ACS Cent. Sci.* **2**, 621–630 (2016).

196. Li, J. *et al.* Conformational equilibria and intrinsic affinities define integrin activation. *EMBO J.* **36**, 629–645 (2017).

197. Jankowska, K. I. *et al.* Integrins modulate T cell receptor signaling by constraining actin flow at the immunological synapse. *Front. Immunol.* **9**, 1–19 (2018).

198. Baker, R. G. *et al.* The Adapter Protein SLP-76 Mediates " Outside-In " Integrin Signaling and Function in T Cells ▯ †. **29**, 5578–5589 (2009).

199. Boerth, N. J., Judd, B. A. & Koretzky, G. A. Functional Association between SLAP-130 and SLP-76 in Jurkat T Cells *. *J. Biol. Chem.* **275**, 5143–5152 (2000).

200. Nolz, J. C. *et al.* WAVE2 Regulates High-Affinity Integrin Binding by Recruiting Vinculin and Talin to the Immunological Synapse ▯. *Mol. Cell. Biol.* **27**, 5986–6000 (2007).

201. Porter, J. C. *et al.* Signaling Through Integrin LFA-1 Leads to Filamentous Actin Polymerization and Remodeling, Resulting in Enhanced T Cell Adhesion. *J Immunol* **168**, 6330–6335 (2002).

202. Law, A. *et al.* Lamellipodin and the Scar/WAVE complex cooperate to promote cell migration in vivo. *J Cell Biol.* **203**, 673–689 (2013).

203. Eto, K. *et al.* The WAVE2 / Abi1 complex differentially regulates megakaryocyte development and spreading : implications for platelet biogenesis and spreading machinery. *Blood* **110**, 3637–3647 (2007).

204. Barone, M. *et al.* Designed nanomolar small-molecule inhibitors of Ena / VASP EVH1 interaction impair invasion and extravasation of breast cancer cells. *PNAS* **117**, 29684–29690 (2020).

205. Dustin, M. L. The immunological synapse. *Cancer Immunol Res.* **2**, 1023–1033 (2015).

206. Hosseini, B. H. *et al.* Immune synapse formation determines interaction forces between T cells and antigen-presenting cells measured by atomic force microscopy. *PNAS* **106**, 17852–17857 (2010).

207. Wang, H. *et al.* ADAP – SLP-76 Binding Differentially Regulates Supramolecular Activation Cluster (SMAC) Formation Relative to T Cell – APC Conjugation The Journal of Experimental Medicine. *J Exp Med.* **200**, 1063–1074 (2004).

208. Roy, N. H. & Burkhardt, J. K. The actin cytoskeleton: A mechanical intermediate for signal integration at the immunological synapse. *Front. Cell Dev. Biol.* **6**, 1–7 (2018).

209. Murugesan, S. *et al.* Formin-generated actomyosin arcs propel t cell receptor microcluster movement at the immune synapse. *J. Cell Biol.* **215**, 383–399 (2016).

210. Callebaut, I., Cossart, P. & Y, P. D. EVH1 / WH1 domains of VASP and WASP proteins belong to a large family including Ran-binding domains of the RanBP1 family. *FEBS* **441**, 181–185 (1998).

211. Jeffrey C. Nolz, Timothy S. Gomez, Peimin Zhu, Shuixing Li, Ricardo B. Medeiros, Yoji Shimizu, Janis K. Burkhardt, Bruce D. Freedman, and Daniel D. Billadeau. The WAVE2 Complex Regulates Actin Cytoskeletal Reorganization and CRAC-Mediated Calcium Entry during T Cell Activation. *Curr Biol.* **16**, 1–7 (2006).

212. Zipfel, P. A. *et al.* Role for the Abi / Wave Protein Complex in T Cell Receptor-Mediated Proliferation and Cytoskeletal Remodeling. *Curr. Biol.* **16**, 35–46 (2006).

213. Dustin, M. L. & Cooper, J. A. The immunological synapse and the actin cytoskeleton : molecular hardware for T cell signaling. *Nat. Immunol.* **1**, 23–29 (2000).

214. Burbach, B. J. *et al.* Distinct Regulation of Integrin-Dependent T Cell Conjugate Formation and NF- ⬚ B Activation by the Adapter. *J. Immunol.* **181**, 4840–4851 (2008).

Appendix:

Abbreviations:

α	Alpha
β	Beta
γ	Gamma
ζ	Zeta
μ	Micro
#	Number
μM	Micromolar
^0C	Degree Celsius
ml	Mililiter
nm	Nanometer
mg	Miligram
μg	Microgram
2-Cl-F	2-Chloro-Phenylalanin
2D	2 Dimensional
3D	3 Dimensional
AA	Amino acids
ActA	Actin assembly-inducing protein
ADAP	Adhesion and degranulation-promoting adapter protein
$ADAP_{MUT}$	Mutant ADAP
$ADAP_{WT}$	Wild-type ADAP
ANOVA	Analysis of variance,
APC	Antigen presenting cell
ARP2/3	Actin related protein 2/3
ATP	Adenosine triphosphate
ATP	Adenosine triphosphate
BSA	Bovin serum albumin
CCL	C-C motif chemokine ligand
CCR	C-C motif chemokine receptor
CD	Cluster of differentiation
Cdc42	Cell division control protein 42 homolog
CFSE	Carboxyfluorescein succinimidyl ester
CNS	Central nervous system
CO_2	Carbon dioxide
cSMAC	Central supramolecular activation cluster
C-Terminal	Carboxy-terminus
CXCL	C-X-C motif chemokine Ligand
CXCR	C-X-C-motif chemokine Receptor
D	Aspartic acid

DAG	DiacylglyceroDCs Dendritic cells
DAMPs	Damage-associated molecular patterns
DBS	Domain binding site
DMSO	Dimethylsulfoxide
DNA	Deoxyribonucleic acid
dNTP	Deoxynucleotide triphosphates
dSMAC	Distal supramolecular activation cluster
E	Glutamic acid
E. coli	*Escherichia coli*
e.g.	*exempli gratia*; for example
EAE	Experimental Allergic Encephalomyelitis
ECM	Extracellular matrix
EDTA	Ethylenediaminetetraacetic acid
EGTA	Ethylene glycol-bis(β-aminoethyl ether)-tetraacetic acid
EMT	Epithelial mesenchymal transition
Ena/VASP	Enabled/Vasodilator-Stimulated Phosphoprotein
EnaH	Enabled Homolog of Drosophila
ERK	Extracellular signal-regulated kinase
Erk	Extracellular signal-related kinase
EVH-1/2	Ena/VASP homology-1/2
EVL	Ena-Vasp-like protein
Exp	Experiment
F	Phenylalanine
FAB	F actin binding site
FACS	Fluorescence-activated cell sorter/sorting
FBS	Fetal bovine serum
Fc	Fragment crystallisable
FCS	Fetal calf serum
Fig	Figure
FPLC	Fast protein liquid chromatography
FSC	Forward scatter cytometry
FYB	Fyn-binding protein
FYN	Feline yes-related protein
GAB	G actin binding site
GADS	Grb2-related adaptor downstream of shc
GAPDH	Glyceraldehyde 3-phosphate dehydrogenase
GEF	GTP exchange factor
GFP	Green fluorescent protein

GM-CSF	Granulocyte-macrophage colony-stimulating factor
GPCR	G protein-coupled receptor
GSH	Glutathion
GST	Glutathione S-transferase
GTP	Guanosine triphosphate
GYF	Glycine-tyrosine-phenylalanine
h	Hours
HEPES	4-(2-hydroxyethyl)-1-piperazineethanesulfonic acid
HIS	Histidine
HLA	Human leukocyte antigens
hSH3	Helical extended Src homology 3
HSPC300/BRICK1	Haematopoietic stem/progenitor cell protein 300
ICAM-1	Intercellular adhesion molecule 1
IDDM	Insulin-dependent diabetes mellitus
IFN-γ	Interferon gamma
IgE	
IgG	Immunoglobulin G
IgM	Immunoglobulin M
IL	Interleukin
IP3	Inositol 1,4,5-triphosphate
IPTG	Isopropyl-β-D-thiogalactopyranoside
IR	Infrared
IS	Immunological synapse
ITAM	Immunoreceptor tyrosine-based activation
ITC	Isothermal titration calorimetry
ITK	IL-2-inducible T-cell kinase
K_D	Dissociation constant
KD	Knock-down
kDa	Kilodalton
L	Leucine
LAT	Linker for activation of T-cells
LCK	Lymphocyte-specific protein tyrosine kinase
LC-MS	Liquid chromatography–mass spectrometry
LFA-1	Lymphocyte function-associated antigen-1
LNs	Lymph nodes
LPS	Lipopolysaccharide
m/z	Mass to charge ratio
M0	Non-activated macrophages
M1	Pro-inflammatory macrophages

3

M2	Anti-inflammatory macrophages
MAPK	Mitogen-activated protein kinase
mDia1	Mammalian diaphanous-related formin 1
Mena	Mammalian enabled
Mena^{INV}	Mena invasive
MHC	Major histocompatibility complex
MHC	Major histocompatibility complex
Min	Minute
mRNA	messenger RNA
MS	Mass spectrometry
MS	Multiple sclerosis
MS/MS	Tandem mass spectrometry
MWCO	Molecular weight cut-off
Nap1/ Hem-2	Nucleosome assembly protein 1
NCK	Non-catalytic region of tyrosine kinase
NF-κB	Nuclear factor κ-light-chain-enhancer of activated B-cells
Ni-NTA	Nickel-Nitrilotriacetic acid
NK	Natural killer
NLS	Nuclear localization signals
NMR	Nuclear magnetic resonance
N-Terminal	Amino-terminus
OVA peptide	Ovalbumin
P	Proline
PAGE	Polyacrylamide gel electrophoresis
PAMPs	Pathogen-associated molecular patterns
PBS	Phosphate-buffered saline
PCR	Polymerase chain reaction
PDB	Protein Data Bank
PE	Phycoerythrin
PET	Polyethylene terephthalate
PFA	Paraformaldehyde
PH domain	Pleckstrin homology domain
pH	potential of hydrogen
PI3K	Phosphoinositide 3-kinase
PIP2	Phosphatidylinositol-(4,5)-bisphosphate
PKCθ	Protein kinase C theta
PLCγ1	Phospholipase C gamma 1
PMA	Phorbol-12-myristate-13-acetate
PML	progressive multifocal leukoencephalopathy
PMSF	Phenylmethylsulfonyl fluoride
PPII	Proline type II

Pro	Proline
ProM	Proline mimetic
PRRs	Pattern recognition receptors
PRS	Proline rich sequence
pSMAC	Peripheral supramolecular activation cluster
PTB	Protein tyrosine binding
PTK	Protein tyrosine kinases
RA	Rheumatoid arthritis
RAC	Ras-related C3 botulinum toxin substrate 1
RAP1	Ras proximite protein 1
RAPL	Regulator for cell adhesion and polarization enriched in lymphoid tissues
Ras	Rat sarcoma
RhoA	Ras homology family member A
RIAM	Rap1-GTP-interacting adapter molecule
RNA	Ribonucleic acid
RPM	Revolutions per minute
RTKs	Receptor tyrosine kinases
S	Serine
SDS	Sodium dodecyl sulfate
SDS-PAGE	Sodium dodecyl sulfate polyacrylamide gel electrophoresis
SEER	Surveillance, Epidemiology, and End Results
SEM	Standard error of the mean
SFKs	Src family of protein tyrosine kinases
SH2/3	Src homology 2/3
shRNA	Small hairpin RNA
SIP	Sphingosine 1 phosphate
SKAP55	Src kinase-associated phosphoprotein of 55
SKAP-HOM	SKAP-55 homolog
SLAP	Src-like adapter protein
SLAP120	SLP76 associated phosphoprotein of 120 kDa
SLAP130	SLP76 associated phosphoprotein of 130 kDa
SLE	Systemic lupus erythematosus
SLP76	SH2 domain containing leukocyte protein of 76
SMAC	Supramolecular activation cluster
SRA1	Steroid Receptor RNA Activator 1
SSC	Side scatter cytometry
Tab	Table
TAE	Tris-acetate-EDTA

TAM	Tumor associated macrophages
TCEP	Tris (2-carboxyethyl) phosphine hydrochloride
TCR	T-cell receptor
TFA	Trifluoroacetic Acid
TGF-β	Transforming growth factor β
Th	T helper
Th1/2	T helper cell 1/2
TIRF	Total Internal Reflection Fluorescence
TLR	Toll-like receptor
TME	Tumor microenvironment
TNF-α	Tumor necrosis factor-α
Treg	Regulatory T-cell
TSH	Thyrotropin-stimulating hormone
US	United States
UTR	Untranslated region
V	Voltage
VASP	Vasodilator-stimulated phosphoprotein
VAV	Proto-oncogene vav
VAV1	Vav guanine nucleotide exchange factor 1
VCA	Verprolin, cofilin, acidic
VCAM-1	Vascular cell adhesion molecule 1
VEGF	Vascular endothelial growth factor
VLA-4	Very late antigen-4
W	Tryptophan
WASP	Wiskott-Aldrich syndrome protein
WAVE	WASP verprolin homologous protein
WAVE2	WASP verprolin homologous protein-2
WAVE2$_{MUT}$	Mutant WAVE2
WAVE2$_{WT}$	Wild-type WAVE2
WB	Western Blot
WRC	WAVE regulatory complex
ZAP70	ξ-chain associated protein of 70 kDa

List of Figures:

List of Tables:

Acknowledgment